INFORMATION TO USERS

This manuscript has been reproduced from the microfilm master. UMI films the text directly from the original or copy submitted. Thus, some thesis and dissertation copies are in typewriter face, while others may be from any type of computer printer.

The quality of this reproduction is dependent upon the quality of the copy submitted. Broken or indistinct print, colored or poor quality illustrations and photographs, print bleedthrough, substandard margins, and improper alignment can adversely affect reproduction.

In the unlikely event that the author did not send UMI a complete manuscript and there are missing pages, these will be noted. Also, if unauthorized copyright material had to be removed, a note will indicate the deletion.

Oversize materials (e.g., maps, drawings, charts) are reproduced by sectioning the original, beginning at the upper left-hand corner and continuing from left to right in equal sections with small overlaps. Each original is also photographed in one exposure and is included in reduced form at the back of the book.

Photographs included in the original manuscript have been reproduced xerographically in this copy. Higher quality 6" x 9" black and white photographic prints are available for any photographs or illustrations appearing in this copy for an additional charge. Contact UMI directly to order.

UMI

A Bell & Howell Information Company
300 North Zeeb Road, Ann Arbor MI 48106-1346 USA
313/761-4700 800/521-0600

Vibrational Studies of Phosphoryl Transfer Enzymes: ras-p21•MgGTP and Myosin S1•MgADP-Vanadate

by

Jianghua Wang

A dissertation submitted to the Graduate Faculty in Physics in partial fulfillment of the requirements for the degree of Doctor of Philosophy. The City University of New York

1999

This manuscript has been read and accepted for the Graduate Faculty in Physics in the satisfaction of the dissertation requirement for the degree of Doctor of Philosophy.

9/27/97
Date

Chair of Examining Committee

12/15/98
Date

Executive Officer

Supervisory Committee

The City University of New York

ABSTRACT

Vibrational Studies of Phosphoryl Transfer Enzymes: ras-p21•GTP and Myosin S1·MgADP-Vanadate

by

Jianghua Wang

Advisor: Professor Robert H. Callender

We have measured the Raman spectra of monophosphate compounds in aqueous solution. The measured frequencies were correlated with P••O valence bond order by using a modification of the Hardcastle-Wachs procedure. The P••O bond order and bond length in phosphates can be determined from vibrational spectra by using the derived bond order/stretching frequency correlation and the bond length/bond order correlation of Brown and Wu .

The Raman and infrared spectra of guanosine 5'-diphosphate (GDP) and guanosine 5'-triphosphate (GTP) in aqueous solution were also examined. Frequency shifts were observed as Mg^{2+} complexes with GDP and GTP in aqueous solution. These results suggested that Mg^{2+} binds to GDP in a bidentate manner to the α,β P••O bonds and in a tridentate manner to the α,β and γ P••O bonds of Mg•GTP. We have analyzed the previously obtained isotope edited Raman difference spectra of 1:1 complexes of Mg•GDP and Mg•GTP in ras-p21. Frequency changes of the phosphate groups were observed when Mg•GDP, Mg•GTP bind to the protein. Employing both the previous

empirical relationships between bond orders/lengths and frequencies as well as vibrational analysis from *ab initio* calculations, the spectral changes can be explained by the change of the Mg^{2+} binding sites and hydrogen-bonding. Implications of these structural results for the reaction mechanism of GTP hydrolysis catalyzed by the GTPase are discussed.

We have analyzed previously obtained isotope edited Raman difference spectra of the non-bridging V••O bonds of vanadates, both in solution, and when bound to the myosin S1•MgADP complex. By use *of ab initio* calculations on a model of the vanadate binding site in myosin, the angles between the non-bridging V••O bonds and between these bonds and the apical bonds in the myosin S1•MgADP-Vi complex were determined. The summed bond order of the two apical bonds between the attacking and leaving group oxygens with the central vanadium ion in the S1•MgADP-Vi complex was found to increase only slightly compared with the bond order of the ester V-O bond of a monoester vanadate model compound in solution, suggesting an S_N2 like mechanism for the phosphoryl transfer reaction catalyzed by myosin.

ACKNOWLEDGMENTS

I would like to express my sincere gratitude to Professor Robert H. Callender for his guidance and patience during the course of this thesis work. His ideas are essential parts of all the research work.

I would like to thank Dr. Hua Deng for leading me into an active research field. His suggestion, extensive experiences and clear discernment are always good guidance for my research. I thank him for sharing these happiness and the frustrating moments of my research work.

I feel grateful to Drs. Marilyn Gunner, William Ray and Michael Green for their valuable advice. I would like to thank Drs. John Burgner, Martin Webb and Ralph Yount for synthesizing compounds and protein samples used in my research work.

I would like to thank Dr. Miriam Gulotta for reading and improving the English of the thesis. I would also like to thank Drs. Rudolf Gilmanshin, Larry Senak, Dongguang Xiao, Zhongmo Ju, Hui Zhong and Ruhong Zhou for their generous help.

Finally, I would like to thank all my family members for their encouragement and help in all these years.

To the memory of my mother, Azhu Lu and my father, Ronglin Wang

Table of Contents

LIST OF TABLES

LIST OF FIGURES

LIST OF ABBREVIATIONS

p21	gene product of the human c-H-ras proto-oncogene
p21(G12D)	point mutation of p21 at residue Gly12 by Asp
p21(G12P)	point mutation of p21 at residue Gly12 by Pro
p21(G12V)	point mutation of p21 at residue Gly12 by Val
ADP	adenosine 5' diphosphate
ATP	adenosine 5' triphosphate
GDP	guanosine 5' diphosphate
GTP	guanosine 5' triphosphate
(β-$^{18}O_3$)GDP	guanosine 5' diphosphate with ^{18}O labeled on the three oxygen atoms of β-phosphate.
($\alpha\beta$-^{18}O;β-$^{18}O_3$)GDP	guanosine 5' diphosphate with ^{18}O labeled on the three oxygen atoms of β-phosphate and the P_α-O-Pβ linkage oxygen.
(β-$^{18}O_2$;$\beta\gamma$-^{18}O)GTP	guanosine 5' triphosphate with ^{18}O labeled on the two oxygen atoms of β-phosphate and the P_γ-O-Pβ linkage oxygen.
(γ-$^{18}O_3$)GTP	guanosine 5' triiphosphate with ^{18}O labeled on the three oxygen atoms of γ-phosphate
GMPPCP	guanyle (β,γ-methylene)-triphosphate
GppNHp	guanosine 5'-(β,γ-imido)-triphosphate

CHAPTER 1

Introduction

A very large number of proteins either bind phosphate or catalyze phosphoryl transfer reactions. The common mechanistic feature of phosphoryl transfer reactions is that the group being transferred is the phosphoryl group $-PO_3^{2-}$ (not phosphate, $-OPO_3^{2-}$). Despite the ubiquity of these enzymes, very little is known about how the various enzymes bring about catalysis. The solution mechanism of phosphate hydrolysis of dianionic phosphate monoesters, $RO\text{-}PO_3^{2-}$, is well investigated. The strength of the attacking nucleophile, water or hydroxide for example, matters little to rates of hydrolysis. The pK_a of the leaving group is key, however, with more stable leaving groups undergoing faster cleavage (Bourne & Williams, 1984; Kirby, 1967; Jones, 1984; Admiraal, 1995; Herschlag, 1987). These and other studies suggest that phosphoryl transfer involving monoester dianionic phosphate in aqueous solution is via a primarily dissociative pathway, with a 'metaphosphate-like' transition state (Herchlag & Jencks, 1990). Here, the extensive bond breaking of the old bridging O-P bond has occurred before the new bond forms, that is, $RO^{-}\cdots PO_3^{-}\cdots {}^{-}OR'$. The sum of the bond order of the broken bond and the incipient new bond is significantly less than one. However, the phosphoryl transfer reaction of monoester dianionic phosphate catalyzed by enzymes may proceed via different pathways in various enzymes. Recent studies on protein-tyrosine phosphatase (Zhao & Zhang, 1996) and alkaline phosphatase (Hollfelder & Herschlag, 1995) suggest dissociative transition states. In contrast, an associative mechanism would involve substantial bond formation by the attacking nucleophile before expulsion of the old RO^- group. This appears to be the mechanism of phosphoryl transfer reaction catalyzed by

phosphoglucomutase (PGM) (Deng et al., 1993). In another process, bond-making and bond-breaking are approximately synchronous and part of the energy for breaking the old bond is furnished by forming the new one (S_N2 like). The sum of the bond orders for the forming and breaking bonds is close to the bond order of the original P-O ester bond. It has been proposed that ras-p21 catalyzes hydrolysis of the γ-phosphate from bound GTP via an in-line S_N2/associative mechanism (Schweins & Warshel, 1996) based on linear free energy relationships. However, the partially dissociative mechanism can't be excluded. Direct bond information will be needed to further study this problem. The phosphate hydrolysis mechanism in other phosphoryl transfer enzymes is still unknown. Here Raman spectroscopy is used to study the mechanism of two phosphoryl transfer enzymes, ras-p21 and myosin subfragment-1 (S1).

Guanine nucleotide binding proteins are involved a variety of key cellular processes such as signal transduction, cell growth and differentiation, protein synthesis, and protein transport. ras-p21, like other proteins under the generic term of 'G-proteins', is believed to be involved in a growth promoting signal transduction process (see Barbacid, 1987; Gibbs et al., 1984). These proteins share common sequence elements, have a highly homologous structure (Wooley and Clark, 1989; Bourne et al., 1990,1991; Boguski and McCormik, 1993), and their biochemical activities are tightly regulated by the nature of the bound nucleotide. In general, GTP-binding proteins are in an 'active' state when complexed with GTP, and in an 'inactive' state when complexed with GDP (Wooley and Clark, 1989). It is well known that GTP-binding proteins exhibit a GTPase activity that recycles the protein back to its inactive GDP-bound form. The rate of this reaction is crucial for the corresponding timing of the regulated process; the longer a guanine nucleotide binding protein remains in its active GTP-bound state, the longer it will transmit and also amplify a certain signal.

Hence, the rate of GTP hydrolysis is of great importance for the right timing of many processes in a cell. The p21 protein itself possesses intrinsic GTPase activity. In vivo, this intrinsic activity is greatly enhanced by GAP (GTPase activating protein). GAP can enhance the GTPase activity of p21 by at least a factor of $4x10^3$ (Bollag and McCormick, 1991). Mutations may slow the reaction rate of these biologically active signaling proteins. For example, mutations in positions 12, 13, and 61 of ras p21 significantly reduce its GTPase activity, impair the protein's ability to hydrolyze GTP (Fasano et al. 1984) and render it insensitive to activation by GAP (Adari et al., 1988). Therefore, the protein remains in the active, growth promoting GTP-bound state, which can lead to cancer. Thus, an understanding of the GTPase mechanism of p21 and the effect of GAP on this mechanism is of importance for an understanding of the molecular basis of cancer. The 'hot spots' in the oncogenic p21 proteins include residues 12 (normally Gly-12) and 61 (normally Gln-61). The role of Gln-61 in the mechanism of p21 is of particular interest since mutations of this residue in the GAP/ras p21 complex reduce the rate of GTP hydrolysis by more than 4 orders of magnitude (Sigal et al., 1988) and are found to be responsible for cell transformation (Fasano et al., 1984). The same mutations in the isolated p21 change the hydrolysis rate by only 1 order of magnitude (Fasano et al., 1984).

It .is generally believed that phosphotransferases require at least one divalent cation complexed directly to phosphoryl group oxygens for catalytic activity. One can postulate various possible catalytic functions of the Mg^{2+} ion, such as shielding of the negative charge on the attacked γ-phosphate, increasing the acid strength of the leaving group or activation of the nucleophile (Cooperman, 1976; Knowles, 1980). Mg^{2+} can also be involved in the stabilization of the transition state of the reaction. The precise role of the metal ion for the guanine nucleotide binding proteins has not been proven and may

indeed be different for each enzyme, as can be seen from the fact that there is no preferred ligation pattern of the metal ion to the enzyme or the phosphate atoms for the related enzymes (see e.g. Eckstein, 1985). The GTPase activity of guanine nucleotide binding proteins has been shown to be absolutely dependent on the presence of certain divalent ions (Gilman, 1987).

Extensive studies have been carried on the biological properties of ras-p21 (Wittinghofer et al., 1991). Expression of the recombinant ras-p21 proteins has resulted in an abundance of sample that has made it feasible to investigate these proteins completely via X-ray crystallography, NMR and vibrational spectroscopy. It is very important to understand, at atomic level, how normal and mutant ras-p21 proteins interact with GDP and GTP at active and inactive site, as well as how these interactions are involved in the GTP hydrolysis in proteins.

X-ray crystallographic studies have revealed the structure of p21 protein bound with GDP or a GTP analogue (Pai et al., 1989, 1990; Bourne et al., 1991; Schlichting et al., 1990; Krengel et al., 1990; Tong et al., 1990; Milburn et al., 1989; de Vos et al., 1988). The structure contains a central β-sheet consisting of six strands, five helices and nine loops (Figure 1.1). Three loops are particularly important for the function of the protein: loop L1 contains Gly12, which is the most frequently mutated residue in human tumors; loop L2 contains the residue which is believed to be involved in the interaction with GAP such as Asp33; loop L4 contains Gln61, which is highly important for the oncogenic activation of ras-p21. The structures shows that Gln61 makes contact with a water molecule, which is perfectly placed to be the nucleophile attacking the γ-phosphate of GTP. These three loops comprise the active site of molecule centered around the γ-phosphate, where an important interaction can initiate the GTPase reaction (Pai et al., 1989). X-ray structure studies also show several

hydrogen bonding interactions between the nucleotide and p21 protein, both at the guanine ring moiety and at the phosphate moiety. These strong hydrogen bounding interactions are attributed to the high affinity and specificity for GDP and GTP. The kinetic studies have shown that p21 doesn't tolerate many substitutions of GDP and GTP. The affinities of p21 for GMP and ADP are about six orders of magnitude smaller than that of GDP (John et al., 1990). The overall structures of mutant p21 (G12V; G12D) are very similar to that of the wild type p21.

Another phosphoryl transfer enzyme which will be studied is Myosin subfragment 1. Myosin is an enzyme that, in conjunction with actin, transduces the chemical energy from the hydrolysis of ATP into directed mechanical movement. The cytomyosin system of motility is found in all eukaryotic cells where it is directly involved in cytokinesis, cell division, and the movement of organelles. In its most abundant and organized state, it is responsible for muscle contraction. Over the years considerable effort has been devoted toward understanding the molecular origin of the myosin-based motility. Extensive kinetic measurements on both fragments of myosin and muscle fibers have established the chemical and physical features of this process (Greene & Eisenberg, 1980; Trybus & Taylor, 1982). The classic work of Lymn and Taylor provided the first successful description of ATP hydrolysis by myosin which was shown to occur during the time that myosin was dissociated from actin. These studies suggested that the power stroke was associated with product release (Lymn & Taylor, 1971). In addition, kinetic analysis revealed that nucleotide binding and release is a multistep process; suggesting that ATP hydrolysis involves the transition between several discrete conformational states (Smith & Rayment, 1995).

X-ray crystallographic studies of skeletal muscle myosin subfragment-1 have established the overall domain structure and tertiary fold of this complex molecular aggregate (Smith & Rayment, 1996). It is strongly suggested that myosin undergoes conformational changes when it binds to actin and to ATP. In an effort to investigate the nature of the structural transitions that occur during the process of energy transduction, crystals of a series of ATP analogs with a truncated head of myosin from D. discoideum have been formed and their three-dimensional structures determined through x-ray diffraction techniques (Smith & Rayment, 1995). Smith et al. found that the conformational change, which occured when ATP bound to actomyosin and which reduced the affinity of myosin for actin, was caused by the binding of the γ– and β-phosphate groups of nucleotide.

In myosin, ATP hydrolysis is not coincident with the force-generating step (Lymn & Taylor, 1971; Goldman, 1987). Instead, ATP binding initially reduces the affinity of myosin for actin, after which hydrolysis of ATP occurs rapidly and results in a metastable ternary complex between myosin, ADP, and inorganic phosphate. In this state the equilibrium constant for the myosin + ATP reaction is between 1 and 10 for sketel muscle depending on the temperature and ionic strength (Bagshaw & Trentham, 1973,1974; Taylor, 1977). Release of the hydrolysis products is catalyzed by rebinding to actin which is accompanied by the energy transduction step. Vanadate inhibits the myosin ATPase activity by forming, in absence of actin, a long-lived complex with MgADP that is believed to mimic either the transition state for hydrolysis or the (ADP, Pi) state (Goodno, 1979; Goodno & Taylor, 1982). The half-life for dissociation of this complex at 0 ^{o}C is ~4 days (Goodno, 1979, 1982; Werber et al., 1992). Interestingly, the rate of inhibition is considerably less than the diffusion limit for binding. Thus, formation of the inhibitory ternary complex has been

interpreted as a multistep process, in which there is initial formation of an equilibrium complex, followed by slow isomerization to form the inhibited state. Furthermore, ADP•V_i reduces the binding affinity of myosin for actin ($1.5x10^{-3}$ M^{-1}), although less than that induced by the ADP, P_i state under the same conditions. Actin also increases the rate of release of vanadate by 10^5 compared to that of myosin•ADP•P_i alone, although the release of vanadate is still slow. The actin-activated ATPase activity of myosin is about 90% inhibited by ADP•V_i at high vanadate concentrations (Goodno & Taylor, 1982); however, there is some indication that this is due in part to the formation of polymeric vanadate ions (Smith & Eisenberg, 1990). Spectroscopic studies of spin-labeled myosin subfragment 1 have also shown that the ADP•V_i complex exhibits many of the structural properties of the (ADP, P_i) state (Wells & Bagshaw, 1984). Consequently, the ADP•V_i complex is often considered to be close to the confirmation of myosin at the start of the power stroke. Formation of metastable, yet dynamic, ternary myosin•ADP•P_i state is an unusual feature for an enzyme. The MgADP•V_i complex provides an opportunity to arrest the contractile cycle at a critical point and provides a chance to study this important state.

Vanadate is believed to be a transition state analog for the phosphate in many hydrolysis reactions (Ray et al., 1993; Deng et al., 1993). The orthovanadate ion is a potent inhibitor of many enzymes that catalyze phosphoryl transfer. It is an effective inhibitor in part because it has very similar size and charge to inorganic phosphate, but also, because it readily increases its coordination sphere to five and exhibits considerable plasticity in its bond distances. These structural changes allow this ion to adopt a trigonal bipyramidal coordination that has been proposed to mimic the conformation of the phosphate group at the transition state expected for the phosphoryl transfer

which has been observed in the Magnesium(II)·ADP·Vanadate complex of the dictyostelium discoideum myosin motor domain (Rayment et al., 1993).

Vibrational spectroscopy gives detailed information about the vibrational motions of atoms in molecules. Because these vibrations are sensitive to chemical changes, vibrational spectroscopy is a good tool for studying them. The conformation of a molecule may be probed and the ionization states of its polar groups are easily determined, particularly for small molecules. Also for protein-ligand interactions, like hydrogen bonding which perturb a molecule's electronic distribution, result a modified vibrational force field and vibrational frequency shifts. Thus, the changes observed in the vibrational spectra of a bound ligand are a direct measurement of how a protein acts upon it. Our group has previously succeeded in obtaining the classical Raman spectra of a small molecule bound to a protein by difference spectroscopy technique (Yue et al., 1984; Chen et al., 1987; Callender et al., 1988; Deng et al., 1987). The changes between the spectrum of a ligand bound protein and that of ligand in solution yield much information about the protein-ligand interactions.

The interaction between ras-p21 proteins and guanine nucleotides at the phosphate moiety, as well as the differences between the interactions between wild type and mutant p21 proteins, have previously been studied in our group by Raman spectroscopy (Weng et al., 1994; Xiao, 1995). This work is a continuation of those studies. In parallel to the experiments, ab initio calculations of normal mode frequencies were also performed. These calculations help with the assignments of the observed bands and are also valuable for proposing studies relating measurements of kinetic ^{18}O isotope effects to vibration frequencies. In addition, theoretical and experimental work was performed on solutions of monophosphate, diphosphate (GDP) and triphosphate (GTP). The studies of phosphates in solution are necessary for the

interpretation of the spectra found in the enzyme measurements. We also report here our results on another phosphoryl transfer enzyme, Myosin subfragment-1 (S1). We have used Raman spectroscopy to determine the structure of the vanadate moiety in the S1•MgADP•Vi complex, vanadate in solution, and vanadate bound in S1. A complete vibrational analysis is presented using both the *ab initio* method and the empirical method. The results are compared to those from X-ray crystallographic studies. Implications of our results for the mechanisms of ATP hydrolysis by myosin will also be discussed. In addition, this work will also form a strong basis for interpreting the results of vibrational studies of phosphoryl transfer in further studies of other enzyme systems.

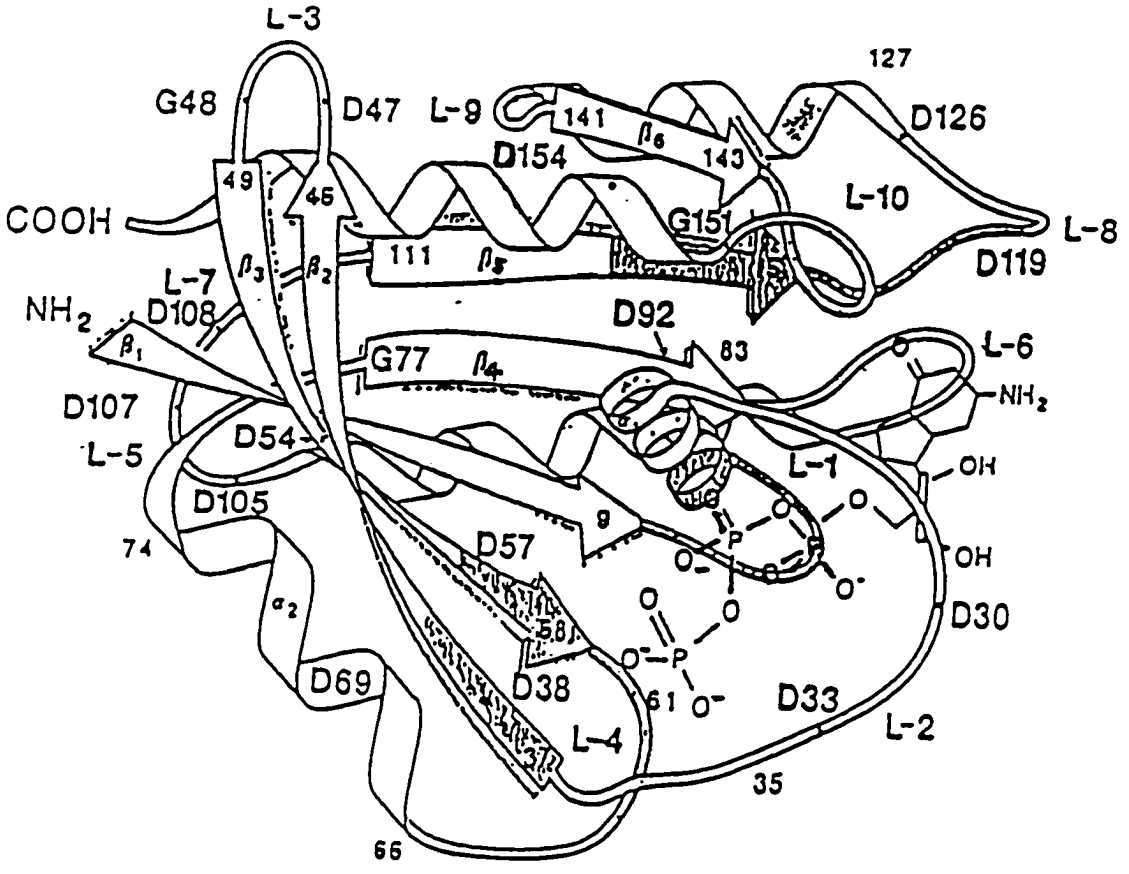

Figure 1.1 Ribbon diagram of truncated human Ha-ras p21 (1-166), showing the positions of several of the markers discussed in the text [adapted from Bourne et al. (1991)].

CHAPTER 2

Raman Difference Spectroscopy

There are several common structural probes. Two of the most powerful, X-ray crystallographic studies and multi-dimensional NMR spectroscopy, provide coordinates for each atom that makes up the enzyme and enzyme-substrate complex. From this, it is often possible to surmise qualitatively the types of interactions present in the complex and to make educated guesses as to the catalytic pathway. However, these probes do not characterize the electronic distributions between atoms and bonds, and these distributions are keys to understanding the bond breaking/bond making steps in catalysis. For example, vibrational spectra are affected by hydrogen bonding which perturbs a molecule's electronic distribution, and results in a modified vibrational force field and vibrational frequency shifts. It is thus evident that vibrational spectroscopy, which is sensitive to the electronic distributions between atoms as well as to geometry of the bonds and the masses of the bonded atoms would be useful as a complementary structural probe. The changes observed in the vibrational spectrum of a bond ligand are a direct measure of how a protein acts upon it.

2.1 Raman Scattering

In ordinary Raman scattering, we are concerned with the two-photon-process whereby photon (k_1,υ_1) is absorbed, photon (k_2,υ_2) is created, and the molecule undergoes a transition from state $|k\rangle$ to state $|m\rangle$. Energy conservation requires that $h(\upsilon_1-\upsilon_2)=E_m-E_k$. Figure 2.1 shows some of the possible consequences of photon-molecule interactions, in which the upward-pointing arrows indicate a photon absorbed and the downward-pointing arrows

indicate the release of a photon. The states of molecule $|k\rangle$ and $|m\rangle$ both are ground electronic states and the molecule is brought up to a virtual energy state by photon (k_1,υ_1) in the normal Raman scattering process. When $\upsilon_2 = \upsilon_1$, that is called Rayleigh scattering. When $\upsilon_2 < \upsilon_1$, the scattered radiation frequency υ_2 is said to be stokes-shifted from the incident frequency υ_1; anti-stokes-shifted radiation is obtained when $\upsilon_2 > \upsilon_1$ (Struve, 1989). The energy difference $h(\upsilon_2 - \upsilon_1)$ normally matches either a molecular vibrational-rotational or rotational level difference υ_{vib} and the frequency υ_1 is usually some readily generated visible frequency in conventional Raman spectroscopy. In such cases, $|\upsilon_2 - \upsilon_1| / \upsilon_1 << 1$. For the stokes and anti-stokes, the difference comes from the molecular vibrational level at the same ground electronic state. For resonance Raman scattering, the molecule is brought to a real electronic excited state so that intensity of the scattered light is generally enhanced. The pre-resonance Raman scattering is a process between normal and resonance Raman Scattering. Since the intensity of the Stokes line is several orders higher than that of the anti-Stokes line, the feeble anti-Stokes scattering is usually ignored in conventional Raman spectroscopy and only the Stokes spectrum is recorded. The frequencies of Raman peaks are properties solely of the electronic ground state of a molecule, but their intensities are functions of both ground- and excited-state electronic structures.

2.2 Group Frequency

Raman and IR spectroscopies offer the enormous advantage that they permit qualitative identification of compounds by examining their group vibrations: a given group or bond in a molecule will produce spectral features characterizing this group or bond. This is one of the most useful aspects of vibrational spectroscopy. Furthermore, the group frequencies allow for an initial

vibrational assignment, which often determines the quality of the fit of a force field. In order to apply the group frequency concept to a part of a molecule, the motion in a given normal mode must be essentially localized within that group.

Thus group frequencies are of importance to chemists in general for the identification and qualitative interpretation of compounds. However, they are also extremely important to vibrational spectroscopists involved in the calculation of normal modes of vibrations and molecular force fields. A closer inspection of the PED (potential energy distribution), based on group frequencies, isotopic data can give a good vibrational assignment. Group frequencies find their maximum utility when they give intense features, when they occur in a spectral region that is free from the other intense features, and when small variations in the group frequency can be correlated with conformational and environmental changes. The group frequencies have been used with great success to study hydrogen bonding interactions. For example, the protein amide I band (C=O stretch) in the region between 1600~1700 cm^{-1}, and amide III band (peptide N-H bending) in the region 1200~1300 cm^{-1} are correlated to the secondary structure of the peptide backbone (Carey, 1982; Tu, 1982).

2.3 Instrumentation

Figure 2.2 shows the typical instrumental set-up of our Raman experiment. A laser beam is introduced through the sample. The scattered light is collected at 90° and focused on the entrance slit of a monochromator. The gratings in the monochromator disperse the incoming light into a spectrum of frequencies. This spectrum is transformed into an electronic signal by a detector, and then sent to a computer for analysis.

The laser sources available in our laboratory are a 4-Watt argon ion laser from Spectra Physics (Model 165), a 5-Watt krypton ion laser (Model INNOVA 400) and a 10-Watt argon ion laser (Model INNOVA 200, Coherent Radiation Inc.). The sample holder can hold a double or a triple split cuvette specially designed for measuring several spectra under the same conditions, and each sample space of the split cell has a dimension of 2.5mmx2.5mm. The cuvette is set on a computer-controlled stage which can be moved to within 1μm accuracy. Raman spectra are measured by a Triplemate spectrometer (Spex Industries), equipped with a solid state detector system (Model DIDA-100 water cooled photodiode array and a model ST-100 detector controller; Princeton Instruments), or a charge coupled device (CCD) system (CCD model LN/CCD-1152UV liquid nitrogen cooled and a model ST-135 detector controller; Princeton Instruments). Data are acquired, stored, and analyzed on a Macintosh computer (Apple, Cupertino Ca). Spectral lines are calibrated against known Raman lines of toluene and are accurate to within $\pm 2 cm^{-1}$. The resolution of the instruments is typically set to 6 cm^{-1} full width at half maximum.

2.4 Raman Difference Technigues

Despite the obvious value of Raman spectroscopy, its use has been greatly hampered because of spectral crowding. Many vibrational modes contribute to the spectrum of a protein at each frequency, and this results in a spectrum which is very difficult to interpret. Our laboratory developed a difference Raman spectroscopy technique which makes vibrational spectroscopy of proteins practical. Isotope labeling obviates the problems associated with band identification.

To study protein-ligand interactions, we intend to measure the Raman spectra of bound ligands or other small protein molecular moieties. However,

the signals coming from the ligands are generally overwhelmed by background vibrational bands from the protein itself. Difference Raman spectroscopy can overcome this difficulty (Yue et al., 1984; Chen et al., 1987). The operator can be represented by:

$$\text{Spectrum(Enzyme}\bullet\text{L) - Spectrum(Enzyme)} = \text{Spectrum(L bound in Enzyme)+Spectrum(protein change)} \quad (2.1)$$

Where L represents a cofactor, inhibitor or substrate of the enzyme.

This procedure may not be suitable for the studies of the interaction between protein and ligand for the phosphate moieties of GDP and GTP because the signal from phosphate is the same order as that from protein change. An alternative route that can get the difference spectra of these protein-ligand complexes is represented by:

$$\text{Spectrum(Protein}\bullet\text{L)-Spectrum(Protein}\bullet\text{L}^*\text{)} = \text{Spectrum(L - L}^*\text{ bound in protein)} \quad (2.2)$$

where L^* is isotopically labeled L at certain positions.

There are no protein changes caused by isotope editing because L and L^* have same chemical properties.

To get accurate difference spectra and to avoid artifacts, a split cell is used to measure several samples (Figure 2.2). The temperature and humidity in the room, where the measurements are taken, are kept nearly constant. Arrangements like these are made to reduce the influences of different optical

properties for the different samples, and to control the environmental fluctuations which may affect accuracy of forming the difference spectrum. The long term drift of the optical system can be canceled out if the spectra are taken in a sequential way and the spectra are lined up before adding them. A detailed procedure of the alignment is described as follows: assume sample A is a stable protein-ligand complex, sample B is another stable protein-ligand complex different from A. The spectra of A and B are measured in a $A_1B_1A_2B_2....A_nB_n$ fashion, with each run taking 10 to 20 minutes. The sets of data are then checked by the subtraction A_n-A_{n-1}, A_n-A_{n-2}, ...,A_n-A_1 and B_n-B_{n-1}, B_n-B_{n-2},... B_n-B_1. Every subtraction should give a flat featureless background. If the difference spectrum shows features of a derivative-like band for narrow mark bands which are invariant between two spectra, the subtracted spectrum could be shifted first and then subtracted. The amount of the shifting, usually 0.01 to 0.8 $cm^{-1,}$ is determined by the disappearance of the derivative peaks in the difference spectra. Assume I(u) is the Raman intensity of a spectrum, δ is a small shift, then the amount of the shift is

$$\Delta I(\nu) = \frac{\partial I(\nu)}{\partial \nu}\delta \tag{2.3}$$

If a band is Gaussian with intensity at center I(0) and the full width at half-maximum Γ, we find that

$$\Delta I_{max} / I(0) = 1.4\delta / \Gamma \tag{2.4}$$

therefore, the amount of shift is

$$\delta = \Gamma \Delta I_{max} / (1.4 I(0)) \tag{2.5}$$

The relative factor for a Lorentzian band should be 1.9 instead of 1.4. If the spectroscopic features can not be corrected by shifting, the corresponding spectrum should be discarded. All the spectra taken from the same sample are then added together as A and B. To get the difference spectrum, B is subtracted

from A. The disappearance of protein characteristic bands, i.e. amide I band at 1600~1700 cm^{-1} region, methylene band around 1450 cm^{-1} , amide III band at 1200~1300 cm^{-1} region and phenylanaline as round 1000 cm^{-1} should be taken as the criteria of the extent of the subtraction.

For the ras-p21 proteins studied here, the intensity of the largest nucleotide peak is about 6% of that of the protein amide I peak. With careful measurement, intensity differences as little as 0.1% of the most intense Raman bands can be detected by our experimental system.

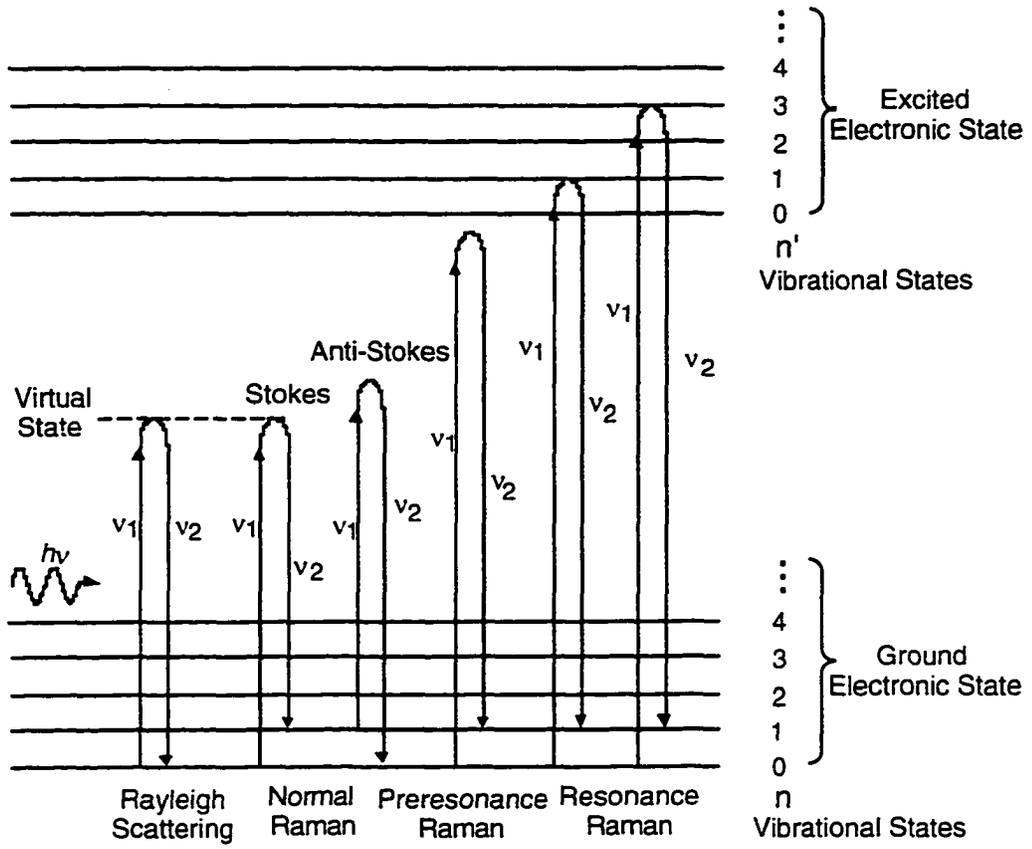

Figure 2.1 The energy diagram of photon-molecule interactions. In Rayleigh scattering, the molecule absorbs a photon with an energy υ_1 and creates a photon with an energy $\upsilon_2=\upsilon_1$; in normal Raman (NR), the molecule is elevated to a virtual state by a photon and then releases another photon with an energy difference $\nu_{vib}=\upsilon_2-\upsilon_1$ (Raman shift); in resonance Raman (RR), the molecule is elevated to a electronic excited state by a photon and then releases another photon with an energy difference ν_{vib}, and the band intensities are usually orders of magnitude greater.

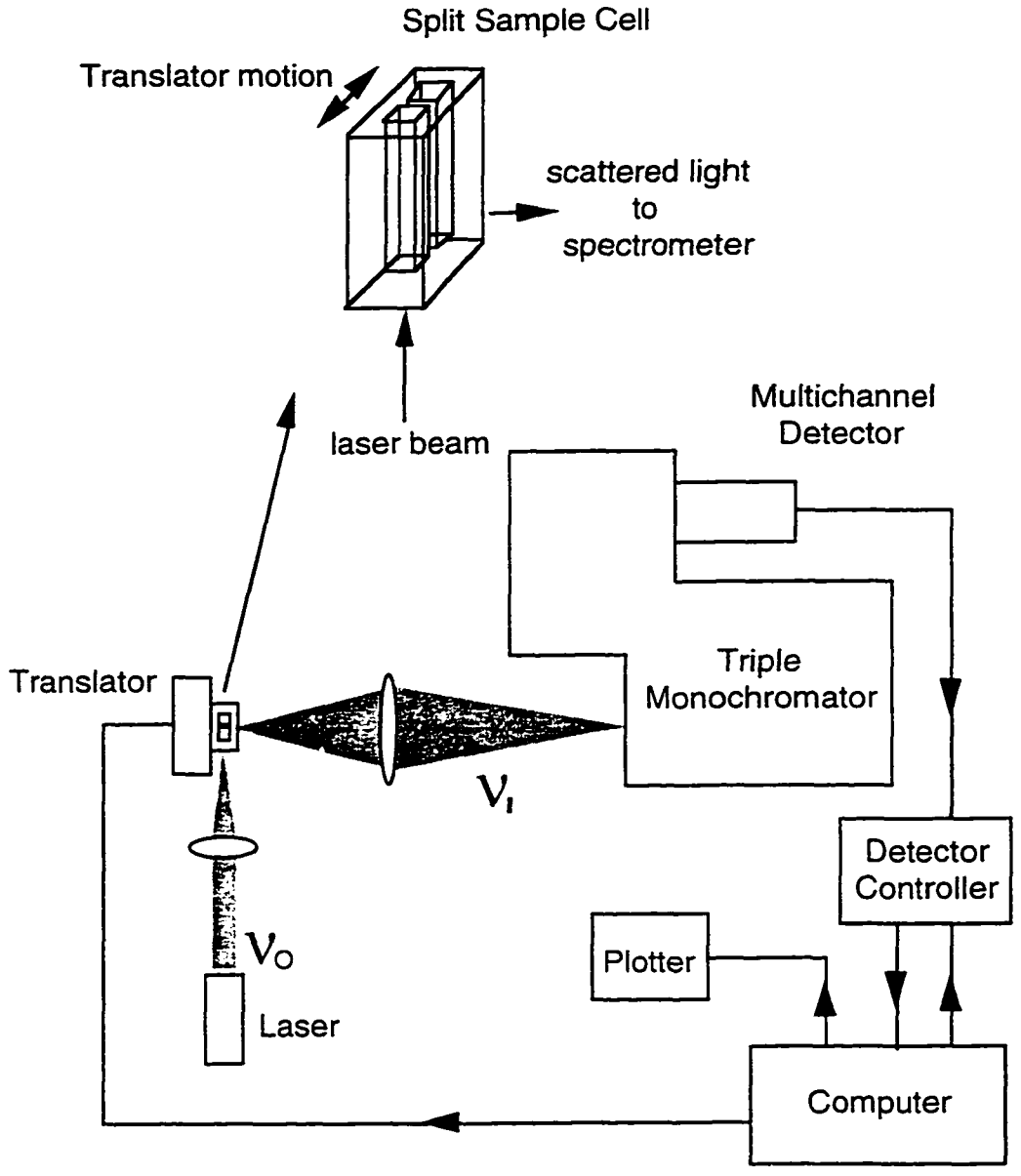

Figure 2.2 A scheme for the Raman measurement setup. The monochromatic light emitted from a laser source is introduced through the sample. The scattered light is focused on the entrance slid of a triplemate monochromator. The spectrometer disperses the incident light into a spectrum and focuses it on to a detector. The spectrum is converted into electrical signals by a charge coupled device (CCD), and then transferred to a Apple computer for analysis.

CHAPTER 3

Normal Mode Analysis

Normal modes analysis can be used to quantitatively study protein-ligand interaction. There are two typical methods: empirical method and ab initio method. The empirical method treats molecules classically as coupled harmonic oscillators consisting of point masses connected by springs with a defined equilibrium geometry. The normal modes are the solutions of the equations of motion of the given system. The ab initio method treats molecular interactions at the quantum level. The observed physical quantities are interpreted as the expectation value of the operator over the wavefunctions ($\langle k | \hat{A} | k \rangle$).

3.1 Classical Normal Mode Analysis

In the calculations, the atoms in a molecule are assumed to oscillate about their equilibrium position on a harmonic potential surface. For nonlinear (linear) molecules, there exits 3N-6 (3N-5) vibrational modes, which are associated with the 3N-6 (3N-5) fundamental vibrational transitions accessible via infrared and Raman spectroscopies.

3.1.1 Internal coordinate and symmetry coordinate

The principles of the computations appear very straightforward: set up the potential energy matrix in Cartesian or mass-weighted Cartesian coordinates and then use standard diagonalizing methods to get the energy eigenvalues of this matrix. However, the difficulty comes from setting up the potential energy matrix in order to calculate 3N-6 vibrational frequencies. A 3Nx3N potential energy matrix, which requires $3N(3N+1)/2$ force constants, needs to be defined. Thus, for a simple molecule such as water, there are six Cartesian force

constants and only three vibrational frequencies, so there are too many independent force constants. Furthermore, if in another computation the molecule is oriented differently in the coordinate system, all force constants may be different. Therefore, chemists prefer to choose some coordinates with "chemical meaning": in terms of an angle deformed or bond stretch. These coordinates are known as "internal coordinates" in which the potential energy is expressed in terms of significant groupings. The transformation between internal and Cartesian displacement coordinates is given by the **B** matrix in many textbooks (Wilson et al., 1955; Diem, 1993):

$$\mathrm{R}=\mathbf{B}\,\mathrm{x} \tag{3.1}$$

Symmetry coordinates, which are defined as linear combinations of certain internal coordinates, can be used to significantly reduce the size of matrices by breaking an overall energy matrix into smaller independent submatrices. This greatly simplifies the calculation of the eigenvalues.

3.1.2 GF method

The potential energy, V, can be expressed in internal coordinates or cartesian coordinates. The potential energy of molecule can be expanded in a Taylor series about the equilibrium geometry in terms of the internal coordinates, R, or the Cartesian coordinates, x.

$$\begin{aligned} 2V &= R^T FR \\ &= x^T B^T FBx \end{aligned} \tag{3.2}$$

where

$$F_{ij} = \frac{\partial^2 V}{\partial R_i R_j}$$

Therefore, in the cartesian coordinate system

$$F_x = B^T F B \tag{3.3}$$

The kinetic energy, T, may be written in terms of internal coordinates

$$\begin{aligned} 2T &= \dot{x}^T M \dot{x} = \dot{R}^R B^T M B R \\ &= \dot{R}^T G^{-1} \dot{R} \end{aligned} \tag{3.4}$$

where, M is the mass matrix and

$$G^{-1} = B^T M B \tag{3.5}$$

The vibrational problem leads to a secular equation

$$\det | \, GF - E \, | = 0 \tag{3.6}$$

This is the famous "GF matrix method".

3.1.3 Raman Intensity and depolarization ratio

The basic theory of Raman scattering was developed by Placzek in 1934. The Raman intensity Igm->gn for the transition from the vibrational state gm to the vibrational state gn, both in the ground electronic state g, is proportional to the square of the corresponding term in the polarizability tensor and is given by

$$I_{gm->gn} \propto I_0 \nu^4 \sum_{\sigma\rho} |(\alpha_{\sigma\rho})_{mn}|^2 \tag{3.7}$$

where

$$(\alpha_{\sigma\rho})_{mn} = \sum_k \frac{< n|\mu_\rho|k >< k|\mu_\sigma|m >}{\nu_{mk} - \nu_0 + i\Gamma_k} + \frac{< n|\mu_\sigma|k >< k|\mu_\rho|m >}{\nu_{nk} + \nu_0 + i\Gamma_k} \tag{3.8}$$

The I_0, ν are the intensity and frequency of incident light, repectively; $(\alpha_{\sigma\rho})_{mn}$ is the component of the polarizability tensor; μ is the induced dipole ($\mu = \alpha\varepsilon$); ε is the electric vector of incident light.

To distingish the Raman bands, the depolarization ratio has been proved to be very useful. The depolarization ratio is defined as the ratio of the scattered intensity which is polarized perpendicular to ε, that is, in the direction of the propagation of the incident light, to the intensity parallel to ε . For linear polarized incident light, the depolarized ratio of intensities is given by (Wilson et al. 1955, Page 46)

$$\rho_l = \frac{3\beta^2}{45\alpha^2 + 4\beta^2} \tag{3.9}$$

where

$$\alpha = \frac{1}{3}(\alpha_1 + \alpha_2 + \alpha_3)$$

$$\beta^2 = \frac{1}{2}[(\alpha_1 - \alpha_2)^2 + (\alpha_2 - \alpha_3)^2 + (\alpha_3 - \alpha_1)^2] \tag{3.10}$$

3.2 Ab initio

Over the last 30 years, scientists developed several very sophisticated software packages for ab initio molecular electronic structure calculations, such as, Gaussian and Gamess. They are based on quantum theory and can be used to calculate molecular geometry, force fields and molecular properties such as electronic dipole polarizability and magnetizability which measure the response of a molecule to an external electric field, and have the ability to deal with the electron correlation.

The crucial task in quantum theory is to solve the Schrodinger equation

$$H\Psi = E\Psi \tag{3.11}$$

Unfortunately, it is difficult to solve this equation rigorously in most cases. In ab initio calculation, several alternative methods are used to solve the equation: Here three typical methods are introduced: variation principle, perturbation theory and self-consistent field theory. The details can be found in most quantum mechanics textbooks.

3.2.1 Variation principle

Born and Oppenheimer (1927) showed that, to a very good approximation, the motions of the nuclei and the electrons can be considered separately. Unfortunately, the complexity of electron interactions still makes the problem very difficult to solve. An elegant approach is afforded by the variation principle

$$E = \int \psi^{*} \hat{H} \psi d\tau \,/\, \int |\psi|^{2} d\tau \tag{3.12}$$

In the general case, however, we will never be able to solve the eigenvalue equation exactly, so our approximate wavefuction will never satisfy $H\Psi = E\Psi$. It turns out that for any approximate wavefunction Ψ_a with the correct boundary conditions, if we calculate

$$\tilde{E} = \int \psi_a^{*} \hat{H} \psi_a d\tau \,/\, \int |\psi_a|^{2} d\tau \tag{3.13}$$

The variation principle guarantees that the energy calculated from the equation will always be higher than the 'true' energy, and this gives a criterion for the accuracy of the guess. This result is proved in many quantum mechanics

textbooks, and relies on the fact that the approximate wavefunction Ψ_a can be expressed in terms of the exact eigenfunctions Ψ_k as

$$\psi_a = \sum C_k \psi_k \tag{3.14}$$

where $H\Psi_k = E_k\Psi_k$.

3.2.2 Perturbation theory

Perturbation theory is another powerful method. We can rewrite the Himiltonian as

$$H = H_0 + H^{(1)} + H^{(2)} + \cdots \tag{3.15}$$

Thus if $H_0\ \Psi_k^{(0)} = E_k^0\ \Psi_k^{(0)}$, it is easy to derive

$$E_k = E_k^{(0)} + E_k^{(1)} + E_k^{(2)} + \ldots \tag{3.16}$$

where

$$E_k^{(1)} = \int \psi_k^{(0)} \hat{H}^{(1)} \psi_k^{(0)} d\tau$$
$$E_k^{(2)} = \sum_{m \neq k} \frac{\{\int \psi_k^{(0)} \hat{H}^{(1)} \psi_m^{(0)} d\tau\}^2}{E_m - E_k} \tag{3.17}$$

3.2.3 Self-consistent fields

In 1927, Hatree and Fock proposed the self-consistent field method. The basic physical idea of the SCF method is that each electron moves in an average field due to the nuclei and remaining electrons and so the effect of electron repulsion is formally included. For a 2-electron atom whose electrons are labeled 1 and 2, electron 1 occupies orbital ϕ_1, and corresponds to an electron density -e ϕ_1^2. the potential seen by electron 2 is

$$V = -\frac{Ze^2}{4\pi\varepsilon_0|R-r_2|} + \frac{e^2}{4\pi\varepsilon_0}\int\frac{\phi_1^2(r_1)}{|r_1-r_2|}d\tau_1 \qquad (3.18)$$

and we can write formally one-electron eigenvalue equation for electron 2.

$$\left\{-\frac{\hbar^2}{2m}\nabla_2^2 + V\right\}\phi_2 = E\phi_2 \qquad (3.19)$$

Obviously ϕ_1 should be known to calculate ϕ_2 etc., and some kind of iterative calculation will be necessary in order to calculate ϕ_1 and ϕ_2. Also, the actual form of interaction is much more complicated than given above.

For molecular calculation, Gaussian orbitals, which have an exponential part, exp(-a r^2), are widely used in molecular structure calculations although they have defects. A very large number of Gaussian atomic orbital basis sets are available, and many software packages store a selection internally.

3.2.4 Force fields

As calculations on small molecules show, the ab initio HF method systematically overestimates the diagonal force constants. This is due partly to the neglect of electron correction and partly to the basis set truncation. At the present it seems impractical to improve the wave function to a point where systematic errors would be absent. Therefore, a set of empirical scale factors is introduced according to the scheme (Pulay et al., 1981)

$$F'_{ij} = (x_i x_j)^{1/2} F_{ij} \qquad (3.20)$$

where F'_{ij} is the scaled force constant, F_{ij} is the theoretical one, and x_i, x_j are scale factors for the coordinates i and j, respectively. Usually a number of similar coordinates share a common scale factor. The values of the factors are determined by least-squares fitting to the observed spectra. The factors are expected to be transferable and can be used to reproduce the observed data. We will apply these methods to study phosphoryl transfer enzyme myosin S1 in the following chapters.

There are other empirical scaling schemes in use, which employ a common scale factor for all coupling (off-diagonal) elements of the force field in valence coordinates. It is difficult to see why physically different off-diagonal elements should share the same scale factor, unless one assumes that coupling terms are not very significant in a properly chosen valence coordinate system, and therefore their scaling is unimportant. This argument is not valid, however, in a highly coupled system. For coupling constants which are unusually large, or important because they connect two near-degenerate zeroth-order frequencies, the introduction of separate scale factors are necessary, such as in phosphate case.

CHAPTER 4

Vibrational Studies of Monophosphate and Vanadate

4.1 Bond order, bond length and frequency

Bond order can be expressed in several different ways. Regardless of how it is expressed, there usually is a presumed relationship between bond order and bond strength which, in turn, can be expressed in different ways, e.g., in terms of an equilibrium force constant or a bond dissociation energy. In the present context we use valence bond order, s, defined in terms of bond lengths so that Σs for all chemical bonds to a given atom are equal to its formal valence (Brown, 1992).

Since "valence electrons" are the primary determinants of chemical bonds, a variety of relationships between valence bond order and bond strength have been proposed, dating to Pauling (Eckstein, 1985). In fact, a linear relationship between valence bond order and υ^2, the square of the stretching frequency of a bond, where stretching frequency is taken as a measure of bond strength, was proposed shortly after Pauling's paradigm appeared (Badger & Bauer, 1937). This υ-s relationship, which is based on the classical concept of a harmonic oscillator, has gained acceptance among spectroscopists because of the accuracy with which $s = c\upsilon^2 + d$, plus a small number of empirical parameters, correlates s and υ for a variety of simple molecules with integral values of s (Gordy, 1946). However, Gordy's original parameter set fails to provide a satisfactory measure of valence bond order for some tetrahedral molecules, especially those that contain multiply bonded atoms that are best described as resonance hybrids, e.g. phosphates and vanadates.

Bond length, r, also is a measure of bond order (subsequently we drop the adjective, valence) although s-r relationships tend to be entirely empirical. The

s-r relationship developed by Brown and associates (Brown & Wu, 1976; Gilman, 1987) eq 4.1 , holds for a much wider variety of bonds than Gordy-type s-υ

$$s = (r/r_1)^{-p} \qquad (4.1)$$

relationships. In fact, eq 4.1 can be applied to bonds with a nonintegral bond order in asymmetric environments, i.e., the relationship is independent of bond angles. The parameters r_1 and p of eq 4.1 have been assigned on the basis of extensive compilations of atomic distances obtained via crystallography, and unique values are available for most elements more electropositive than oxygen. These assignments were made by treating a crystal as a continuous network such that Σs for each atom in the network is as close as possible to its valence or formal oxidation state. Hence, s is expressed in "valence units", vu, and specifies the average number of electron pairs that participate in a bond. This approach is particularly useful for describing the bonds within molecules that can be considered as resonance hybrids.

Later Hardcastle and Wachs (Hardcastle & Wachs, 1991) showed that the vibrational frequency of a bond between two given atoms, e.g., a V••O bond, also can be related to bond length, r, within a series of compounds containing such bonds: eq 4.2,

$$\ln \upsilon = br + c \qquad (4.2)$$

where υ is the vibrational frequency, b and c are empirical parameters. They then combined eqs 4.1 and 4.2 so that the stretching frequency of a given type of bond could serve as a determinant for nonintegral bond order. The relationship

thus obtained was tested by examining the correlation between stretching frequency and the summed vanadium-oxygen bond order, Σs_{VO}, using 14 different crystalline V(IV) and V(V) vanadium oxides that exhibit a variety of bonding patterns and geometries. The basic assumption in this treatment is that V••O bonds in crystalline vanadium oxides can be treated as independent oscillators and that the frequency of the symmetric stretching mode can be related to bond order. The relationship that provides a reasonable fit for their extensive data set takes the form

$$s=[a \ln (\upsilon_O/\upsilon)]^{-p} \qquad (4.3)$$

where the value of p is the same as in eq 4.1 and thus is the Brown and Wu exponent for a bond between two specified atoms. Both a and υ_O are adjustable parameters that are related to the parameters in equations 4.1 and 4.2. These were adjusted by curve-fitting so that each value of s_{VO} is close to the value calculated via the Brown-Wu relationship on the basis of a direct bond-length measurement. Hence, in this system, stretching frequency can be used as a direct measure of the average number of electron pairs per V••O bond. The same approach also has been used successfully to analyze the bonding within a group of molybdenum oxides (Hardcastle & Wachs, 1991). Later Ray *et al.* (Ray et al., 1993a) applied a variant of this approach to aqueous solutions of natural abundance phosphoric acid and its anions in an attempt to relate bond order to stretching frequency in solution. However, in all these studies, it has been unclear what should be used for frequency, υ in eq. 4.3: the symmetric, υ_s, or the asymmetric, υ_a, stretch of the PO bonds or some specific combination.

The present chapter begins where the study of Ray *et al.* (Ray et al., 1993a) ends and provides a validation of the frequency selection in that paper, plus

other assumptions, as well as a modification of the s-υ equation described therein. To accomplish this, a simple normal mode analysis was used to assess the relative importance of the parameters upon which PO frequencies in phosphates depend. *Ab initio* calculations were used in conjunction with this analysis to check the validity of various approximations which simplify the analytical expressions. This combined approach shows that the symmetric and asymmetric stretching frequencies of phosphates (and related compounds such as vanadates) depend not only on the stretching force constant of the bonds between the central atom and the surrounding oxygens but also on molecular geometry. In addition, it shows that in the case of phosphates (and vanadates) appropriate combinations of the symmetric and asymmetric stretching frequencies can be used to obtain both the stretching force constant and the angular geometry of the PO (or VO) bonds. In fact, the fundamental frequency, υ, defined as below, depends almost entirely on the force constant and thus is indeed the appropriate parameter to be used to develop frequency-bond order relationships. In addition, the symmetric and asymmetric stretching frequencies for the four different P$\underline{\bullet\bullet}$O bonds and three different P-OH bonds in [$^{16}O_4$] and [$^{18}O_4$] phosphoric acid and its three anions were measured in solution under the same conditions by Raman and FT-IR spectroscopy. The derived s-υ relationship from this data is expected to hold quite accurately for P$\underline{\bullet\bullet}$O bonds with differences in bond order at least as large as those encountered in aqueous solutions of phosphates.

Such υ-r relationships can be important in structure-function studies. For example, changes in P-O bond length of phosphates in range of 0.1 Å or less may occur during binding to phosphoryl transfer enzymes. Such changes, due to enzyme-substrate interactions, may be an important aspect of the catalytic power of the enzyme. The present study shows that the stretching frequencies

of phosphates bound to proteins (Callender & Deng, 1994; Deng et al., 1993) can be used to assess changes in the P••O bonding of such compounds that could accompany the binding process with a substantially greater accuracy than by use of diffraction data from such systems.

Some conventions are used in this chapter. PO is used to designate either P••O or P-OH bonds unless a distinction between these is necessary. The fundamental stretching frequency for P••O or P-OH bonds, υ, is an average frequency defined as $\upsilon^2 = (\upsilon_s^2 + n_a\upsilon_a^2)/(n_a+1)$, where υ_s and υ_a are the symmetric and asymmetric modes for these bonds, respectively, and n_a the degeneracy of the asymmetric modes. A superscript 16 or 18 is used when a distinction between bonds in normal and [$^{18}O_4$] phosphates is necessary. PO bond order is designated by s, although sP••O and sP-OH sometimes are used for clarity.

4.2 Theoretical Models

To determine which of the vibrational frequencies of a phosphate, υ_a, υ_s, or υ, is the most appropriate for constructing a bond order-frequency relationship, a vibrational analysis of phosphoric acid and its anions was conducted using the empirical Wilson-FG method. *Ab initio* quantum mechanical methods were employed to validate some of the assumptions used to simplify the derived equations from this method. As is outlined below, the empirical analysis shows that υ, as opposed to υ_s or υ_a, depends almost entirely on the force constant and is largely independent of bond angles when coupling can be ignored. Although the analysis presented here focuses on the non-bridging P••O bonds of phosphoric acid and its anions, a variation of this analysis can be used for the P-OH bonds in these compounds. In addition, the same analysis holds for V_O

bonds in vanadate molecules. The following four sections emphasize the empirical approach; the fifth section describes *ab initio* calculations.

Phosphoric Acid. Since there is only one P••O bond in H_3PO_4, $\upsilon = \upsilon_a = \upsilon_s$. If one can ignore coupling between P••O stretching modes and other vibrational modes that involve P-OH groups (see below) and if the stretching frequency of the P••O bond can be considered as localized (i.e. a strict diatomic oscillator), its frequency is given by the following equation:

$$\upsilon^2 = f_S/\mu \qquad (4.4)$$

where f_S is the stretching force constant for the P••O bond and μ is the reduced mass of the P••O group. For $f_S^{18} \equiv f_S^{16}$, $\upsilon^{16}/\upsilon^{18}$ would equal 1.039. The observed ratio, 1.032 (±0.002) (see below), is consistent with the assumption that the P••O stretching mode is localized to a sufficient extent that motional coupling in H_3PO_4 can be ignored for our purposes.

Monoanionic Phosphate. There are two P••O bonds in $H_2PO_4^-$. The frequencies of their stretching modes can be computed analytically by the Wilson-FG method and simplified considerably if the coupling terms between the P••O stretching modes and the O••P••O bending mode (Bansil et al., 1980) as well as the vibrational interactions with the two -OH groups can be ignored. The unimportance of these interactions for our purposes was verified by vibrational analysis using the *ab initio* methods described below. Thus, according to the Wilson-FG method, the effect of O••P••O bending on P••O stretching can be formulated as in eqs 4.5 and 4.6 if the coupling constant for the two stretching modes is C_{ss}, and the bending force constant and bond angle for the O••P••O group is f_b and θ, respectively. (Note that since $\theta > 90°$ for $H_2PO_4^-$), $\cos\theta < 0$).

$$\upsilon_s^2 = \left\{\left(\frac{1}{\mu}+\frac{\cos\theta}{M_p}\right)\left(f_s+C_{ss}\right)\sqrt{1+\Delta\left(f_s,C_{ss},f_b,\theta\right)}\right\} \qquad (4.5)$$

$$\upsilon_a^2 = \left(\frac{1}{\mu}-\frac{\cos\theta}{M_p}\right)\left(f_s-C_{ss}\right) \qquad (4.6)$$

Here, is the reduced mass of the P••O bond, M_p is the mass of the phosphorus, and & is a function of the bending and stretching force constants, the atomic masses, the P••O bond length, and θ. Subsequent *ab initio* calculations (see below) provide values for the force constants and bond lengths of $H_2PO_4^-$ that are required to evaluate &, which comes to about 0.05 (see below). Hence, for this system the bending of the O••P••O constellation contributes little to the symmetric stretching of the P••O bonds and eq 4.6 may be rewritten as

$$\upsilon_s^2 = \left(\frac{1}{\mu}+\frac{\cos\theta}{M_p}\right)\left(f_s+C_{ss}\right) \qquad (4.7)$$

Another way to validate the accuracy of eqs 4.6 and 4.7 is to assess how systematic changes in the bending force constant affect υ_a and υ_s, again using *ab initio* procedures. As will be seen below, υ_a exhibits virtually no dependence on the bending force constant, in accord with eq 4.6, whereas the symmetric stretching is reduced by only 10 cm^{-1} from 1249 cm^{-1} when f_b is set to zero in these calculations (Table 4.1). Hence, for the present system eqs 4.6 and 4.7 provide sufficiently accurate descriptions of υ_a and υ_s for our purposes.

Alternatively, *ab initio* procedures can be used, together with known values of and M_P plus measured values of υ_a and υ_s, to calculate values for θ and f_s/C_{ss}, about 123° and 10, that seem reasonable. Or, conversely, eqs 4.6 and 4.7 plus reasonable values of the above parameters provide a rationale for the observed υ_a/υ_s ratio (Table 4.4).

Eqs 4.6 and 4.7 also show that both υ_s and υ_a are functions of molecular geometry, and that an altered geometry, i.e., a change in θ, will change these two frequencies *in opposite directions*. However, their average or 'fundamental' frequency, as determined by $\upsilon = [(\upsilon_s^2 + \upsilon_a^2)/2]^{1/2}$, will be essentially independent of geometry if the coupling constant for the two P••O groups, C_{ss}, is much smaller than the force constant for stretching, f_s. In such case, the square of the average or fundamental frequency will approach $f_s/$, i.e., will approach the expression for υ^2 in the case of H_3PO_4 (eq 4.4), where there is only a single P••O bond. Thus, although the stretching force constant f_s is numerically smaller in $H_2PO_4^-$ because the P••O bond strength is lower than in the monoanion, the fundamental frequency of the P••O stretching mode in $H_2PO_4^-$ is primarily a function of the same reduced mass as in H_3PO_4, and the $\upsilon^{16}/\upsilon^{18}$ ratio should be essentially the same for both species. This expectation is consistent with *ab initio* calculations and with experimental observations (see below).

Dianionic Phosphate. The Wilson-FG equations for the P••O stretching modes in dianionic phosphoric acid HPO_4^{2-}, which contains three P••O bonds, are similar to those above. *Ab initio* calculations again show that f_b exerts a small influence on the stretching frequencies. Setting $f_b = 0$ simplifies the equation enormously. The following expressions thus are obtained for υ_s and the doubly degenerate υ_a of a $-PO_3^{2-}$ group with symmetry C_{3v} symmetry (HPO_4^{2-}), or C_{3d} symmetry (PO_3^-).

$$\upsilon_s^2 = \left(\frac{1}{\mu} + 2\frac{\cos\theta}{M_p}\right)\left(f_S + 2C_{ss}\right) \qquad (4.8)$$

$$\upsilon_a^2 = \left(\frac{1}{\mu} - \frac{\cos\theta}{M_p}\right)\left(f_S - C_{ss}\right) \qquad (4.9)$$

The expression for υ_a (eq 4.9) is the same as that for the monoanion (eq 4.6), whereas the contribution of the angle-dependent term to υ_S (eq 4.8) is increased by a factor of two compared with that in monoanion (eq 4.7). Hence, υ_S likely is more sensitive to a geometrical change in the PO_3 moiety than is υ_a. However, the average P••O stretching frequency υ, given by $\upsilon = [(\upsilon_s^2 + 2\upsilon_a^2)/3]^{1/2}$, is much less dependent on geometry than υ_S, and υ^2 will approach $f_S/$ in the limiting case when $f_S >> C_{SS}$. As in the case for phosphate monoanion, the ratio of f_S/C_{SS} can be estimated from equations 4.8 and 4.9 using the observed values of υ_S and υ_a (Table 4.3) and the bond angle θ calculated by *ab initio* methods. Here θ is about 110°, which yields a f_S/C_{SS} ratio of about 15. Since in this case $\upsilon^2 = \frac{f_S}{\mu}\left(1 + 2\cos\theta\frac{C_{ss}}{f_S}\frac{\mu}{M_p}\right)$, the effect on υ^2 produced by the increased degeneracy of the asymmetrical mode, relative to that for $H_2PO_4^-$, is largely compensated by a larger f_S/C_{SS} ratio and a smaller value of $|\cos\theta|$.

Trianionic Phosphate. A treatment for tetrahedral PO_4^{3-} similar to that for OPO_4^{2-} yields the following expression for υ_S and triply degenerate υ_a:

$$\upsilon_s^2 = \left(\frac{1}{\mu} + 3\frac{\cos\theta}{M_p}\right)\left(f_S + 3C_{ss}\right) \qquad (4.10)$$

$$\upsilon_a^2 = \left(\frac{1}{\mu} - \frac{\cos\theta}{M_p}\right)\left(f_s - C_{ss}\right) \qquad (4.11)$$

Although the angle, θ, between each O••P••O constellation is the same for a molecule with perfect T_d symmetry, most of the geometric dependence of the stretching modes will be eliminated in the fundamental stretching mode, defined by $\upsilon = [(\upsilon_s^2 + 3\upsilon_a^2)/4]^{1/2}$, even for PO_4^{3-} with imperfect T_d symmetry. As above, υ^2 will approach f_s/ if $f_s >> C_{ss}$, but an even larger f_s/C_{ss} ratio is required. The f_s/C_{ss} ratio estimated by equation 4.10 and 4.11 using the observed values υ_s and υ_a (Table 4.3) is about 12, i.e., somewhat smaller than for HPO_4^{2-}. This means that eq 4.4 may not apply as well to PO_4^{3-} as to the other phosphates. However, in constructing a υ-s relationship (see below) PO_4^{3-} remains a choice reference molecule because its P••O bond order not only is unusually low (and thus is an appropriate reference for low-frequency P••O bonds) but its P••O bond order is defined by its structure.

Ab initio vibrational analysis of the P••O stretching modes of phosphoric acid and its anions. Ab initio frequency calculations were performed on phosphoric acid and its three anions, as well as on metaphosphate (PO_3^-) to evaluate the contribution of O••P••O bending modes and P-OH stretching modes to the frequencies of P••O stretching modes. Such calculations also were used to determine whether the $\upsilon^{16}/\upsilon^{18}$ ratio for the various P••O bonds can be considered as a constant and thus to assess how extensively the normal stretching mode is localized. The results of the calculations at HF/3-21g* level are shown in Tables 4.1 and 4.2 for phosphate molecules and Table 4.3 for vanadate molecules.

The calculated values of υ_s and υ_a for P••O stretching modes are about 20% higher than the corresponding experimental values for phosphoric acid and

its anions (see below). This difference arises partly because frequency calculations at the HF level overestimate the stretching force constant and partly because calculations are performed on isolated molecules, whereas the experimental values are influenced by the interactions between P••O bonds and water molecules. However, these differences do not affect our inquiry about the validity of using the simple relationship between the fundamental frequency and the force constant for the P••O stretching mode, eq 4.4, concerning the possible coupling among stretching and bending modes.

The data in Table 4.1 indicate that the dependence of the P••O stretching modes on O••P••O bending and P-OH stretching motions in a series of phosphates is quite small, as reflected by the small effect on the P••O stretching mode frequencies when the relevant force constants are set to zero. When the bending force constant is set equal to zero, the fundamental P••O stretching frequency changes only by 0.1-2% within this series. Similarly, when the force constant for P-OH stretching is set to zero, the frequency of the P••O stretching mode changes by no more than 1.5%. Thus, ignoring the force constants for O••P••O bending and P-OH stretching in the analytical analysis of the phosphate P••O stretching normal modes is justified. Our results also indicate that while P-OH stretching modes also are reasonably well behaved i.e., not particularly influenced by HO-P-OH and O••P••O bending modes, they are somewhat more sensitive to P••O stretching modes. Thus, for comparison, when the force constants for the P-OH stretching modes are set to 0, the average frequency of the P••O stretching modes shifts to lower frequencies by less than 5 cm^{-1} for mono and dianionic phosphate although the shift is about 16 cm^{-1} for phosphoric acid; in contrast, when the force constants for the P••O stretching modes are set to 0, P-OH stretching frequencies shift to higher frequencies for phosphoric acid and its anions by 20 cm^{-1} or more (Table 4.1).

Table 4.2 lists the P••O stretching frequencies of a series of phosphates and their ^{18}O labeled counterparts calculated as above. Also shown in Table 4.2 are calculated values for the $\upsilon^{16}/\upsilon^{18}$ ratios for these phosphates. These ratios range from 1.032 to 1.038 and thus are close to the uncoupled value, i.e., the value expected on the basis eq 4.4 (1.039). Interestingly, the ratios calculated by *ab initio* methods are intermediate between the uncoupled and observed values (see below). Even for metaphosphate, the calculated ratio is 1.038, which is within about 0.4% of the average value calculated for the other phosphate compounds.

Table 4.3 shows similarly for vanadates that the dependencies of the V_O stretching modes on the O••V••O bending and V-OH stretches are small, varying the fundamental frequency by only 0.5-3.0 % when they are set to zero. Thus the simplifications made in the analytical analysis of the P••O stretch normal modes of for phosphates hold equally well for vanadates. The *ab initio* calculations show that the $\upsilon^{16}/\upsilon^{18}$ ratio is 1.044 for H_3VO_4, 1.043 for $H_2VO_4^-$, 1.042 for HVO_4^{2-}, 1.043 for VO_4^{3-}. The value calculated for a VO diatomic oscillator is 1.045. Thus, like the phosphate results, the fundamental frequency associated with vanadate molecules behaves quite well as an isolated oscillator. All these results show, interestingly, that the relatively large difference between υ_s and υ_a for the phosphates versus the relatively small difference for vanadates arises mostly from the different angles between the nonbridging bonds of the vanadate and phosphate, and from the different masses of vanadium and phosphorus.

4.3 A Bond order/stretching frequency empirical corrrelation

Values of υ_s, υ_a, and υ for the P••O bonds in aqueous solutions of $[^{16}O_4]$- and $[^{18}O_4]$ phosphoric acid and the various anions of both are recorded in Table

4.4. The symmetric stretching modes are well defined, but asymmetric modes are rather broad and exhibit somewhat different values in Raman and IR spectra. Hence, the values in Table 4.3, some of which differ slightly from previously reported values, are the average of several measurements. The last column of Table 4.3 gives the measured value of the fundamental frequency ratio, $\upsilon^{16}/\upsilon^{18}$, for the different P••O bonds in the data base. The standard deviation of the individual values, 0.002, from the average value of this ratio, 1.032, is that expected if the ratio were constant, throughout, and error for a given frequency is 2 cm^{-1}.

In an earlier study, (Ray et al., 1993a) a correlation between bond order and PO stretching frequencies for phosphates in aqueous solution was formulated by defining bond order so that Σs_{PO} for the four PO bonds of phosphoric acid and its anions is 5 and assuming that when s=1 the stretching frequency of P-OH and P••O groups is the same i.e., that the parameters a and b in eq 4.3 are the same for P-OH and P••O groups. (In that study (valence) bond order was referred to as bond strength.) However, the current study shows that P-OH and P••O stretching frequencies should not be combined in constructing a bond order/frequency correlation. Not only is the frequency of P-OH stretching modes more sensitive to motional coupling with P••O and other P-OH groups than that of the P••O stretching mode, the effect of coupling on P••O and P-OH stretching modes is *opposite* (Table 4.1). Thus, at least small differences can be expected between the apparent force constants for P••O and P-OH bonds at s=1 when f_S is calculated via eq 4.4 , and these differences should be reflected by differences in parameters a and b in eq 4.3.

Therefore, the previously determined a and b parameters, eq 4.3, (eq 4 in Ray et al., 1993a) are modified herein. This modification involves using only P••O bonds to evaluate parameters. Since there are only a limited number of

compounds where both the structure and the P••O stretching frequency have been determined, only two reference compounds seemed appropriate for use in this process. These represent extremes for a structure-frequency relationship involving phosphates. One is the phosphate trianion, with a low stretching frequency (Table 4.3), and a defined bond order, 1.25 vu; the other is F_3PO, with short P••O bonds (1.436 Å, Bishop et al., 1981) and the highest known P••O stretching frequency (1415 cm^{-1} Tran-Dinh et al., 1975). Using eq 4.1 with r_1 = 1.62 Å and p = 4.29, the P••O bond order in F_3PO is calculated as 1.68 vu. Eq 4.3 thus becomes:

$$s_{P\underline{\bullet\bullet}O} = [0.175 \ln(224.500 / \upsilon^{16}_{P\underline{\bullet\bullet}O})]^{-4.29} \qquad (4.13)$$

The P••O bond order for several phosphates, calculated according to eq 4.13, is listed in Table 4.5 and compared with that calculated previously (using eq 4 in Ray et al., 1993a). The differences actually are quite small, but would become significant if an extrapolation to substantially larger or smaller bond orders was used. Also listed in Table 4.5 are P••O bond lengths for the same phosphates calculated from sP••O by using eq 4.1 with r_1 = 1.62 Å and p = 4.29 (Brown & Wu, 1976).

The P••O bond lengths in crystalline disodium methylphosphate are 1.512, 1.512, 1.514 Å, (Klooster, 1992) in excellent agreement with the length determined from vibrational data (entry 7, Table 4.5; difference = 0.002 Å). Similarly, the reported P••O stretching frequency of triphenylphosphine oxide (1190 cm^{-1}, Aldrich Library of FT-IR spectra), yields a P••O bond length of 1.486 Å, also in good agreement, difference = 0.004 Å, with the reported P••O bond length of 1.482 Å determined by X-ray crystallography (Lariucci, 1986).

The bridging P-OH or P-OR bond order in an anion of phosphoric acid or a phosphate ester, or the bond-order sum, can be estimated by using the P••O stretching frequency to estimate sP••O (eq 4.13) and subtracting sP••O from 5.0 vu, the sum defined by the approach used herein. (When eq 4.13 is used to calculate $s_{P\text{-}OH}$ or $s_{P\text{-}OR}$ the results are about 5% too high or 5% too low, respectively.)

As discussed in previous sections for isolated bonds, the ratio $\upsilon^{16}/\upsilon^{18}$ should be a constant at 1.039. Although both the calculated and measured values of this ratio are somewhat lower, about 1.033 and 1.032, respectively (Tables 4.2 and 4.3), if this difference is ignored, a correlation between the bond order and P••O stretching frequencies from ^{18}O labeled phosphate can be derived by substituting $1.032\upsilon^{18}$ for υ^{16} in eq 4.13. However, although $\upsilon^{16}/\upsilon^{18}$ = 1.032 is a reasonable approximation for 1.039, there appears to be a slight trend in the data of Table 4.4; this ratio seems to decrease in the series from phosphate trianion to phosphoric acid. Thus, parameter a in eq 4.3 for υ^{16} may differ slightly from that for υ^{18}. One the other hand, Figure 4.1 shows a plot of $\ln \upsilon^{18}$ against $\ln \upsilon^{16}$ plus the least squares line calculated for these data points:

$$\ln \upsilon^{18} = 1.0195 \ln \upsilon^{16} - 0.1647$$

When this result is used, the bond order-frequency correlation for the ^{18}O labeled phosphate is given by the following equation.

$$s^{18}_{P\underline{\bullet\bullet}O} = [0.1717 \ln(241{,}360 / \upsilon^{18}_{P\underline{\bullet\bullet}O})]^{-4.29} \qquad (4.14)$$

According to the data in Table 4.4, as P••O bond order decreases within the series, $(HO)_3PO$ to $HOPO_3^{2-}$, P-OH bond order increases, as it must if $\Sigma s_{PO} = 5.0$

vu. In other words, a change in the bonding of one PO group in the PO_4 moiety is compensated by opposite changes in the bonding of the other three PO groups. This conclusion, together with the observation that $\upsilon^{16}/\upsilon^{18}$ is essentially constant within the above series i.e., that $\upsilon^{16}\text{-}\upsilon^{18} \approx 0.032\upsilon^{16}$, provides an insight into the origin of the $[^{18}O_4]$ equilibrium isotope effect (EIE) that accompanies the successive protonation of the oxygens of PO_4^{3-} (Knight et al., 1986). Thus, the binding of a proton to PO_4^{3-} produces a decrease in the bond order of one P••O group and a corresponding increase in s_{PO} for the other three PO bonds. To the extent that zero point energy (ZPE) differences, which are related to $\upsilon^{16}\text{-}\upsilon^{18}$, dominate the expression for the $[^{18}O_4]$ equilibrium isotope effect (EIE) on proton binding (Cook, 1991), altered PO bonding should make only a minor contribution to this isotope effect. Thus, weakening of the P••O bond that is protonated (decreased P••O bond order) should produce a direct EIE, whereas the strengthening of the remaining P••O bonds (increased P••O bond order) should produce an inverse EIE that largely compensates the direct EIE. In fact, the net ZPE difference calculated by use of eqs 4.13 and 4.14, < 1 cm^{-1}, would contribute a factor of only 0.001 to the EIE. The small size of the calculated contribution relative to the observed EIE, 0.019 (Knight et al., 1986) suggests that the observed effect is produced by differences in ^{16}O-H and ^{18}O-H stretching modes.

In conclusion, the present study shows that the square of the fundamental frequency, υ, of the P••O bonds in phosphates (or the V_O bonds in vanadates) is proportional to the force constant for these bonds and is relatively insensitive to the angle between them. The fundamental frequency also is quite insensitive to coupling with other normal modes. Thus, υ is the appropriate parameter to employ in attempting to formulate bond frequency/bond order relationships. By employing the Hardcastle and Wachs (Hardcastle & Wachs,

1991) form of the bond frequency/bond order relationship that was validated earlier for vanadates together with an exponential parameter relating bond order to bond length for phosphate (Brown, 1992; Gilman, 1987), a bond order-bond frequency relationship was derived for $[^{16}O_4]$- and $[^{18}O_4]$-phosphates (eqs 4.13 and 4.14, respectively). With these relationships and Brown's bond order-bond length relationship (eq 4.1) bond lengths and bond orders can be derived from P••O vibrational frequencies. The error in these relationships is estimated as about 0.04 vu, or about 0.004 Å, as judged by comparisons of derived bond lengths of P••O bonds from frequency data to the results from small molecule crystallographic data. This approach provides insights into the origin of some $[^{18}O_4]$ isotope effects that accompany the reactions of phosphates.

Table 4.1. P_O stretching frequencies for isolated [$^{16}O_4$]-phosphate molecules, calculated by an *ab initio* procedure, plus the effect on these frequencies of setting the values of various force constants to zero[a].

Species	Force Field[b,c]	Frequency(P=O)[d]			Force Field[e]	Frequency(P-O)[d]		
		υ_s	υ_a	υ		υ_s	υ_a	υ
H_3PO_4	Full set	1471	-	1471	Full set	963	957	959
	f_b=0	1463	-	1463	f_b=0	964	956	960
	$f_{s(P-O)}$=0	1455	-	1455	$f_{s(P=O)}$=0	1007	957	982
$H_2PO_4^-$	Full set	1249	1489	1374	Full set	905	953	929
	f_b=0	1239	1489	1370	f_b=0	905	953	929
	$f_{s(P-O)}$=0	1247	1488	1373	$f_{s(P=O)}$=0	953	954	954
HPO_4^{2-}	Full Set	1070	1325	1246	Full set	788	-	788
	f_b=0	1066	1310	1234	f_b=0	-	-	-
	$f_{s(P-O)}$=0	1073	1325	1247	$f_{s(P=O)}$=0	808	-	808
$CH_3PO_4^{2-}$	Full Set	1068	1327	1247	Full set	729	-	729
	f_b=0	1067	1315	1238	f_b=0	-	-	-
	$f_{s(P-O)}$=0	1085	1326	1251	$f_{s(P=O)}$=0	744	-	744
PO_4^{3-}	Full Set	963	1146	1103				
	f_b=0	963	1123	1085				

[a]Calculations performed at the hf/3-21g* level.

[b]In this table, P=O is used for P_O.

[c]In this column, f_b refers to the O_P_O bending force constant except in H_3PO_4. where it refers to O_P-O bend.

[d]All values are in cm^{-1}

[e]In this column, f_b refers to the HO≅P≅OH bending force constant

Table 4.2. P_O stretching frequencies for isolated [$^{16}O_4$]- and [$^{18}O_4$]-phosphate molecules calculated by an *ab initio* procedure.[a]

Species	Bond Type	[$^{16}O_4$]-phosphate[b]			[$^{18}O_4$]-phosphate[b]			$\upsilon^{16}/\upsilon^{18}$
		υ_s	υ_a	υ	υ_s	υ_a	υ	
H_3PO_4	P_O	1471	-	1471	1424	-	1424	1.033
$H_2PO_4^-$	P_O	1249	1489	1374	1199	1450	1330	1.033
HPO_4^{2-}	P_O	1070	1325	1246	1018	1291	1207	1.032
$CH_3PO_4^{2-}$	P_O	1068	1327	1247	1015	1289	1205	1.035
PO_4^{3-}	P_O	963	1146	1103	908	1115	1067	1.034
PO_3^-	P_O	1133	1453	1355	1068	1408	1306	1.038

[a]Calculations performed at the hf/3-21g* level.

[b]All values are in cm^{-1}

Table 4.3. V_O stretching frequencies for isolated [$^{16}O_4$]-vanadate molecules, calculated by an ab initio procedure, plus the effect on these frequencies of setting the values of various force constants to zero[a].

Species	Force Field[b,c]	Frequency(V=O)[d]			Force Field[e]	Frequency(V-O)[d]		
		υ_s	υ_a	υ		υ_s	υ_a	υ
H_3VO_4	Full set	1310	-	1310	Full set	879	983	948
	f_b=0	1301	-	1301	f_b=0	877	971	941
	$f_{s(V-O)}$=0	1317	-	1317	$f_{s(V=O)}$=0	888	983	952
$H_2VO_4^-$	Full Set	1200	1214	1207	Full set	779	845	813
	f_b=0	1190	1214	1202	f_b=0	777	845	812
	$f_{s(V-O)}$=0	1206	1214	1210	$f_{s(V=O)}$=0	797	845	821
HVO_4^{2-}	Full Set	1068	1088	1081	Full set	648	-	648
	f_b=0	1055	1070	1065	f_b=0	-	-	-
	$f_{s(V-O)}$=0	1073	1088	1083	$f_{s(V=O)}$=0	657	-	657
$CH_3VO_4^{2-}$	Full Set	1057	1086	1076	Full set	582	-	582
	f_b=0	1045	1067	1060	f_b=0	-	-	-
	$f_{s(V-O)}$=0	1050	1069	1063	$f_{s(V=O)}$=0	593	-	593
VO_4^{3-}	Full Set	944	894	907				
	f_b=0	944	858	880				

[a]Calculations performed at the hf/3-21g* level.

[b]In this table, V=O is used for V_O.

[c]In this column, f_b refers to the O_V_O bending force constant except in H_3VO_4, where it refers to O_V-O bend.

[d]All values are in cm^{-1}

[e]In this column, f_b refers to the HO≡V≡OH bending force constant

Table 4.4. Raman stretching frequencies for [$^{16}O_4$]- and [$^{18}O_4$]phosphates.[b]

Species	Bond Type	[$^{16}O_4$]-phosphate[a]			[$^{18}O_4$]-phosphate[a]			$\upsilon^{16}/\upsilon^{18}$
		υ_s	υ_a	υ	υ_s	υ_a	υ	
H_3PO_4	P_O	1177	-	1177	1143	-	1143	1.030
$H_2PO_4^-$	P_O	1078	1159	1119	1040	1129	1085	1.031
$D_2PO_4^-$	P_O	1084	1190	1138	1048	1155	1103	1.033
HPO_4^{2-}	P_O	990	1084	1054	950	1053	1020	1.033
DPO_4^{2-}	P_O	989	1085	1054	952	1055	1022	1.031
$MePO_4^{2-}$	P_O	983	1097	1060	945	1070	1030	1.030
$MePO_4^{2-}$ (crystal)	P_O	974	1117	1071	931	1090	1040	1.031
PO_4^{3-}	P_O	938	1010	992	882	982	958	1.036
							1.032	0.002
H_3PO_4	P_OH	891	1010	972	849	979	938	1.036
$H_2PO_4^-$	P_OH	878	943	911	838	918	879	1.036
HPO_4^{2-}	P_OH	858	-	858	833	-	833	1.030

[a]All values are in cm^{-1}

[b]Measurements were taken by H. Deng (Ray et al., 1993a).

Table 4.5. P_O Bond order and bond length calculated from Raman stretching frequencies.

Species	$\upsilon(cm^{-1})$	Bond order[a]	Bond length (Å)[b]
H_3PO_4	1177	1.44 (1.44)	1.489
$H_2PO_4^-$	1119	1.38 (1.37)	1.503
$D_2PO_4^-$	1138	1.40 (1.40)	1.498
HPO_4^{2-}	1054	1.31 (1.30)	1.520
DPO_4^{2-}	1054	1.31 (1.30)	1.520
$MePO_4^{2-}$	1060	1.32 (1.31)	1.518
$MePO_4^{2-}$ (crystal)	1071	1.33 (1.32)	1.515

[a]Calculated according to eq. 13 from values of υ(P_O) in Table 4.4 (and reproduced in column 2). Numbers in parantethes are calculated by Eq.4 in Ray et al. (1993a).
[b]Calculated according to eq. 4.1 with r_l = 1.62 Å and p=4.29.

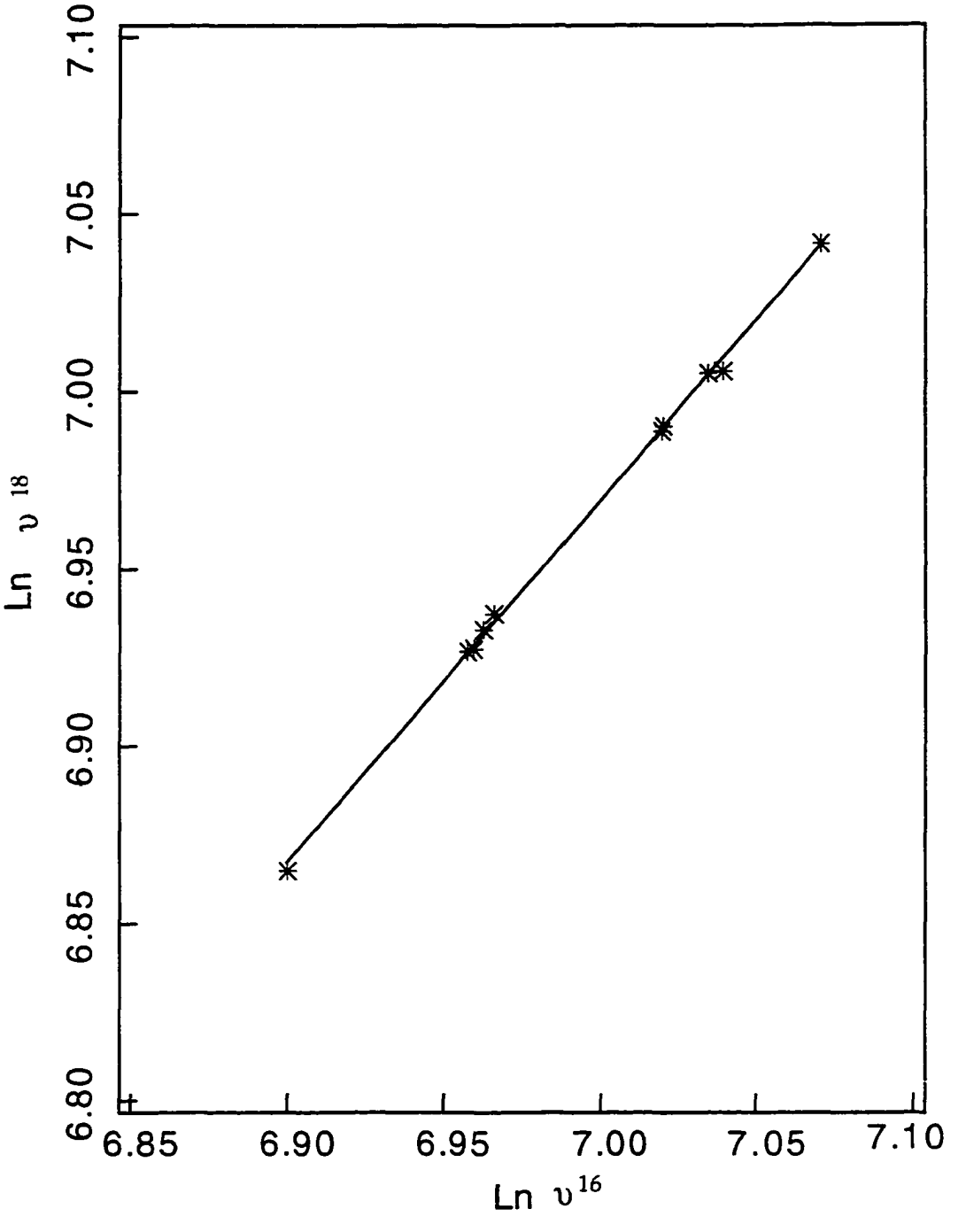

FIGURE 4.1. Logarithmic plot (base e) of fundamental stretching frequencies for the P••O groups of [$^{18}O_4$] phosphates versus those for the corresponding [$^{16}O_4$] phosphates. The experimental data in Table 4.4 are shown. Two additional data points are from FTIR measurements; the straight line is the least squares fit.

CHAPTER 5

Vibrational Study of Phosphate Modes in GDP and GTP in Aqueous Solution

Vibrational spectroscopy has often been used in the study of the conformational structure of nucleotides (Hardcastle & Wachs, 1991; Lewis et al., 1975). A common goal in these investigations is to establish correlations between vibrational spectra and specific structural features of nucleotides in solution, in protein complexes, and in nucleic acid assemblies. Of particular interest are Raman and infrared bands that correspond to vibrational modes localized in the phosphate group of the purine nucleotides, adenosine 5'-triphosphate (ATP) and guanosine 5'-triphosphate (GTP). These are involved in important phosphoryl transfer reactions in proteins that have to do with energy transduction, such as the muscle proteins and the transmembrane pump proteins (ATPases), and the large number of guanine nucleotide binding proteins. The latter group is involved a variety of key cellular processes such as signal transduction, cell growth and differentiation, protein synthesis and protein transport (Boguski & McCormick, 1993; Bourne et al., 1990; Bourne et al., 1991; Wooley & Clark, 1989). The binding site of these proteins most often contain Mg^{2+} or Ca^{2+}, although the function of the divalent cation is still not clear. Nucleotides normally bind to these proteins as their complex with Mg^{2+}, and the metal ion is probably involved in binding both, providing a bridge between phosphate oxygens and amino acids, and in catalysis of triphosphate hydrolysis, for example by helping to neutralize the diphosphate leaving group (Cleland, 1967). Therefore, knowledge of the structures of these nucleotides and their interactions with metal ions both in solution and in protein binding sites is of considerable interest.

ATP complexed with Mg^{2+} in aqueous solution has been studied extensively by spectroscopic methods. NMR studies have yielded several models for the Mg•ATP complex: β monodentate (Tran-Dinh et al., 1975), β,γ-bidentate (Cohen & Hughes, 1962; Lewis et al., 1975), α,β,γ-tridentate (Bishop et al., 1981), a mixture of α,β-, β,γ- and α,γ-bidentate (Ramirez & Marecek, 1980), and α,β,γ-tridentate with smaller extent of α coordination (Huang & Tsai, 1982). The coordination sites of Mg•ATP have also been investigated by Raman and infrared spectra (Takeuchi et al., 1988). Takeuchi et al. concluded that the Mg·ATP 1:1 complex is a mixture of β, γ-bidentate and α, β, γ-tridentate. A number of X-ray crystallographic studies of GDP, GTP in protein active sites have been reported (Sprang, 1997; Pai et al., 1990; Tong et al., 1991; Wittinghofer et al., 1991). However, few studies on GTP in aqueous solution have been performed.

In this study, Raman and infrared spectra of GDP, GTP and their isotopomers (scheme 5.1) in aqueous solution were measured as were their Mg^{2+} complexes. Assignments of the phosphate bands in the spectra of GTP and GDP in aqueous solution are made on the basis of ^{18}O labeling of the phosphate group and known intensity patterns with Raman and IR spectroscopies. Large frequency shifts of phosphate modes were observed upon Mg^{2+} complexation to GDP and GTP.

5.1 Assignments of Infrared and Raman Bands of GDP at pH 5.0

Figure 5.1 shows the Raman (a, b) and infrared spectra (a', b'), respectively, of GDP and its ^{18}O labeled derivatives in aqueous solution at pH 5.0. One oxygen atom of the β-phosphate is protonated at this pH (pKa=6.3, scheme 5.1). The diphosphate moiety is composed of two $>PO_2^-$ groups and four P-O single bonds. Each $>PO_2^-$ group has C_{2v} symmetry which leads to a symmetric P$\underline{\bullet\bullet}$O

stretch mode, $\upsilon_s(PO_2^-)$, and an antisymmetric stretch mode, $\upsilon_a(PO_2^-)$. The symmetric stretch motions of the two $>PO_2^-$ groups are often strongly coupled to form an in-phase combination, $\upsilon_s(\text{in-}PO_2^-)$, and an out-of-phase combination, $\upsilon_s(\text{out-}PO_2^-)$, while the two antisymmetric modes $\upsilon_a(\alpha\text{-}PO_2^-)$, $\upsilon_a(\beta\text{-}PO_2^-)$ are not strongly coupled (Shimanouchi et al., 1964; Takeuchi et al., 1988). In general, the intensity of the in-phase symmetric stretch mode is strong in Raman but weak in IR while the intensity of the out-of-phase symmetric stretch mode is strong in IR but weak in Raman, so is the intensity of the antisymmetric stretch mode. However, the antisymmetric stretch band is broad while the band of symmetric stretch mode, either in-phase or out-of-phase, is sharp.

Antisymmetric stretch mode, $\upsilon_a(PO_2^-)$, of the two $>PO_2^-$ groups are expected in the 1250-1150 cm^{-1} region (Shimanouchi et al., 1964). In Figure 5.1a', a broad infrared spectra appears at 1227 cm^{-1} . Upon ^{18}O-substitution at the β position, the intensity of the 1227-cm^{-1} peak is reduced and a new peak appears at 1176 cm^{-1} (Figure 5.1b'). Thus, the intensity of the 1227-cm^{-1} band in Figure 5.1a' can be assigned to arise from the overlap of the antisymmetric stretch modes, $\upsilon_a(\beta\text{-}PO_2^-)$ and $\upsilon_a(\alpha\text{-}PO_2^-)$. The band of the antisymmetric mode $\upsilon_a(\beta\text{-}P^{18}O_2^-)$ moves to 1176 cm^{-1} band in Figure 5.1b', but the intensity of the 1176-cm^{-1} band may also have contribution from the guanosine ring which has a band at 1179 cm^{-1} in the Raman spectrum (Figure 5.1b). In Figure 5.1b', the virtually unshifted infrared component at 1227 cm^{-1} is assigned to the antisymmetric stretch mode $\upsilon_a(\alpha\text{-}PO_2^-)$.

The PO_2^- symmetric stretch modes, $\upsilon_s(PO_2^-)$ are expected around 1100 cm^{-1} (Shimanouchi et al., 1964). The 1109(1110)-cm^{-1} band in Figure 5.1a(5.1a') can be assigned to the in-phase combination, $\upsilon_s(\text{in-}PO_2^-)$, and the band at 1080(1080) cm^{-1} in Figure 5.1a(5.1a') can be assigned to the out-of-phase combination, $\upsilon_s(\text{out-}PO_2^-)$, on the basis of the following observations: (1) upon ^{18}O-

substitution at the β position, the strong and sharp Raman band at 1109 cm^{-1} (in Figure 5.1a) shifts down to 1098 cm^{-1} (in Figure 5.1b) and the strong infrared band at 1080 cm^{-1} (in Figure 5.1a') shifts down to 1050 cm^{-1} (Figure 5.1b'). These frequency shifts (10, 30 cm^{-1}) are less than the ^{18}O shift of the P••O symmetric stretch modes in monophosphates (40-cm^{-1}, either monoionic or dianionic) indicating that there are considerable mixing of the stretch motions of the PO bonds of α,β-phosphate groups; (2) both bands are sharp, which is characteristic of symmetric stretch modes; (3) the intensity of 1109-cm^{-1} band is strong in Raman but weak in IR while the intensity of 1080-cm^{-1} band is strong in IR but weak in Raman. These assignments are consistent with the observations in the spectra of (β-$^{18}O_3$)GDP (Figure 5.1b, 5.1b'): the stretch motions of the two phosphate groups are still coupled and the intensity of the in-phase mode at 1098 cm^{-1} is strong in Raman but weak in IR (1096 cm^{-1}), while the intensity of the out-of-phase mode at 1050 cm^{-1} is strong in infrared but weak in Raman. The 1096-cm^{-1} and 1050-cm^{-1} bands mainly involves P••O stretch of α-PO_2^- and β-$P^{18}O_2^-$ group, respectively. The 984-cm^{-1} band is very likely to involve the P-O stretch mode of the linkage P-O-P (Shimanouchi et al., 1964; Takeuchi et al., 1988).

Table 5.1 summarizes all the position and band assignments

5.2 Assignments of Infrared and Raman Bands of GDP at pH 7.5.

Figure 5.2 shows the Raman (a, b) and infrared spectra (a', b'), respectively, of GDP and its ^{18}O derivatives in aqueous solution at pH 7.5. The β-phosphate group is dianionic at pH 7.5 (Scheme 5.1). The diphosphate moiety is thus composed of a $>PO_2^-$ group and a $-PO_3^{2-}$ terminal group. The a $>PO_2^-$ group has approximate C_{2v} symmetry which leads to a symmetric P••O stretch mode, υ_s(α-PO_2^-), and an antisymmetric stretch mode, υ_a(α-PO_2^-). The β-PO_3^{2-} group

has C_{3v} symmetry; therefore it has a symmetric P••O stretch mode, $\upsilon_s(\beta\text{-}PO_3^{2-})$, and a doubly degenerate antisymmetric stretch mode, $\upsilon_a(\beta\text{-}PO_3^{2-})$. The symmetric stretch motions of the two phosphate groups are not strongly coupled because the bond orders of the two groups are quite different. The intensities of both symmetric stretch modes are strong in Raman but weak in IR while the intensities of the antisymmetric stretch modes are weak in Raman and strong in IR. In general, the antisymmetric stretch bands are broad while the bands of symmetric stretch modes are sharp. The antisymmetric stretch mode $\upsilon_a(\alpha\text{-}PO_2^-)$ is expected to lie within 1250-1150 cm^{-1}, the $\upsilon_s(\alpha\text{-}PO_2^-)$ and $\upsilon_a(\beta\text{-}PO_3^{2-})$ modes within 1100-1150 cm^{-1}, and the symmetric stretch mode, $\upsilon_s(\beta\text{-}PO_3^{2-})$ within 900-1000 cm^{-1} (Shimanouchi et al., 1964).

In the FTIR spectra of Figure 5.2a', a broad infrared band at 1205 cm^{-1}, which is invariant upon ^{18}O labeling at the β-position, can then be assigned to the antisymmetric stretch mode of the α-phosphate group, $\upsilon_a(\alpha\text{-}PO_2^-)$. A strong and sharp Raman band at 1089 cm^{-1} of unlabeled GDP (Figure 5.2a), which is also virtually unshifted (1087 cm^{-1}, Figure 5.2b) upon ^{18}O labeling at the β-position, is assigned to the symmetric stretch mode, $\upsilon_s(\alpha\text{-}PO_2^-)$. The infrared spectra of unlabeled GDP shows a strong and broad band at 1115 cm^{-1} (Figure 5.2a'), which upon ^{18}O-substitution at the β position shifts down to 1089 cm^{-1} (Figure 5.2b'). Thus, the 1115 cm^{-1} infrared band is assigned to the antisymmetric stretch mode, $\upsilon_a(\beta\text{-}PO_3^{2-})$. The intensity of the broad peak at 1115 cm^{-1} in the infrared spectrum may also have a contribution from the symmetric stretch mode $\upsilon_s(\alpha\text{-}PO_2^-)$ at 1089 cm^{-1} observed in the Raman spectrum (Figure 5.2a') since the two frequencies are quite close but the symmetric mode is expected to be weak, but not zero, in the IR.

Upon ^{18}O-substitution of the oxygens at the β position, the 943-cm^{-1} peak in the Raman spectrum (Figure 5.2a) is shifted down and splits into two peaks at

900 and 919 cm^{-1} (Figure 5.2b). We assign the observed intensity of the 943-cm^{-1} peak (Figure 5.2a) as arising from the $\upsilon_S(\beta\text{-}PO_3^{2-})$ motion and the P-O stretch of the P-O-P linkage. The $\upsilon_S(\beta\text{-}PO_3^{2-})$ mode is shifted to 900 cm^{-1} upon ^{18}O labeling while the $\upsilon(P_\beta\text{-}^{18}O)$ is shifted to 919 cm^{-1} (Figure 5.2b). This assignment is confirmed by the Raman difference spectra formed between GDP and ($\alpha\beta$–^{18}O;$\beta\text{-}^{18}O_3$)GDP (unpublished data), which show clear positive intensity at 944 cm^{-1} and negative intensity at 895 cm^{-1}.

Table 5.2 summarizes all the position and band assignments.

5.3 Assignments of Infrared and Raman Bands of GTP at pH 5.0

Figure 5.3 shows the Raman (a-c) and infrared spectra (a'-c'), respectively, of GTP and its ^{18}O derivatives in aqueous solution at pH 5.0. One of the oxygen atom of the γ-phosphate is protonated at this pH (Scheme 5.1). The triphosphate moiety consists of three PO_2^- groups and six P-O single bonds. Each PO_2^- group has approximately C_{2v} symmetry which leads to a symmetric P=O stretch mode $\upsilon_S(PO_2^-)$ and an antisymmetric stretch mode $\upsilon_a(PO_2^-)$. The symmetric stretch motions of the three PO_2^- groups are often strongly coupled to form an in-phase combination $\upsilon_S(\text{in-}PO_2^-)$ and two out-of-phase combinations $\upsilon_S(\text{out-}PO_2^-)$ while the three antisymmetric modes $\upsilon_a(\alpha\text{-}PO_2^-)$, $\upsilon_a(\beta\text{-}PO_2^-)$ and $\upsilon_a(\gamma\text{-}PO_2^-)$ are not strongly coupled. The intensity of the in-phase symmetric stretch mode is strong in Raman but weak in IR while the intensities of both out-of-phase symmetric stretch modes are strong in IR but weak in Raman, so are the intensities of the antisymmetric stretch modes. However, the antisymmetric stretch bands are broad while the symmetric stretch bands, either in-phase or out-of-phase, are sharp.

The antisymmetric stretch modes $\upsilon_a(PO_2^-)$ of the three PO_2^- groups are expected in the 1250-1150 cm^{-1} region (Shimanouchi et al., 1964). The infrared

spectrum of unlabeled GTP shows a broad absorption band at 1239 cm^{-1} (Figure 5.3a'). Upon ^{18}O-substitution at the γ position, the 1239-cm^{-1} band shifts to 1235 cm^{-1} with reduced intensity and a new peak appears at 1179 cm^{-1} (Figure 5.3c') Upon ^{18}O-substitution at the β position, the 1239-cm^{-1} band shifts down to 1227 cm^{-1} with weak shoulder at 1200 cm^{-1} (Figure 5.3b'). Therefore, the 1239-cm^{-1} band (Figure 5.3a') can be assigned to an overlap band of the antisymmetric stretch modes of the three PO_2^- groups $\upsilon_a(\alpha\text{-}PO_2^-)$, $\upsilon_a(\beta\text{-}PO_2^-)$ and $\upsilon_a(\gamma\text{-}PO_2^-)$. The 1235-$cm^{-1}$ band (Figure 5.3c') is due to an overlap band of $\upsilon_a(\alpha\text{-}PO_2^-)$, $\upsilon_a(\beta\text{-}PO_2^-)$ and the band at 1175 cm^{-1} (Figure 5.3c') is thus assigned to $\upsilon_a(\gamma\text{-}P^{18}O_2^-)$. The 1227-$cm^{-1}$ band (Figure 5.3b') is assigned to an overlap of $\upsilon_a(\alpha\text{-}PO_2^-)$, $\upsilon_a(\gamma\text{-}PO_2^-)$ and the 1200-cm^{-1} shoulder (Figure 5.3b') is ascribed to $\upsilon_a(\beta\text{-}P^{18}O_2^-)$. It is reasonable to conclude that $\upsilon_a(\alpha\text{-}PO_2^-)$ is about 10 cm^{-1} lower than $\upsilon_a(\beta\text{-}PO_2^-)$ (Takeuchi et al., 1988): the frequencies of $\upsilon_a(\alpha\text{-}PO_2^-)$ and $\upsilon_a(\beta\text{-}PO_2^-)$ are around 1230 cm^{-1} and 1240 cm^{-1}, respectively. The weak band of $\upsilon_a(\gamma\text{-}PO_2^-)$ is around 1210 cm^{-1} which is overlapped by the tail of $\upsilon_a(\alpha\text{-}PO_2^-)$.

The PO_2^- symmetric stretch modes are expected around 1100 cm^{-1} (Shimanouchi et al., 1964). In Figure 5.3a and 5.3a', the Raman band at 1123 cm^{-1} (labeled 1124 cm^{-1} in the infrared spectrum) can be assigned to the in-phase combination, $\upsilon_s(\text{in-}PO_2^-)$, and two infrared bands 1097 and 1079 cm^{-1} are assigned to the out-of-phase combination, $\upsilon_s(\text{out-}PO_2^-)$, based on the following observations: (1) Upon ^{18}O-substitution at the $\beta(\gamma)$-position, the strong and sharp Raman band at 1123 cm^{-1} shifts down to 1108(1120)cm^{-1} (Figure 5.3b, 5.3c), strong infrared band at 1079 cm^{-1} shifts down to 1052(1050) cm^{-1} (Figure 5.3b', 5.3c') and strong infrared band at 1097 cm^{-1} shifts down to 1080(1079) cm^{-1} (Figure 5.3b', 5.3c'); (2) All three bands are sharp, which is characteristic of symmetric stretch modes; (3) The intensity of 1123-cm^{-1} band is strong in the Raman but weak in IR while the intensities of 1097, 1079-cm^{-1} bands are strong

in IR but weak in Raman. (Figure 5.3a, 5.3a'). The two out-of-phase modes show dramatic changes in the infrared intensity distribution upon ^{18}O isotopic label because of the changes in the mode mixing pattern (Figure 5.3b', 5.3c'). In the β,γ-^{18}O labeled GTP spectra, the bands at 1052 (Figure 5.3b') and 1050 cm^{-1} (Figure 5.3c') are predominantly related with the stretch motions of the ^{18}O-substituted phosphate group while bands labeled at 1080 (Figure 5.3b') and 1079 cm^{-1} (Figure 5.3c') are involved the stretch motions of the unlabeled PO_2^- group. The 966, 923-cm^{-1} bands are very likely to involve the P-O stretch motions of the main chain.

Table 5.1 summarizes all the assignments for the modes of GTP and the isotopically labeled GTPs.

5.4 Assignments of Infrared and Raman Bands of GTP at pH 7.5.

Figure 5.4 shows the Raman and infrared spectra of GTP and labeled GTP in aqueous solution at pH 7.5. At this pH, the triphosphate moiety is composed of two $>PO_2^-$ groups and one $-PO_3^{2-}$ terminal group. The symmetric stretch motions of the two $>PO_2^-$ groups are often strongly coupled to form an in-phase combination $\upsilon_S(\text{in-}PO_2^-)$ and an out-of-phase combination $\upsilon_S(\text{out-}PO_2^-)$ because their bond orders, hence force constants and characteristic vibrational frequencies, of the two $>PO_2^-$ groups are quite close. However, the two antisymmetric modes, $\upsilon_a(\alpha\text{-}PO_2^-)$ and $\upsilon_a(\beta\text{-}PO_2^-)$, are not strongly coupled (Shimanouchi et al., 1964; Takeuchi et al., 1988). The γ-PO_3^{2-} group has approximate C_{3v} symmetry which leads to a symmetric $P\underline{\bullet\bullet}O$ stretch mode $\upsilon_S(\gamma\text{-}PO_3^{2-})$ and a doubly degenerate antisymmetric stretch mode $\upsilon_a(\gamma\text{-}PO_3^{2-})$. The symmetric stretch motion of γ-phosphate is not coupled with the other two phosphate groups because the bond orders of the non-bonded P-O bonds are quite different for the α and β $>PO_2^-$ groups compared to the γ-PO_3^{2-} moiety.

The intensity of the in-phase symmetric stretch mode is strong in Raman but weak in IR while the intensity of the out-of-phase symmetric stretch mode is strong in IR but weak in Raman as is the intensity of the antisymmetric stretch mode. In additon, as in the case of GDP, the antisymmetric stretch band is broad while the band of symmetric stretch mode, either in-phase or out-of-phase, is sharp. These attributes aid in identification.

Antisymmetric stretch modes, $\upsilon_a(PO_2^-)$, of the two $>PO_2^-$ groups are expected in the 1150-1250 cm^{-1} region (Shimanouchi et al., 1964). In Figure 5.4a', a broad infrared band appears at 1233 cm^{-1}. Upon ^{18}O-substitution at the β position, the 1233-cm^{-1} band shifts down to 1220 cm^{-1} with a weak shoulder band at 1190 cm^{-1} (Figure 5.4b'). Thus, the intensity of the 1233-cm^{-1} band can be assigned to arise from the overlap of the antisymmetric stretch modes, $\upsilon_a(\alpha\text{-}PO_2^-)$ and $\upsilon_a(\beta\text{-}PO_2^-)$. The 1220 cm^{-1} band (Figure 2b') is assigned to the antisymmetric stretch mode of the α-phosphate group, $\upsilon_a(\alpha\text{-}PO_2^-)$. This band of the antisymmetric stretch mode $\upsilon_a(\beta\text{-}P^{18}O_2^-)$ moves to 1190-cm^{-1} in $(\beta\text{-}^{18}O_2;\beta\gamma\text{-}^{18}O)$GTP. It is reasonable to conclude that the antisymmetric stretch mode of unlabeled β-phosphate $\upsilon_a(\beta\text{-}PO_2^-)$ should be higher than $\upsilon_a(\alpha\text{-}PO_2^-)$. Hence, the 1229 cm^{-1} band of the $(\gamma\text{-}^{18}O_3)$GTP spectrum (Figure 5.4c') is due to the overlap of the antisymmetric stretch modes $\upsilon_a(\alpha\text{-}PO_2^-)$ and $\upsilon_a(\beta\text{-}PO_2^-)$.

The PO_2^- symmetric stretch modes, $\upsilon_s(\text{in-}PO_2^-)$ and $\upsilon_s(\text{out-}PO_2^-)$, are expected near 1100 cm^{-1} (Shimanouchi et al., 1964). The degenerate stretch mode $\upsilon_a(\gamma\text{-}PO_3^{2-})$ close to the position of $\upsilon_s(\text{in-}PO_2^-)$. However, the strong sharp Raman band at 1116 cm^{-1} (Figure 5.4a), which is invariant upon ^{18}O labeling at the γ-position (Figure 5.4c) but shifts down to 1102 cm^{-1} upon ^{18}O labeling at β-position (Figure 5.4b), can be assigned to in-phase combination $\upsilon_s(\text{in-}PO_2^-)$ of α,β-phosphate groups since its intensity is strong in Raman but weak in IR. The 1087-cm^{-1} Raman band (Figure 5.4a), which is invariant upon ^{18}O labeling at γ-

position (Figure 5.4c) but shifts to 1060 cm^{-1} upon ^{18}O labeling at the β-position (Figure 5.4b), is thus assigned to the out-of-phase mode. The strong, broad infrared band at 1119 cm^{-1} (Figure 5.4a'), which shifts down to 1082 cm^{-1} (Figure 5.4c') upon ^{18}O-substitution at the γ position, is assigned to the antisymmetric stretch mode of γ-phosphate group, $\upsilon_a(\gamma\text{-}PO_3^{2-})$. The 1082-$cm^{-1}$ (Figure 5.4c') band can assigned to $\upsilon_a(\gamma\text{-}P^{18}O_3^{2-})$. Upon ^{18}O-substitution at the β position, a broad infrared band appears at 1102 cm^{-1} which is composed of $\upsilon_a(\gamma\text{-}PO_3^{2-})$ and $\upsilon_s(\text{in-}PO_2^-)$ (Figure 5.4b').

The symmetric stretch mode, $\upsilon_s(\gamma\text{-}PO_3^{2-})$, is expected around 900-1000 cm^{-1} (Shimanouchi et al., 1964). In Figure 5.4a', the intensity of the observed Raman 927-cm^{-1} band most likely arises from the overlap of two modes: the symmetric stretch mode of the γ-phosphate, $\upsilon_s(\gamma\text{-}PO_3^{2-})$, and a P-O stretch mode υ(P-O) of the $P_\beta\text{-}O\text{-}P_\gamma$ linkage. This is based on the following observations: (1) upon ^{18}O-substitution at the γ position, a strong Raman band at 900 cm^{-1} appears (Figure 5.4c); (2) the Raman intensity of the 891 cm^{-1} band is enhanced on (β-$^{18}O_2$;βγ-^{18}O)GTP (Figure 5.4b); (3) the infrared band at 927 cm^{-1} shifts to 905 cm^{-1} because of isotope ^{18}O labeling at γ position (Figure 5.4c'). Thus, the 900 cm^{-1} Raman band (Figure 5.4c) is assigned to the symmetric stretch mode of $\upsilon_s(\gamma\text{-}P^{18}O_3^{2-})$. The 891 cm^{-1} (Figure 5.4b) band is assigned to the P-O stretch mode $\upsilon(P\text{-}^{18}O)$ of the $P\gamma\text{-}O\text{-}P\beta$ linkage (Figure 5.4b). In Figure 5.4b, the Raman band at 995-cm^{-1} is most likely due to the P-O stretch mode of the $P\alpha\text{-}O\text{-}P\beta$ linkage (Takeuchi et al., 1988).

Table 5.2 summarizes all the assignments for the modes of GTP and the isotopically labeled GTPs.

The infrared and Raman spectra of ATP and caged ATP have been reported (Takeuchi et al., 1988; Barth, 1995; Barth, 1997). The frequencies of symmetric and antisymmetric modes of $>PO_2^-$ groups of ATP are very close to

those assigned here for GTP at either pH value, as is expected. For the γ-PO_3^{2-} group, the frequency of the antisymmetric mode of GTP is also very near that of ATP. However, the frequencies of the symmetric mode are quite different. Our assignment of $\upsilon_S(\gamma\text{-}PO_3^{2-})$ at 927 cm^{-1} is based primarily on the Raman spectra of ^{18}O isotope labeling at γ-position. Takeuchi et al. suggested that the $\upsilon_S(\gamma\text{-}PO_3^{2-})$ mode of ATP lies near 1000 cm^{-1} based on infrared spectra. This needs further study using isotope labeled ATP, particularly since the infrared intensity of the symmetric stretch mode $\upsilon_S(\gamma\text{-}PO_3^{2-})$ is weak.

5.5 Effect of Mg^{2+} complexation on the phosphate modes

Interaction of Mg^{2+} with GDP: Since the pK_a of the β-PO_3^{2-} group decreases when GDP (or the γ-PO_3^{2-} group of GTP) is complexed with Mg^{2+}, we only present the data obtained at pH 7.5 as this is the likely ionization state of GDP and GTP in protein complexes. Figure 5.5a and 5.5a' show the Raman and infrared spectra of Mg•GDP 1:1 complex at pH 7.5, respectively. Large frequency shifts due to Mg^{2+} binding are observed for the vibrations localized to the α-PO_2^- group. The symmetric stretch vibration of $\upsilon_S(\alpha\text{-}PO_2^-)$ shifts up by 5 cm^{-1} from 1089 cm^{-1} in free GDP (see Table 5.2) to 1094 cm^{-1} in the complex (Figure 5.5a). The $\upsilon_a(\alpha\text{-}PO_2^-)$ shifts up by 10 cm^{-1} to 1215 cm^{-1} (Figure 5.5a'). This is direct evidence that Mg^{2+} interacts with the α-PO_2^- group in Mg•GDP. Furthermore, the infrared spectrum shows that the antisymmetric stretch mode $\upsilon_a(\beta\text{-}PO_3^{2-})$ of the β-phosphate group shifts up by 8 cm^{-1} in the complex (Figure 5.5a') while the frequency of $\upsilon_S(\beta\text{-}PO_3^{2-})$ is virtually unchanged (Figure 5.2a', 5.5a'). This suggests that Mg^{2+} interacts with the β-PO_3^{2-} group in Mg•GDP.

Interaction of Mg^{2+} with GTP: The Raman and infrared spectra of Mg•GTP 1:1 complex at pH 7.5 are shown in Figure 5.6a and 5.6a', respectively. Figure 5.6b and 5.6c show the spectra of Mg•(β-$^{18}O_3$)GTP 1:1 complex and

Mg•(γ-$^{18}O_3$)GTP 1:1 complex, respectively. The band arising from the overlap of the antisymmetric stretch modes, $\upsilon_a(\alpha\text{-}PO_2^-)$ and $\upsilon_a(\beta\text{-}PO_2^-)$, has a large frequency shift, from 1233 cm^{-1} in free GTP (Figure 5.4a') to 1247 cm^{-1} in the complex (Figure 5.6a'). Upon ^{18}O labeling at β-position, the antisymmetric stretch modes, $\upsilon_a(\alpha\text{-}PO_2^-)$ and $\upsilon_a(\beta\text{-}P^{18}O_2^-)$, are clearly resolved (Figure 5.4b', 5.6b'). The $\upsilon_a(\alpha\text{-}PO_2^-)$ mode shifts from 1220 cm^{-1} in free GTP to 1134 cm^{-1} in the complex and $\upsilon_a(\beta\text{-}P^{18}O_2^-)$ shifts from 1190 cm^{-1} to 1202 cm^{-1} (Table 5.2). Such large frequency shifts are due to the Mg^{2+} interacting with both the $\alpha\text{-}PO_2^-$ and $\beta\text{-}PO_2^-$ groups. The in-phase symmetric mode $\upsilon_s(\text{in-}PO_2^-)$ also upshifts from 1116 to 1122 cm^{-1}, while the frequency of out-of-phase mode is virtually unchanged. The frequency of $\upsilon_a(\gamma\text{-}PO_3^{2-})$ shifts from 1119 to 1128 cm^{-1} while the symmetric mode $\upsilon_s(\gamma\text{-}PO_3^{2-})$ virtually is unshifted. These results provide direct evidence of the binding of Mg^{2+} to the $\gamma\text{-}PO_3^{2-}$ group.

5.6 pKa of Mg•GDP

Figure 5.7 shows that the frequencies of the antisymmetric stretch mode $\upsilon_a(\alpha\text{-}PO_2^-)$, instead of the in-phase $\upsilon_s(\alpha\text{-}PO_2^-)$ as suggested by Heyde & Rimai (Heyde & Rimai, 1971), depend on the value of pH. GDP without Mg^{2+} has a broad strong peak at 1205 cm^{-1} when pH>>pKa $\simeq$6.0 and at 1227 cm^{-1} when pH<<pKa (Figure 5.1 and 5.2). The peak value represents the aspect of protonation of $\beta\text{-}PO_3^{2-}$ group. There are essentially two forms of GDP present, with the following average concentrations: N_1 for protonated GDP, and N_2 for the unprotonated GDP, and the spectrum of interest will consist of two lines at frequencies ω_1 and ω_2 with amplitudes proportional to N_1 and N_2. (The width of the two lines are assumed equal.) This is the situation for pH<<pKa or pH>>pKa, where N_2=0 or N_1=0, respectively. Because the widths of antisymmtric mode $\upsilon_a(PO_2^-)$ (35 cm^{-1}) is larger than the difference of ω_1 and ω_2

(18 cm^{-1}), a broad single line is observed at a frequency $\omega=(\omega_1+\omega_2)/2+0.5*(\omega_1-\omega_2)*(N_2-N_1)/(N_1+N_2)$ (Heyde & Rimai, 1971). The value of pKa determined by this method is slightly different than that derived from the titration method (pK_a=6.3, Dean, 1987). The value of pKa shifts down to 4.7 when GDP mixes with $MgCl_2$ in 1:1 ratio.

5.7 Structure of The Magnesium Complexes

Table 5.2 summarizes the effect of forming Mg•GDP and Mg•GTP complexes at pH 7.5 on the phosphate modes. Of the shifted bands, those due to vibrations localized to one phosphate moiety are of particular interest, because it enables an assessment of the interaction between the cation and the phosphate group. From the table, it is found that the frequency shifts of $\upsilon_a(PO_2^-)$ are twice as large as the frequency shifts of $\upsilon_s(PO_2^-)$. For the terminal PO_3^{2-} group, the symmetric stretch mode is virtually unaffected by the interaction with Mg^{2+} while the antisymmetric mode is shifted up nearly 10 cm^{-1} (Table 5.2). The difference in frequency shift might be related to the strength of Mg^{2+} interaction coordination. However, the difference between the two modes (symmetric and antisymmetric stretch) in frequency shift is more likely due to the fact that the factors which determine the frequencies of these modes involve not only the force constant and effective reduced mass of the atoms contributing to the motion but also to the geometry of the bonds. This is certainly true for the terminal $-PO_3^{2-}$ groups. In this case, the P••O••P bond angle changes that occur when the non-bridging P••O bond orders are changed yield opposite effects on the frequency of $\upsilon_s(\gamma\text{-}PO_3^{2-})$ but are additive in the frequency changes of $\upsilon_a(\gamma\text{-}PO_3^{2-})$ (Deng, Wang, Callender, and Ray, unpublished results). Hence a very small change in frequency may be observed for the symmetric mode even when the P••O bond undergoes substantial bond polarization.

At pH 7.5, the diphosphate chain of Mg•GDP is composed of one $>PO_2^-$ and one $-PO_3^{2-}$ group. Upon Mg^{2+} complex formation with GDP, the frequencies of $\upsilon_a(\alpha\text{-}PO_2^-)$ and $\upsilon_s(\alpha\text{-}PO_2^-)$ are shifted up by 10 and 5 cm^{-1}, respectively (Table 5.2). The antisymmetric stretch mode, $\upsilon_a(\beta\text{-}PO_3^{2-})$, of the $\beta\text{-}PO_3^{2-}$ group shifts up by 8 cm^{-1} while the symmetric mode $\upsilon_s(\beta\text{-}PO_3^{2-})$ is virtually unshifted. Hence, these results show that Mg^{2+} binds to both phosphate groups in a bidentate manner.

The γ-phosphate group of Mg•GTP is unprotonated at pH 7.5 so that the triphosphate chain is composed of two $>PO_2^-$ groups and one $-PO_3^{2-}$ terminal group. In forming the Mg•GTP complex, the $\upsilon_a(\gamma\text{-}PO_3^{2-})$ and $\upsilon_s(\gamma\text{-}PO_3^{2-})$ modes shift 9 and 0 cm^{-1} respectively, about the same as $\upsilon_a(\beta\text{-}PO_3^{2-})$ and $\upsilon_s(\beta\text{-}PO_3^{2-})$ observed in GDP (8, -2 cm^{-1} respectively, Table 5.2). This indicates that Mg^{2+} interacts with $\gamma\text{-}PO_3^{2-}$. For the two $>PO_2^-$ groups in Mg•GTP, the frequency shifts of $\upsilon_a(\beta\text{-}PO_2^-)$ and $\upsilon_a(\alpha\text{-}PO_2^-)$ of 12 and 14 cm^{-1}, respectively, are larger than that of the $>PO_2^-$ group of Mg•GDP (10 cm^{-1}, Table 5.2). Such large frequency shifts indicates that Mg^{2+} binds tightly to both the $\alpha\text{-}PO_2^-$ and $\beta\text{-}PO_2^-$ groups in Mg•GDP. We therefore conclude that the Mg•GTP 1:1 complex at pH 7.5 has Mg^{2+} bound in a tridentate manner to the α,β and γ phosphate groups. Such a solution binding pattern is not necessarily the same as found in proteins. For example, X-ray crystallographic studies of p21, a small guanine binding protein, suggest that p21•Mg•GTP forms a β,γ-bidentate coordination in the active site of the enzyme and p21•Mg•GDP forms a β-monodentate coordination (Tong et al., 1991; Pai et al., 1990).

The present results suggest that the structure of Mg•GTP is aqueous solution is different than that of Mg•ATP, a conclusion reached by previous Raman and infrared spectroscopic studies (Takeuchi et al., 1988). For Mg•ATP, the frequency shifts of $\upsilon_s(\alpha\text{-}PO_2^-)$, $\upsilon_a(\alpha\text{-}PO_2^-)$ and $\upsilon_a(\beta\text{-}PO_2^-)$ at 8, 8, and 9

cm^{-1}, respectively, are close to that of GDP (5, 10, and 8 cm^{-1}), but the frequency shifts of $\upsilon_a(\alpha\text{-}PO_2^-)$ and $\upsilon_a(\beta\text{-}PO_2^-)$ of ATP complexed with Mg^{2+} (4 and 9 cm^{-1}) are smaller than that of GTP (12 and 14 cm^{-1}). This indicates that Mg^{2+} coordination differs between ATP and GTP.

5.8 Structure simulation of Mg•GDP and Mg•GTP

In parallel to the vibrational spectra, we probe the possibility of interpreting the vibrational spectra and the frequency shifts of the Mg^{2+} effect quantitatively by *ab initio* methods. This is done by performing ab initio calculations on methyl di- and triphosphate model compounds. These models are small enough so that calculations are feasible and yet retain the molecular features of the phosphate moiety which may provide useful information for the band assignments of the experimental spectra (Tsuboi, 1987). The model systems also allow the prediction of the spectral change when the configuration of the molecule is changed by external perturbation (Mg^{2+} effect, in our case) (Deng et al., 1992; Deng et al., 1994; Huang et al., 1996). The chemical bond lengths, especially those bonds which contain oxygen, are underestimated by *ab initio* methods at the Hartree-Fock level compared with observed values (Tsuboi et al., 1987). The overestimation of the calculated stretch frequencies (10%) is due to the neglect of electron correlation forces in the calculations, the limited basis set; also the calculations are done in the 'gas phase', which does not allow consideration of the interactions with solvent.

Since we focus on the stretch modes of phosphate groups, we use the methyl di- and tri-phosphate as the model compounds systems for the GDP, GTP normal mode analysis by the *ab initio* method. In this procedure, Cartesian force constants, frequency and the Raman intensity of methyl di-, triphosphates

are calculated by Gaussian 94 program at the HF/3-21+g* level (Frisch et al., 1994).

For isolated methyl diphosphate, the calculated frequencies of α-phosphate group are $\upsilon_s(\alpha\text{-}PO_2^-)$=1077 cm^{-1} and $\upsilon_a(\alpha\text{-}PO_2^-)$=1239 cm^{-1}, respectively (Table 5.3). These frequencies of $\alpha\text{-}PO_2^-$ group (1239, 1077 cm^{-1} in Table 5.3) are close to these experimental spectra lines (1205, 1089 cm^{-1}). For β-phosphate group, the symmetric stretch frequency $\upsilon_s(\beta\text{-}PO_3^{2-})$ is 987 cm^{-1} and the double degenerate antisymmetric stretch frequency $\upsilon_a(\beta\text{-}PO_3^{2-})$ is 1188 cm^{-1} (Table 5.2). It is obvious that those frequencies are overestimated.

To simulate the structure of the Mg•GDP, methyl diphosphate with sodium ion instead of magnesium is used as the model system since the calculation is 'gas phase', which is very sensitive to electronic distribution. The geometry optimization results in a conformation which shows that the Sodium binds to both α and β-phosphate groups. There are large frequency upshifts in the antisymmetric stretch modes of $\alpha\text{-}PO_2^-$ and $\beta\text{-}PO_3^{2-}$ groups (58, 52 cm^{-1}, Table 5.3) which are bigger than that observed in the spectra since the calculations are done in 'gas phase'. That the symmetric mode $\upsilon_s(\beta\text{-}PO_3^{2-})$is virtually unaffected is consistent with the experimental observation (Table 5.2). However, that the $\upsilon_s(\alpha\text{-}PO_2^-)$ of the $\alpha\text{-}PO_2^-$ group are almost unaffected (Table 5.3) is not consistent with the experimental result (Table 5.2). Our calculations show that the antisymmetric stretch modes are very sensitive to the binding of sodium ion while the symmetric modes are insensitive. The main reason probably is due to the ab initio force fields. Therefore, the simulated structure of Mg•GDP is a possible configuration of Mg•GDP in aqueous solution based on the overall consistent frequency shifts.

For the isolated methyl triphosphate, our *ab initio* calculation shows that $\alpha,\beta\text{-}PO_2^-$ groups are not strongly coupled. It is probably due to neglecting the

electron correlation which reduces the effective interaction range. Thus, the difference of the calculated frequencies $\upsilon_s(\alpha\text{-}PO_2^-)$ and $\upsilon_s(\beta\text{-}PO_2^-)$ is 31 cm^{-1} (Table 5.3) which is close to that of $\upsilon_s(\text{in-}PO_2^-)$ and $\upsilon_s(\text{out-}PO_2^-)$ 29 cm^{-1} (Table 5.2). Thus, the calculated symmetric and antisymmetric modes $\upsilon_s(\gamma\text{-}PO_3^{2-})$, $\upsilon_a(\gamma\text{-}PO_3^{2-})$ are overestimated (973, 1168 cm^{-1}, Table 5.3). The calculations also show that $\upsilon_a(\alpha\text{-}PO_2^-)$ is smaller than $\upsilon_a(\beta\text{-}PO_2^-)$. Ihis is consistent with the experimental result.

Ab initio calculation has also been performed to simulate the structure of the Mg•GTP. The model system is methyl diphosphate with a sodium ion instead of magnesium. The geometry optimization results in a conformation (Scheme 5.2) which shows that the sodium ion binds to α,β and γ-phosphate groups. Upon sodium binding to methyl triphosphate, there are large frequency upshifts in antisymmetric stretch modes of $\alpha,\beta\text{-}PO_2^-$ and $\gamma\text{-}PO_3^{2-}$ groups (51, 50, 49 cm^{-1}, see Table 5.3). The overestimation of frequency shifts is due to the calculation being done in "gas phase". The symmetric stretch mode of $\gamma\text{-}PO_3^{2-}$ group is almost unaffected. It is consistent with the observed spectra. The symmetric mode $\upsilon_s(\alpha\text{-}PO_2^-)$ is shifted up 11 cm^{-1} (Table 5.2). That the frequency shifts of the symmetric stretch modes $\upsilon_s(\beta\text{-}PO_2^-)$, $\upsilon_s(\alpha\text{-}PO_2^-)$ are not consistent with experimental results probably comes from the uncoupling of the two $\alpha,\beta\text{-}PO_2^-$ groups. Therefore, the simulated structure of Mg•GTP is a possible configuration of Mg•GTP in aqueous solution based on the overall consistent frequency shifts.

Material and methods GDP and GTP were purchased from Sigma Chemical Co. or Boerhinger Mannhein Co. and used without further purification. ^{18}O-GDP and ^{18}O-GTP were synthesized by Dr. Martin Webb. Raman spectra were measured by instrumentation described in the chapter 2.

All Raman spectra reported here, which were reproduced from Xiao's thesis (Xiao, 1995), were obtained by using the 568.2-nm line of a krypton ion laser (Coherent Radiation Inc., Palo Alto, CA). Band positions are accurate to ±2 cm^{-1}. The sample concentration of GDP and GTP (labeled or unlabeled) was 30mM. For the Mg•GDP and Mg•GTP 1:1 complexes, the concentration was 15mM. Infrared spectra were recorded on a Bruker IFS 66 infrared spectrophotometer equipped with a DTGS detector. The Barium Fluoride Polished 25mm x 2mm-window and 0.025-mm Teflon spacer were used. H_2O was used as the solvent and the background absorption due to the solvent was subtracted from the solution spectra. Band positions are accurate to ±2 cm^{-1}. The sample concentration of GDP and GTP (labeled or unlabeled) was 50mM. For the Mg•GDP and Mg•GTP 1:1 complexes, the concentration was 25mM.

Table 5.1. The frequencies of the phosphate modes in GDP and GTP and their ^{18}O labeled analogs, and their mode assignments at pH 5.0.

Species	Frequency (cm^{-1})	Assignment
GDP	1227	$\upsilon_a(\alpha,\beta\text{-}PO_2^-)$
	1109	$\upsilon_s(\text{in-}PO_2^-)$
	1080	$\upsilon_s(\text{out-}PO_3^{2-})$
GTP	1239	$\upsilon_a(\alpha,\beta,\gamma\text{-}PO_2^-)$
	1123	$\upsilon_s(\text{in-}PO_2^-)$
	1097	$\upsilon_s(\text{out-}PO_2^-)$
	1079	$\upsilon_s(\text{out-}PO_3^{2-})$
$(\beta\text{-}^{18}O_2;\beta\gamma\text{-}^{18}O)GTP$	1227	$\upsilon_a(\alpha,\gamma\text{-}PO_2^-)$
	1179	$\upsilon_a(\beta\text{-}P^{18}O_2^-)$
	1108	$\upsilon_s(\text{in-}PO_2^-)$
	1080	$\upsilon_s(\text{out-}PO_2^-)$
	1050	$\upsilon_s(\text{out-}PO_2^-)$
$(\gamma\text{-}^{18}O_3)GTP$	1235	$\upsilon_a(\alpha,\beta\text{-}PO_2^-)$
	1175	$\upsilon_a(\gamma\text{-}P^{18}O_2^-)$
	1120	$\upsilon_s(\text{in-}PO_2^-)$
	1079	$\upsilon_s(\text{out-}PO_2^-)$
	1050	$\upsilon_s(\text{out-}PO_2^-)$

Table 5.2. The frequencies of the phosphate modes in GDP and GTP and their ^{18}O labeled analogs, their mode assignments, and frequency shifts on complexation with Mg^{2+} at pH 7.5.

Species	Frequency (cm^{-1})	Assignment	Shift (cm^{-1})
GDP	1205	$\upsilon_a(\alpha\text{-}PO_2^-)$	10
	1089	$\upsilon_s(\alpha\text{-}PO_2^-)$	5
	1115	$\upsilon_a(\beta\text{-}PO_3^{2-})$	8
	943	$\upsilon_s(\beta\text{-}PO_3^{2-})$	-2
GTP	1233	$\upsilon_a(\alpha,\beta\text{-}PO_2^-)$	14
	1116	$\upsilon_s(\text{in-}PO_2^-)$	6
	1087	$\upsilon_s(\text{out-}PO_2^-)$	1
	1119	$\upsilon_a(\gamma\text{-}PO_3^{2-})$	9
	927	$\upsilon_s(\gamma\text{-}PO_3^{2-})$	0
$(\beta\text{-}^{18}O_2;\beta\gamma\text{-}^{18}O)GTP$	1220	$\upsilon_a(\alpha\text{-}PO_2^-)$	14
	1190	$\upsilon_a(\beta\text{-}P^{18}O_2^-)$	12
	1102	$\upsilon_s(\text{in-}PO_2^-)$	5
	1060	$\upsilon_s(\text{out-}PO_2^-)$	5
$(\gamma\text{-}^{18}O_3)GTP$	1229	$\upsilon_a(\alpha,\beta\text{-}PO_2^-)$	14
	1116	$\upsilon_s(\text{in-}PO_2^-)$	6
	1087	$\upsilon_s(\text{out-}PO_2^-)$	1
	1082	$\upsilon_a(\gamma\text{-}P^{18}O_3^{2-})$	6
	900	$\upsilon_s(\gamma\text{-}P^{18}O_3^{2-})$	-2

Table 5.3. Frequency Shifts on Complexation with Na^+ simulated by ab initio method (base set hf/3-21+g*).

	Frequency[a]	Mode	Shift[a]
Methyl Di-	1239	$\upsilon_a(\alpha\text{-}PO_2^-)$	+58
phosphate	1077	$\upsilon_s(\alpha\text{-}PO_2^-)$	-1
	1188	$\upsilon_a(\beta\text{-}PO_3^{2-})$	+52
	987	$\upsilon_s(\beta\text{-}PO_3^{2-})$	-3
Methyl Tri-	1280	$\upsilon_a(\beta\text{-}PO_2^-)$	+50
phosphate	1252	$\upsilon_a(\alpha\text{-}PO_2^-)$	+51
	1087	$\upsilon_s(\alpha\text{-}PO_2^-)$	+11
	1056	$\upsilon_s(\beta\text{-}PO_2^-)$	+1
	1168	$\upsilon_a(\gamma\text{-}PO_3^{2-})$	+49
	973	$\upsilon_s(\gamma\text{-}PO_3^{2-})$	+1

[a] In units of cm^{-1}

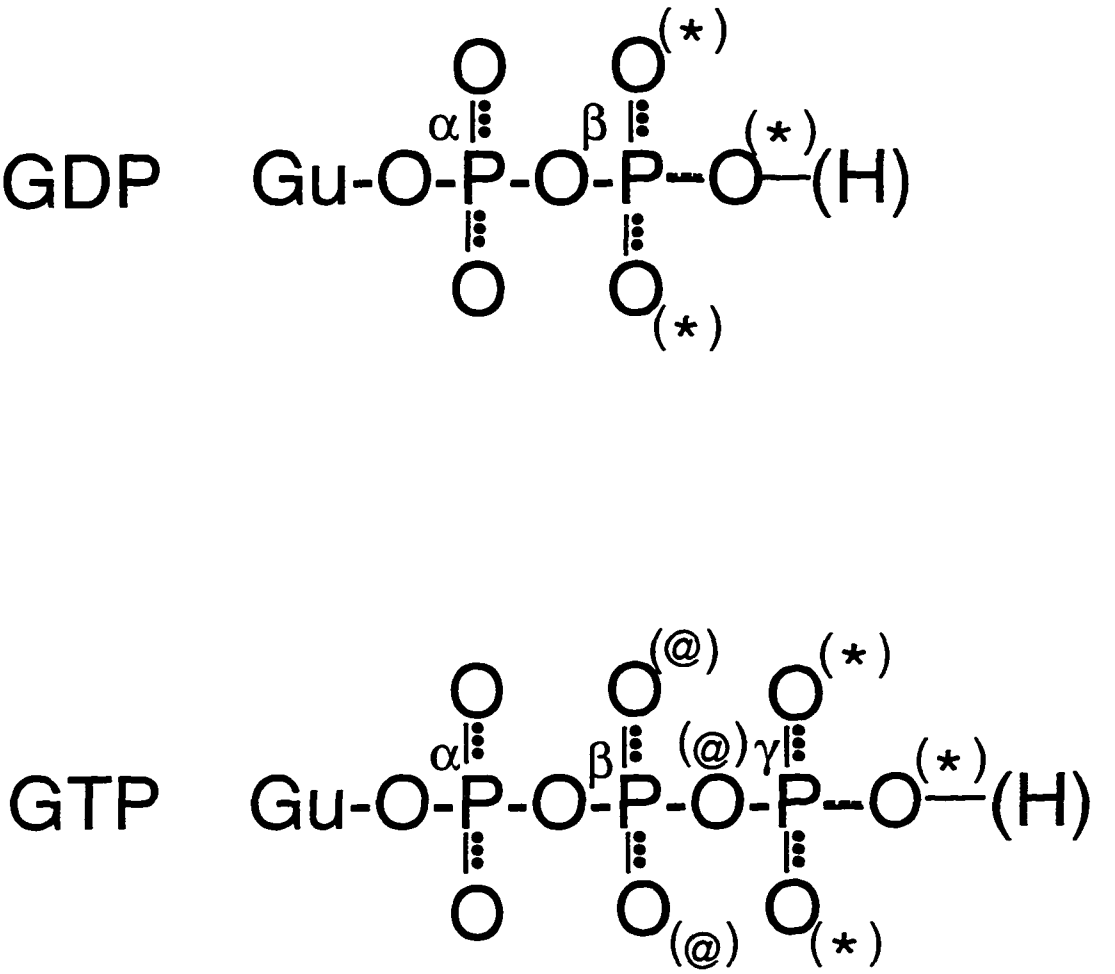

Scheme 5.1. GDP, GTP and their ^{18}O isotopomers in the fully ionized forms and protonated forms (-H). The oxygen atoms marked with (*) or (@) are substituted by ^{18}O for the corresponding isotopic derivatives.

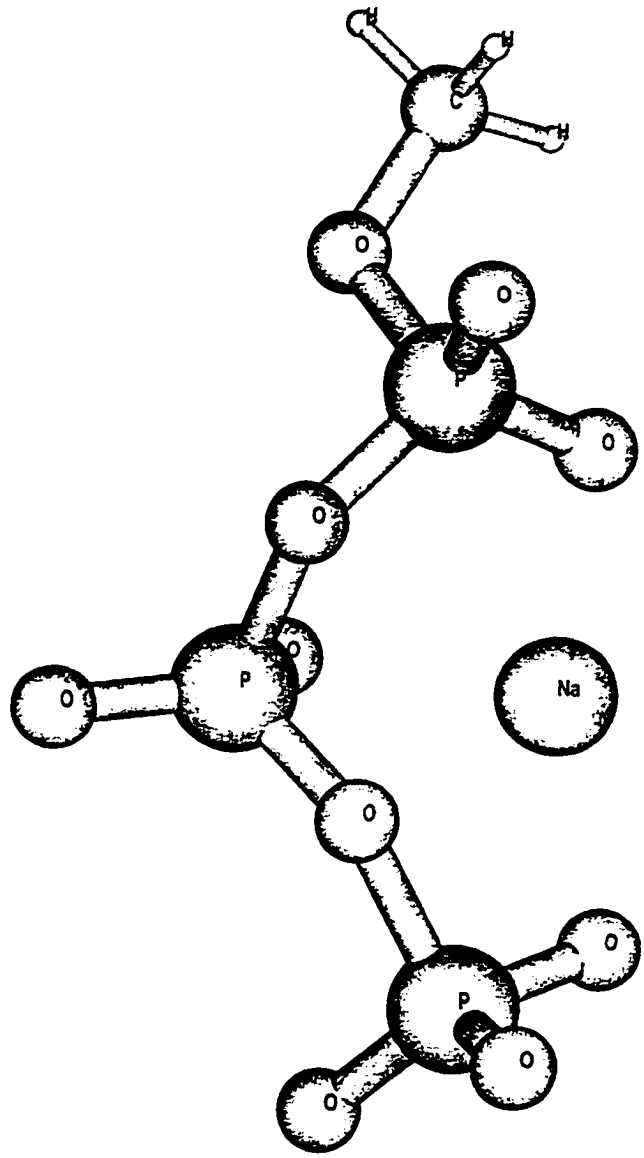

Scheme 5.2 A conformation of metal ion (Na^+) bound to α,β,γ-phosphate groups. Plotted by program Molden (M. W. Schmidt et al.).

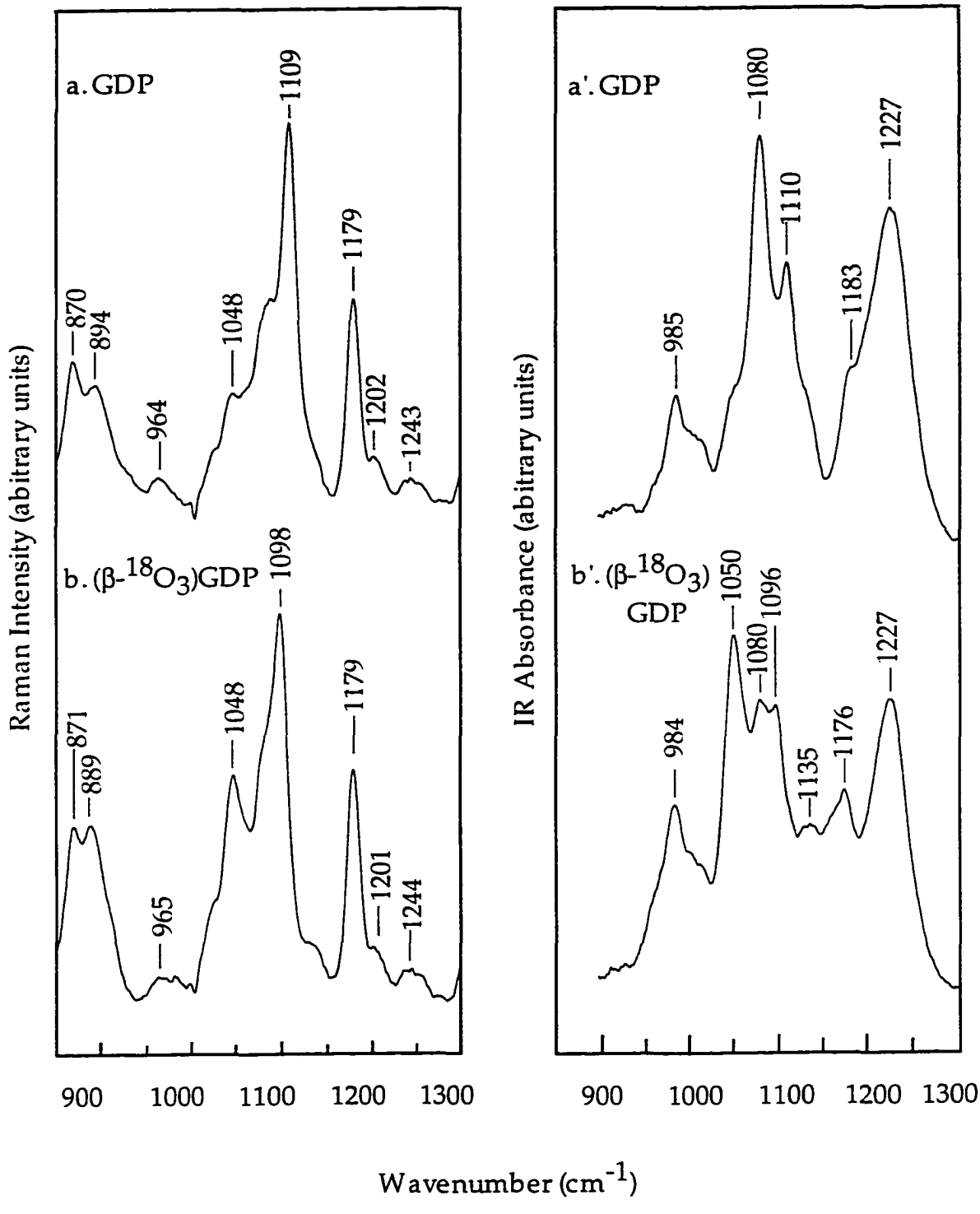

Figure 5.1. Raman (left side) and infrared spectra (right side) of (a,a') GDP and (b,b') (β-$^{18}O_3$)GDP in aqueous solution at pH 5.0. Raman spectra were adapted from Xiao's thesis (1995).

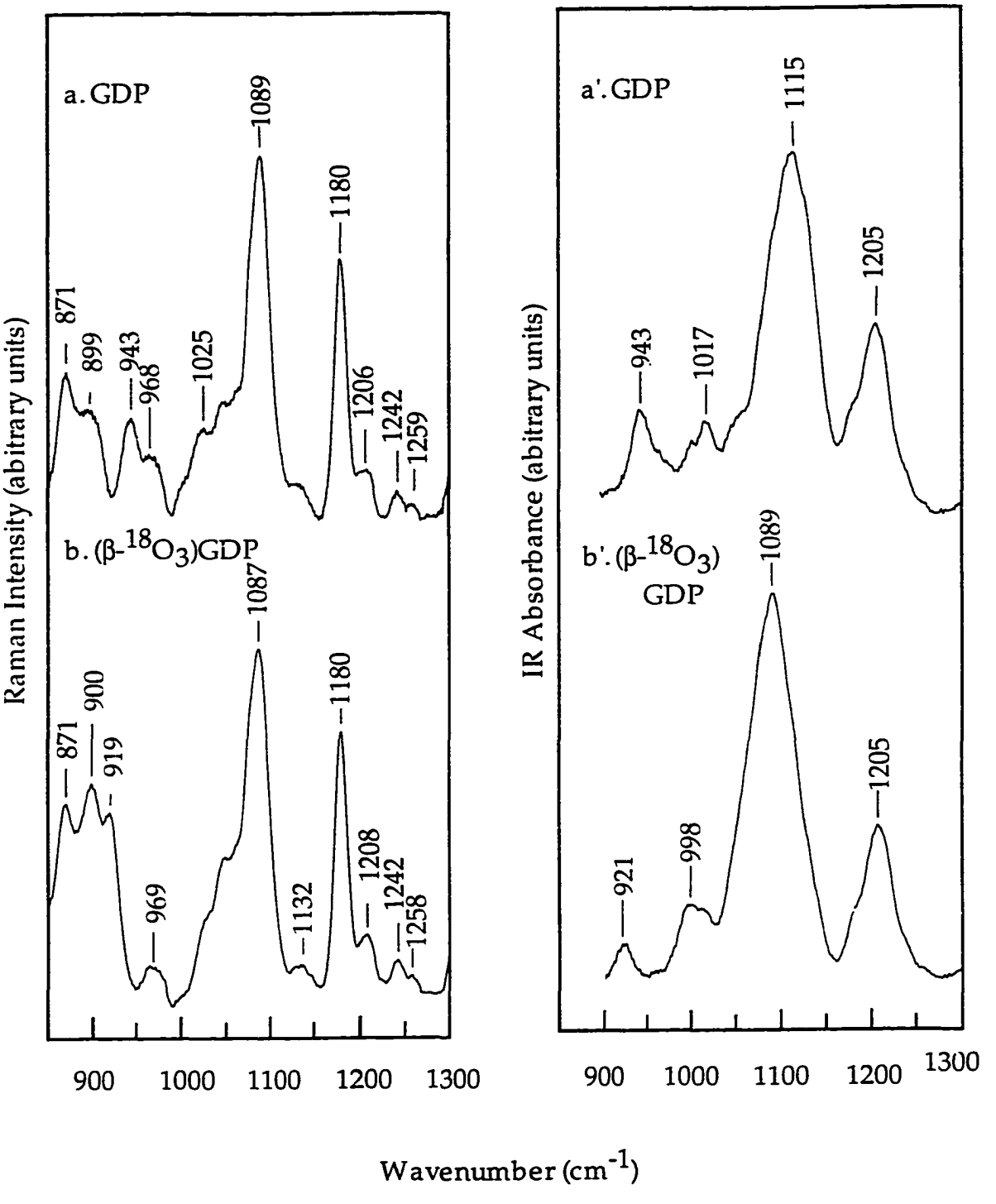

Figure 5.2. Raman (left side) and infrared spectra (right side) of (a,a') GDP and (b,b') (β-$^{18}O_3$)GDP in aqueous solution at pH 7.5. Raman spectra were adapted from Xiao's thesis (1995).

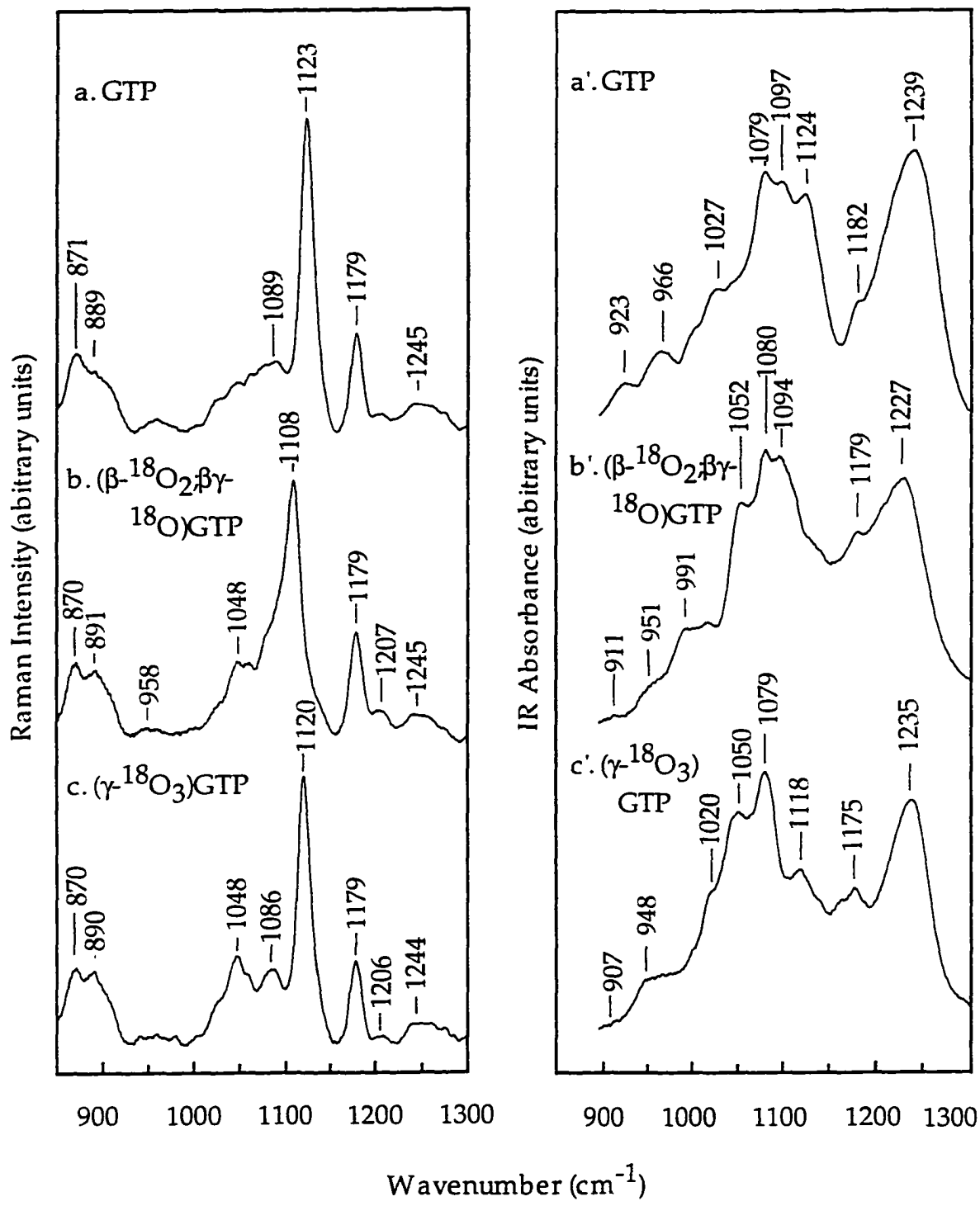

Figure 53. Raman (left side) and infrared spectra (right side) of (a,a') GTP, (b,b')(β-$^{18}O_2$,βγ-^{18}O) GTP and (c,c') (γ-$^{18}O_3$)GTP in aqueous solution at pH 5.0. Raman spectra were adapted from Xiao's thesis (1995).

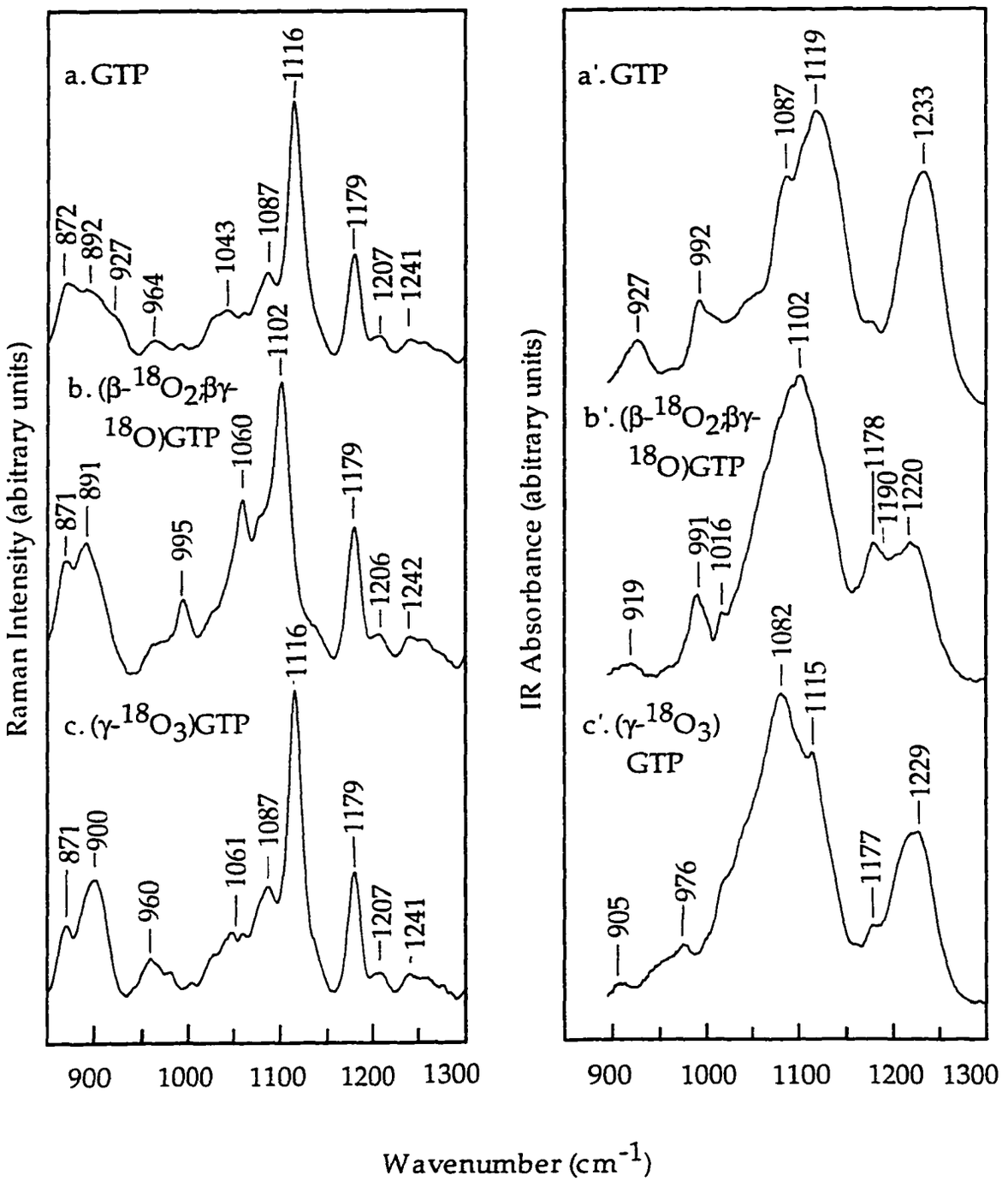

Figure 5.4. Raman (left side) and infrared spectra (right side) of (a,a') GTP, (b,b') (β-$^{18}O_2$,βγ-^{18}O)GTP and (c,c') (γ-$^{18}O_3$)GTP in aqueous solution at pH 7.5. Raman spectra were adapted from Xiao's thesis (1995).

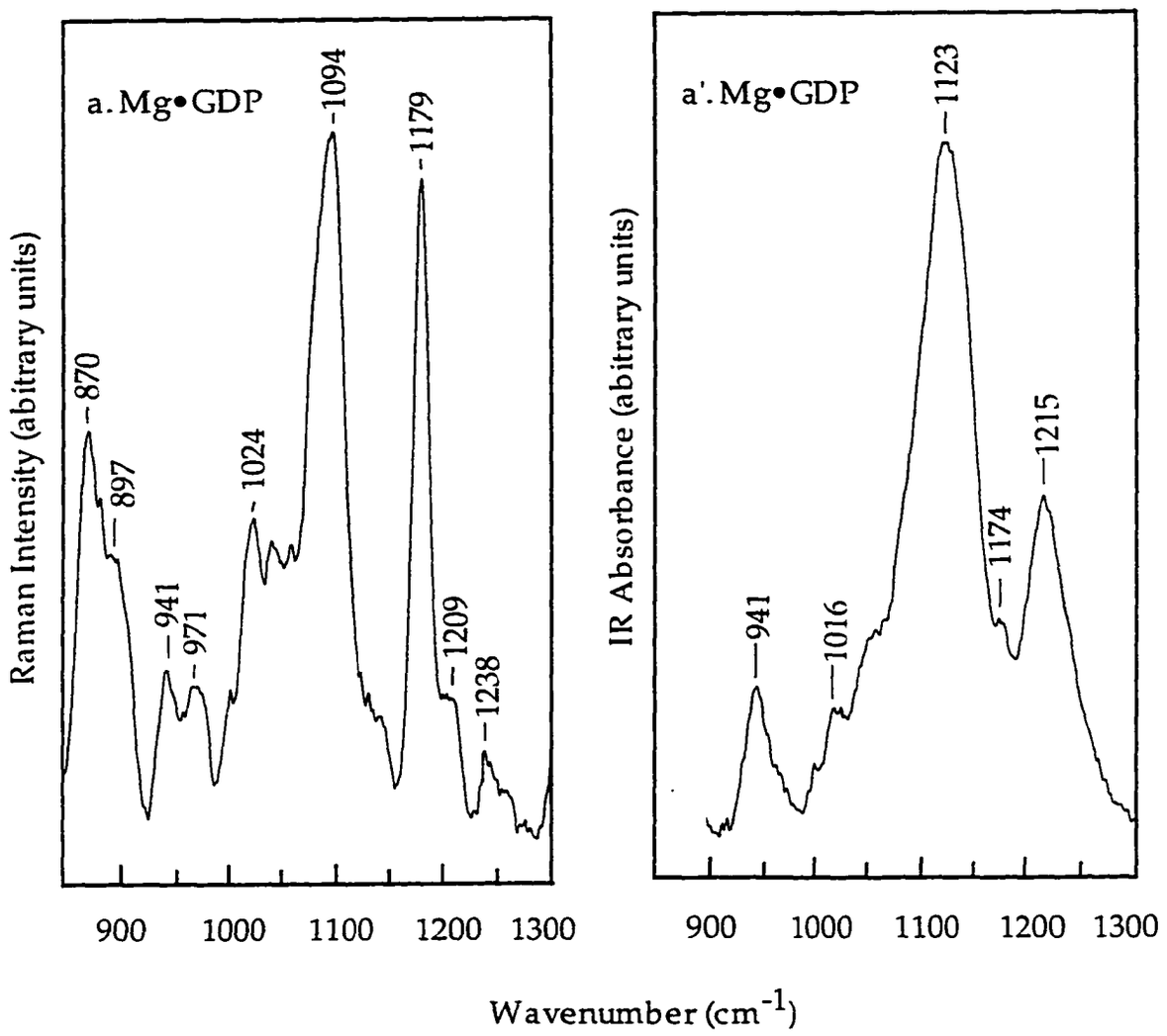

Figure 55. Raman (a, left side) and infrared spectra (a', right side) of Mg•GDP complex in aqueous solution at pH 7.5. The molar ratio of Mg^{2+} and GDP is 1:1. Raman spectrum was adapted from Xiao's thesis (1995).

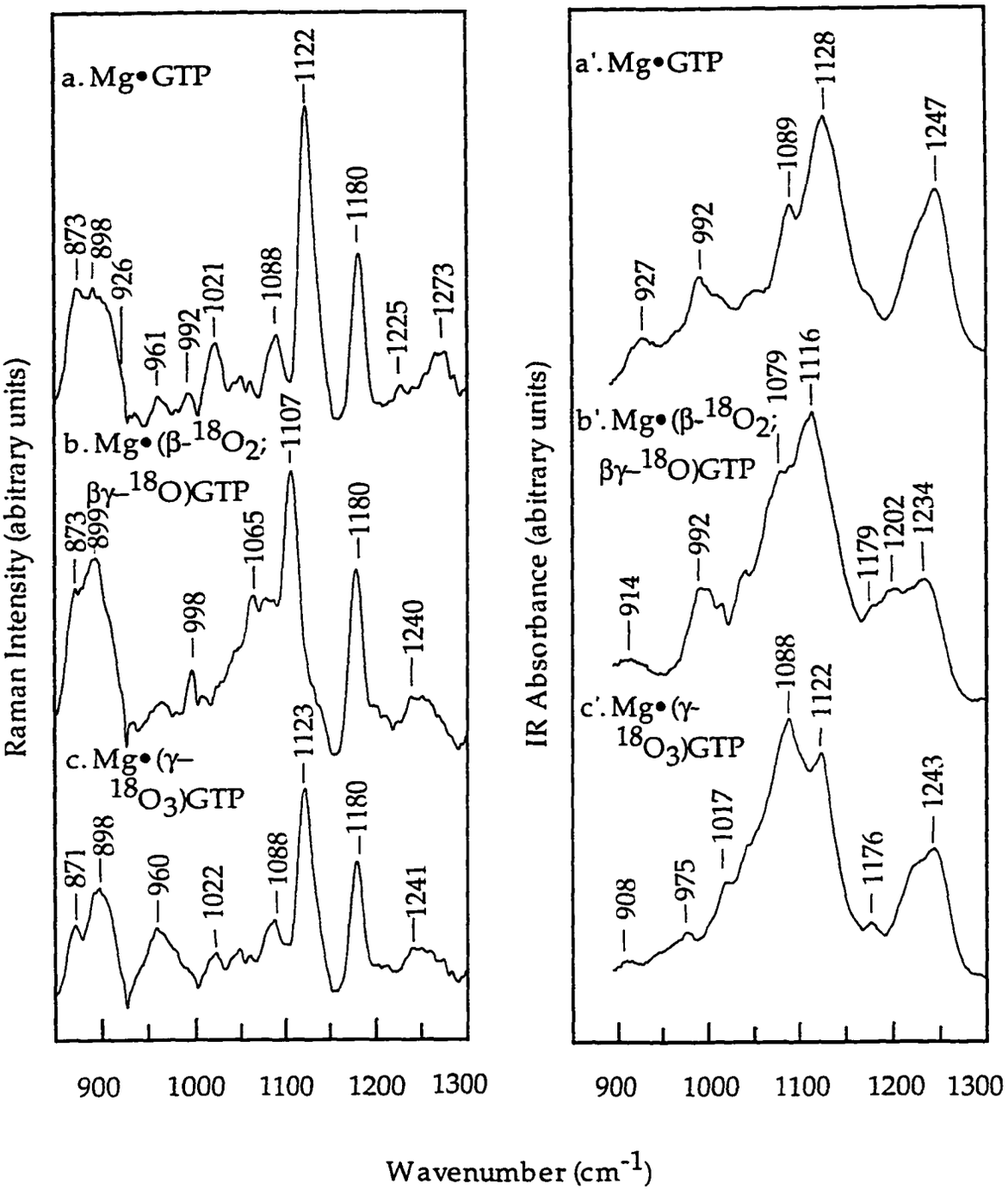

Figure 5.6. Raman (left side) and infrared spectra (right side) of (a,a')Mg•GTP complex, (b,b')Mg•(β-$^{18}O_2$,βγ-^{18}O)GTP and (c,c') Mg•(γ-$^{18}O_3$)GTP in aqueous solution at pH 7.5. The molar ratio Mg^{2+} and GTP and its isotopomers is 1:1. Raman spectra were adapted from Xiao's thesis (1995).

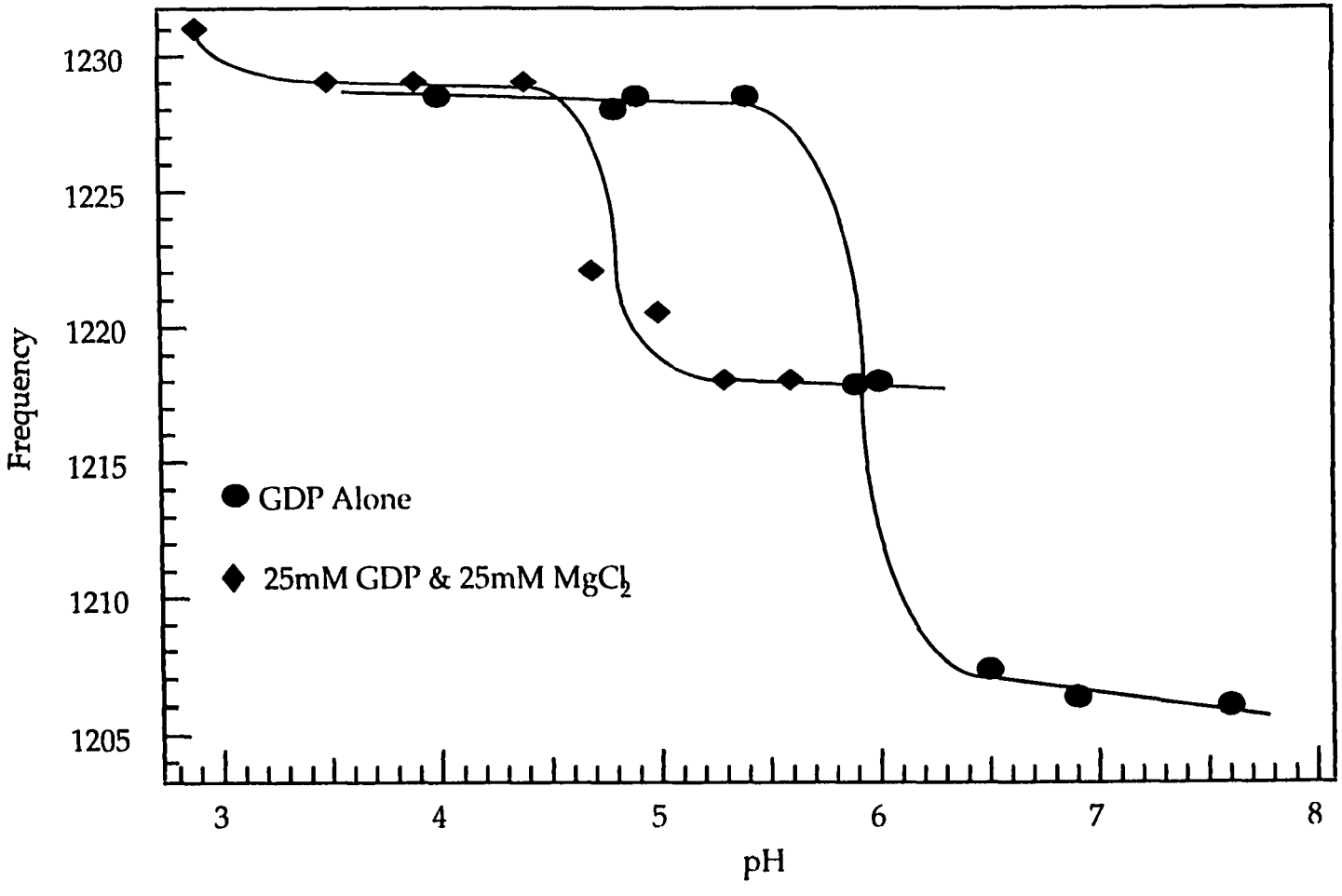

Figure 5.7 pH dependence of the center frequency of the infrared band of diphosphate line for GDP and Mg•GDP complex

CHAPTER 6

Raman Difference Studies of GDP and GTP Binding to c-Harvey ras

In general, GTP-binding proteins are in an 'active' state when complexed with GTP, and in an 'inactive' state when complexed with GDP. The longer a guanine nucleotide binding protein stays at an active state, the longer a certain signal will be transmitted and amplified. Therefore, the rate of GTP hydrolysis is of great importance for the right timing of many processes in a cell. This, in turn has led to great interest in understanding the mechanism of the GTPase reaction in those proetins.

The interactions between GDP/GTP and the apoprotein that are responsible for binding and bringing about protein GTPase activity are not clear, although there has been much progress from x-ray and other structural analyses (see ref. Sprang, 1997, for a review). It is generally believed that phosphoryl transfer involving monoester dianionic phosphate in aqueous solution is via a primarily dissociative pathway, with a metaphosphate-like transition state (Herschlag & Jencks, 1990 and references therein). Here, the bond breaking of the original ester P-O bond is almost complete before significant formation of the new P-O bond, and the sum of the bond orders of the broken and new bond is significantly less than one. However, the mechanism(s) in enzymes is far from clear, and both associative and dissociative transition states have been proposed (see e.g. Zhao & Zhang, 1996; Hollfelder & Herschlag, 1995; Deng et al., 1993; Schweins & Warshel, 1996).

In this chapter, we use Raman difference spectroscopy to study $p21^{ras}$, a protein which plays a central role in signal transduction pathways controlling cell proliferation. It has been shown that Raman difference spectroscopy (Callender & Deng 1994; chapter 4) is well suited for the determination of high

resolution PO bond lengths and bond orders of phosphate complexes in enzymes (Deng et al., 1993; Ray et al., 1993a; Ray et al., 1993b). In such studies, the Raman spectrum of the protein-phosphate complex is measured as is that of the protein. The difference spectrum contains bands arising from the phosphate group. This procedure cannot be used in our study of p21 because this enzyme is unstable without a bound ligand. We therefore have employed isotope editing procedures in this study. The bound nucleotide is replaced by isotopically (^{18}O) labeled nucleotide, and the spectra of the protein-nucleotide and protein-(labeled) nucleotide are taken (Manor et al., 1991; Weng et al., 1994). Bond lengths and bond orders of the nonbridging P$\underline{\bullet\bullet}$O bonds are determined from empirical correlations relating the vibrational stretch frequencies to these quantities (chapter 4; Ray et al., 1993a).

We analyze here the previously obtained Raman difference spectra of GDP and GTP bound to the $p21^{ras}$ protein (Xiao, 1995). Assignemnt of the Raman bands in the ^{18}O derived difference spectra are made on the basis of comparisons to like spectra of GDP/GTP in aqueous solution (chapter 5), band widths and intensities that vary for various normal modes, and the ^{18}O frequency shifts that are evident in the difference spectra. There are substantial changes in the peak positions of many phosphate bands of GDP and GTP upon binding to p21, which have implications for both how these molecules bind to p21 as well as hydrolysis mechanism. The spectral changes are analyzed by employing both the previous empirical relationships between bond orders/lengths and frequencies, as mentioned above, as well as vibrational analysis from *ab initio* calculations.

The Raman spectra of GDP and GTP bound to the p21 protein using difference spectroscopy has been measured (Xiao, 1995). In previous studies (Manor et al., 1991; Weng et al., 1994), "isotope editing" techniques were used for

the measurements of nucleotides bound to the p21 and EF-Tu G-proteins. Since isotope labeling induces spectral shifts in the vibrational modes associated with motions of the labeled atom, all Raman bands, including those of the apoprotein and those of the bound nucleotide that do not involve the isotopic tag, cancel out in the difference spectrum. In our previous studies, the isotopic tag involved positions on the guanine ring in order to study the interactions between the guanine ring and the p21 protein (Manor et al., 1991; Weng et al., 1994). In the results reported here, difference spectra are obtained by ^{18}O labeling of the nucleotide P$\underline{\bullet\bullet}$O bonds and incorporating these nucleotides into the binding site to probe phosphate bond distortions induced by binding.

6.1 Raman Spectra of GDP

Figure 6.1a shows the Raman difference spectrum of GDP and (β-$^{18}O_3$)GDP with 1:1 molar $MgCl_2$ in aqueous solution at pH 7.5 (see chapter 5 for the ^{16}O- and ^{18}O-labeled spectra, Xiao, 1995). The ^{16}O-labeled associated bands show up as positive features while the ^{18}O spectra show up as negative bands in the difference spectrum, yielding what looks like positive/negative derivative features in most cases. The ^{18}O label typically shifts bands from P$\underline{\bullet\bullet}$O vibrations downward 20-40 cm^{-1}. For broad bands where the ^{16}O and ^{18}O band profiles overlap somewhat, there is some cancellation of intensity in the difference spectrum, and the peak frequencies observed in the difference spectrum can be shifted from their proper position (apparently shifting up in the ^{16}O part of the derivative-looking band and shifting down in the ^{18}O part of the difference couple for bands where ^{18}O labeling induces a downshift).

The assignments of the bands observed in the difference spectrum can be made on the basis previous vibrational studies of natural abundance and labeled GDP and GTP (chapter 5). At pH 7.5, the diphosphate moiety of GDP is

composed of a $>PO_2^-$ group and a PO_3^{2-} terminal group. The PO_3^{2-} group has approximately C3v symmetry which leads to a symmetric P••O stretch mode, $\upsilon_S(\beta\text{-}PO_3^{2-})$, and a doubly degenerate antisymmetric P••O stretch mode, $\upsilon_a(\beta\text{-}PO_3^{2-})$. The $>PO_2^-$ group has approximate C_{2v} symmetry which leads to a symmetric stretch mode, $\upsilon_S(\alpha\text{-}PO_2^-)$, and an antisymmetric mode $\upsilon_a(\alpha\text{-}PO_2^-)$. In addition, there are P-O single bond stretch modes of P-O-P linkage.

Three derivative-like bands at 946/900, 1001/990, and 1101/1080 cm^1 (the high frequency denoting the ^{16}O peak position and the low frequency denoting the ^{18}O position) arise from the symmetric P••O stretch mode, $\upsilon_S(\beta\text{-}PO_3^{2-})$ of the $\beta\text{-}PO_3^{2-}$ group, a mode involving significant P-O stretch mode υ(P-O) of the $P\alpha$-O-Pβ linkage, and the symmetric stretch mode $\upsilon_S(\alpha\text{-}PO_2^-)$ of the $\alpha\text{-}PO_2^-$ group, respectively. The assignment of the 1001/990 cm^{-1} couple is based upon the Raman difference spectrum of GDP and ($\alpha\beta\text{-}^{18}O;\beta\text{-}^{18}O_3$)GDP since a strong derivative feature appears at 1002/982 cm^{-1} (unpublished data). Another mode that contains significant P-O stretch motion of the $P\alpha$-O-Pβ linkage is found at approximately 941 cm^{-1} (chapter 5), which shifts down in ($\beta\text{-}^{18}O_3$)GDP to yield the prominent 921 cm^{-1} negative band in the difference spectrum. This assignment is consistent with the Raman difference spectrum of GDP and ($\alpha\beta\text{-}^{18}O;\beta\text{-}^{18}O_3$)GDP in which the 921-$cm^{-1}$ negative bands shifts down to 895-cm^{-1}, overlapping the negative band at 900-cm^{-1} (unpublished data). The positions and assignments of the bands are summarized in Table 6.1.

Figure 6.1b shows the difference spectrum formed between Mg•GDP and Mg•($\beta\text{-}^{18}O_3$)GDP when bound to wild type p21. The spectral features are generally sharper than their solution counterparts, which shows that there is less conformational flexibility for the bound nucleotides and concomitantly less heterogeneous band broadening. There are three major derivative-like bands at 919/886, 996/960 and 1101/1071 cm^{-1} (Figure 6.1b), respectively. These are

very similar to the solution bands observed at 945/921, 1001/982, 1101/1080 cm^{-1} (Figure 6.1a), and they can be assigned as the corresponding mode found in solution. There is an additional feature at 870/854 cm^{-1} which remains unassigned. The shifts of the bands of bound GDP from their respective solution positions are given in Table 6.1. The most important result is that both the symmetric stretch, $\upsilon_S(\beta\text{-}PO_3^{2-})$, and the antisymmetric stretch, $\upsilon_a(\beta\text{-}PO_3^{2-})$, from previous FT-IR studies (Cepus et al., 1997, see Table 6.1) undergo substantial frequency shifts when GDP binds to p21 as does $\upsilon_a(\alpha\text{-}PO_2^-)$. X-ray crystallographic studies shows that the only interaction between the α-phosphate group of the bound GDP molecule and protein is a hydrogen bond between an oxygen atom on the α-phosphate and the main-chain amide group of residue Aln18 (Tong, et al., 1991). In comparison, the β-phosphate group interacts extensively with residues 13 to 17 of the p21 molecule as well as the bound Mg^{2+} (Tong et al., 1991) The downward shifts in frequency show that the non-bonded P••O bonds of the $\beta\text{-}PO_3^{2-}$ group are strongly polarized and indicate a strong interaction between apoprotein and the $\beta\text{-}PO_3^{2-}$ group. Below, the change in bond order of the non-bonded P••O bonds is calculated based on empirical relationships between bond order and vibrational frequencies.

6.2 Raman Spectra of GTP

Raman difference experiments were carried out using two ^{18}O derivatives(Xiao, 1995). In $(\beta\text{-}^{18}O_2;\beta\gamma\text{-}^{18}O)$GTP, the two non-bonded oxygens of the $\beta\text{-}PO_2^-$ moiety were labeled; in $(\gamma\text{-}^{18}O_3)$GTP, the three non-bonded oxygens of the $\gamma\text{-}PO_3^{2-}$ group were labeled. Figure 6.2 shows the Raman difference spectrum of GTP and $(\beta\text{-}^{18}O_2;\beta\gamma\text{-}^{18}O)$GTP with 1:1 $MgCl_2$ in aqueous solution (panel a) and the correponding difference spectrum between the natural abundance and labeled nucleotides bound to p21 (panel b). Figure 6.3 shows

the corresponding difference spectra using (γ-$^{18}O_3$)GTP. All studies were carried out at pH 7.5. At this pH, the triphosphate moiety of GTP is composed of two PO_2^- groups and one γ-PO_3^{2-} group. The γ-PO_3^{2-} group has approximately C3v symmetry which leads to a symmetric P$\underline{\bullet\bullet}$O stretch mode, $\upsilon_s(\gamma\text{-}PO_3^{2-})$, and a doubly degenerate antisymmetric P$\underline{\bullet\bullet}$O stretch mode, $\upsilon_a(\gamma\text{-}PO_3^{2-})$. The symmetric stretch motions of the two PO_2^- groups are often strongly coupled to form an in-phase combination υ_s(in-PO_2^-) and an out-of-phase combination υ_s(out-PO_2^-) while two antisymmetric modes, $\upsilon_a(\alpha\text{-}PO_2^-)$ and $\upsilon_a(\beta\text{-}PO_2^-)$, are not strongly coupled. The Raman intensity of the in-phase combination, υ_s(in-PO_2^-), is much higher than that of the other modes.

In the difference spectrum between the two Mg•GTP complexes (Figure 6.2a), with unlabeled and (β-$^{18}O_2$)nucleotide, there are four major derivative-like bands at 1123/1106, 1088/1065, 1019/999 and 921/894 cm^{-1}, which can be assigned to P$\underline{\bullet\bullet}$O stretch modes related with β-PO_2^- motions. Based on the frequency shifts of ^{18}O isotope labeling, relative Raman intensities, and the positions of the bands (chapter 5), the strongest and sharpest Raman derivative-like band at 1123/1106 cm^{-1} (Figure 6.2a) can be assigned to the in-phase combination, υ_s(in-PO_2^-), of the α,β-PO_2^- groups and the weak derivative-like band at 1088/1065 cm^{-1} (Figure 6.2a) is due to the out-of-phase combination, υ_s(out-PO_2^-). The frequency shifts of υ_s(in-PO_2^-) and υ_s(out-PO_2^-) (17, 23 cm^{-1}) are less than the ^{18}O shift of the P$\underline{\bullet\bullet}$O symmetric stretch modes in monophosphates (40-cm^{-1}, either monoionic or dianionic) indicating that there is considerable mixing to these stretch motions of motions on the PO atoms of the α,β-phosphate groups. The much weaker derivative-like band at 921/894 cm^{-1} (Figure 6.2a) most likely contains P-O stretch motions of the P_γ-O-Pβ linkage. The another derivative-like band at 1019/999 cm^{-1} (Figure 6.2a) thus assigned to a mode containing P-O stretch motions of the $P\alpha$-O-Pβ linkage (see Figure 5.6).

Figure 6.2b shows the Raman difference spectrum formed between Mg•GTP and Mg•(β-$^{18}O_2$;βγ-^{18}O)GTP when bound to wild type p21^{ras} at pH 7.5. Qualitatively, Figure 6.2b is very similar to Figure 6.2a. However, some peak positions are affected by the binding. There are four major derivative-like bands at 1123/1111, 1091/1060, 1025/1009 and 883/867 cm^{-1}, repectively, are just slightly shifted and maintain their relative intensities compared to the solution bands observed at 1123/1106, 1088/1065, 1019/999 and 921/894 cm^{-1} (Figure 6.2a). Hence, these bands can be assigned to shifted modes as assigned in the solution spectra. This is tabulated in Table 6.1.

Figure 6.3a shows the Raman difference spectrum of GTP and (γ-$^{18}O_3$)GTP with 1:1 $MgCl_2$ in aqueous solution at pH 7.5. Upon ^{18}O-substitution at γ-position, the stretch modes related with γ-PO_3^{2-} group are mostly affected. There are three major derivative-like bands at 1121/1105, 1019/1003 and 926/897 cm^{-1}, respectively, which can be assigned to the P$\underline{\bullet\bullet}$O/P-O stretch modes. Based on the ^{18}O isotope labeling, relative Raman intensities and the positions of the bands (see chapter 5), it is clear that the most prominent Raman derivative-like band at 926/897 cm^{-1} (Figure 6.3a) results from the symmetric stretch mode of the γ-PO_3^{2-} group. The 1121/1105-cm^{-1} derivative-like band (Figure 6.3a), which is observed in the Figure 6.2a, is the in-phase combination υ_s(in-PO_2^-) of α,β-PO_2^- groups. The much weaker derivative-like band at 1019/1003 cm^{-1} (Figure 6.3a), which is very similar to 1019/999 cm^{-1} band in Figure 6.2a, is thus assigned as involving P-O stretch motions of the Pα-O-Pβ linkage (chapter 5).

Figure 6.3b shows the Raman difference spectrum formed between Mg•GTP and Mg•(γ-$^{18}O_3$)GTP when bound with to p21^{ras} at pH 7.5. Qualitatively, Figure 6.3b is very similar to Figure 6.3a. However, some peak positions are shifted by the binding. There are three major derivative-like bands

at 1120/1108, 1024/1005 and 917/875 cm^{-1} (Figure 6.3b), respectively, are the shifted bands in the solution spectrum observed at 1121/1105, 1019/1003 and 926/897-cm^{-1} (Figure 6.3a). There is also an additional sharp feature at 885-cm^{-1} which is also observed in the p21:Mg•(^{16}O-β^{18}O)GTP difference spectrum of panel b, Figure 6.2. Its ^{18}O shift is only 10 cm^{-1} when the γ-PO_3^{2-} group is labeled as opposed to a 16 cm^{-1} shift when the β-PO_2^- group is labeled. This mode is thus fairly extended. All these results are tabulated in Table 6.1.

6.3 Ab initio vibrational analysis

Ab initio normal mode analyses were performed to assess how specific interactions contribute to the frequency shifts observed in the binding of GDP and GTP to p21. It is expected that Mg^{2+} interacts strongly with the oxygens and hence alter vibrational frequencies of the polar phosphate bonds. Such interactions will depend on the nucleotide-metal ion distance as well as its relative orientation. Hence, the phosphate frequencies are likely affected differently in solution versus in protein as the geometries are different. Moreover, it is of considerable interest to inquire how water-175, which is in line with the γ-PO_3^{2-} group of p21 bound GTP and is a candidate for the attacking nucleophile, interacts with the γ-phosphate group. All calculations were performed with the guanosine moiety replaced by a methyl group to save computer time. A sodium ion is used to model the effect of Mg^{2+} interacting with GDP(GTP) in aqueous solution and in p21. The reduced charge takes into account, somewhat, screening of the magnesium ion's charge by its surrounding medium. In this way, the modelling allows a semi-quantitative assessment of the spectral changes that take place when the spactial arrangement of the interacting group with respect to the nucleotide is changed and also provides some idea of the size of the spectral changes that can be expected (Deng et al.,

1992; Deng et al., 1994; Huang et al., 1996). It must be stressed that the goal of these calculations is not to determine specifically how the nucleotides bind with p21 from the vibrational data; that would require modeling of the entire binding site, which is outside our present scope. Rather, we are concerned with assessing which interactions are important, in what way they affect the phosphate stretch frequencies, and how symmetric and antisymmetric modes are affected by a putative interaction. The symmetries of these modes are distinctly different and they shift quite differently depending on geometry.

The calculations presented here were performed at the HF/3-21g* level, which we assessed would be provide the most useful information for the following reasons. Chemical bond lengths, especially those bonds which contain oxygen, are underestimated by *ab initio* methods at the Hartree-Fock level compared with those observed values (Tsuboi et al., 1987). Moreover, calculated stretch frequencies are in error by about 10-20% due to the neglect of electron correlation forces in the calculations, the limited basis set (particularly severe for phosphorus), and also that the calculations are done in 'gas phase' which do not treat the interactions with solvent. On the other hand, we have systematically determined all the vibrational frequencies of phosphates of varying ionization states in solution (i.e. PO_4^{3-}, HPO_4^{2-}, $H_2PO_4^{1-}$, H_3PO_4, and $CH_3PO_4^{2-}$) and their ^{18}O labeled analogs. The 'gas phase' *ab initio* calculations at the HF/3-21g* level provides an adequate force field over this entire range of ionization states, overestimating double bond stretches and the ^{18}O shifts by about 15% while underestimating single bond stretches and their ^{18}O shifts by approximately 6%. Trial runs with higher order basis sets at the Hartree Fock level did not significantly improve the agreement; post Hartree Fock calculations were somewhat better but, in view of the limited scope of the calculations herein, do not seem worthwhile. Finally, the HF/3-21g* level basis set does not treat

properly the observed coupling between the $-PO_2^-$ groups of GTP, probably because of the neglect of electron correlation, and results on these modes are not reported.

It is known that most of the phosphate stretch bands of GDP (or GTP) in solution are affected when the Mg•GDP complex is formed (chapter 5). In the analyses of the solution complexes, the geometries of the models used to simulate solution conditions were first optimized at the HF/3-21g* level, and the frequency calculations are then performed on the optimized geometries using the same basis set. The result of freely optimizing geometry indicates that the metal ion binds to both α,β-phosphate groups (structure **I**, Scheme 6.1), as is known from experimental studies. The P••O bond of the terminal β-PO_3^{2-} group directly interacting with the ion is longer than the other two, slightly breaking the C_{3v} symmetry of the terminal group. The C_{2v} symmetry of α-PO_2^- group is also slightly broken. The approximate symmetry classification of the resultant stretch modes were identified based on calculated Raman intensities and depolarization ratios. Table 6.2 lists the symmetric mode $\upsilon_s(\beta\text{-}PO_3^{2-})$ (1050 cm^{-1}) and average antisymmetric stretch mode, $\upsilon_a(\beta\text{-}PO_3^{2-})$ (1335 cm^{-1}). For the α-PO_2^- group, the character of the 1234 and 1368 cm^{-1} modes are also quite close to the symmetric and antisymmetric stretch modes for PO_2 with approximate C_{2v} symmetry, respectively. The shift in frequencies of the phosphate stretch modes induced by the metal ion as obtained by the *ab initio* procedure do a good job at reproducing the direction in the shift of the experimentally measured shifts, although the magnitude can be overestimated. For example, the relative shifts of the important terminal group (in cm^{-1}) are (calculated, measured): $\upsilon_s(\beta\text{-}PO_3^{2-})$ (-3, -2); $\upsilon_a(\beta\text{-}PO_3^{2-})$ (52, 8).

Crystallographic studies of GDP bound to p21 indicate that the binding site magnesium lies outside of the β-phosphate group so that the sodium interacts

only with the one oxygen atom of the β-phosphate group (structure **II**). To simulate the Mg•GDP (and GTP) bound to p21, the metal ion was placed at various positions relative to the phosphate moiety, restricted so as to be close to the position determined by the x-ray crystallographic studies of p21•GDP. The P••O stretch frequencies of the β-PO_3^{2-} group is quite sensitive to the position of the metal ion since the contribution from the interaction between negative charges of -PO_3^{2-} and positive charge of M^+ changes the O••P••O bond angle significantly. The position of the metal ion that is most consistent with the data is one where the M^+-O-P angle is about 20° from that reported in the x-ray structure; this result is tabulated in Table 6.2. The calculated υ_s(β-PO_3^{2-}) mode of the p21•GDP/M^+ shifts down by 34-cm^{-1} compared to solution model structure while υ_a(β-PO_3^{2-}) shifts down 30-cm^{-1}. This can be compared to the shifts found experimentally of -27 and -23, respectively (Table 6.1). The shifts found for the α-PO_2^- phosphate stretches are also in very satisfactory agreement with the experimental shifts (compare Table 6.1 and 6.2). Therefore, the present experimental results, and the simulations, are in reasonable agreement with previous conclusions that Mg^{2+} binds to both α,β-phosphate groups in aqueous solution, while it binds to only the β-phosphate group in p21 (Tong, et al., 1991).

Similar procedures were performed for the Mg•GTP 1:1 complex (solution model structure **III**) and for p21:Mg•GTP (model structure **IV**). The result of geometry optimization shows that the metal ion binds to the α,β and γ phosphate groups in a tridentate manner in the solution model (structure **III**); this is also in agreement with experimental results (chapter 5). The results are listed in Table 6.2. To simulate the Mg•GTP in p21 complex, a sodium ion was placed between γ- and β-phosphate groups so that the sodium interacts only γ,β-phosphate groups as found in the x-ray results. The geometry optimization leads to a conformation whereby the metal ion interacts only with the γ,β-

phosphate groups (structure **IV**), and the results for the γ-PO_3^{2-} group are reported in Table 6.2. The symmetric and antisymmetric stretch modes of the γ-PO_3^{2-} group are virtually unaffected by the metal ion placed in any geometry that is reasonably close to that found in the x-ray results compared to the values obtained from the solution model (**III**). Hence, neither mode shows much of a change in frequency in the calculations for various geometries locating the the metal ion from structure **III** to **IV**.

However, it is observed experimentally that the symmetric stretch shift decreases by 10 cm^{-1}, which is a substantial shift. Since, this observed frequency shift of the symmetric stretch mode $\upsilon_S(\gamma\text{-}PO_3^{2-})$ (Table 6.1) is not due to the interaction of Mg^{2+} with GTP at the binding site of p21, it is useful to examine alternative interactions. In the crystal structure of GppNp complexed with p21, water-175 is in-line with the phosphorus atom of the γ-phosphate of GTP group at a distance of 3.7 Å (Pai et al., 1990; Wittinghofer et al., 1991) . To further simulate the Mg•GTP moiety in p21, a water molecule inline with the bridging P-O bond of methyltriphosphate was placed at various distances, d, (structure **V**). The geometry of the complex, with the γ-phosphorus-water oxygen distance fixed at various lengths, was optimized at HF level with 3-21g* basis set. Table 6.3 shows the results of calculations on several model complexes with P---OH_2 distances ranging from 2.5 Å to 4.0 Å. As can be seen from the Table, the water molecule can have a rather large effect on the symmetric stretch mode. The reason for this is that the frequencies of the symmetric and antisymmetric stretch modes are functions of bond order (force constant) as well as the angle of the O••P••O bond (see structure **V**). The small interaction between the water molecule and the γ-PO_3^{2-} group does not much affect the bond order of the non-bridging P••O bonds (the P••O bond length is hardly affected; see Table 6.3). However, the the O••P••O bond angle 'flattens' out as the water molecule

approaches the central phosphorus atom, and this brings about systematic downward shifts in $\upsilon_S(\gamma\text{-}PO_3^{2-})$ and smaller shifts of $\upsilon_a(\gamma\text{-}PO_3^{2-})$. The best fit to the data is when the water oxygen is about 3.0 Å from the γ-phosphorus; the frequency shift of the symmetric stretch mode $\upsilon_S(\gamma\text{-}PO_3^{2-})$ (9-cm^{-1}) is close to that observed in the Raman difference spectrum (Table 6.1). The stretch frequency shifts are also listed under GTP protein complex (structure **V**), Table 6.2. The central conclusion from these calculations is that the shift observed for $\upsilon_S(\gamma\text{-}PO_3^{2-})$ when GTP binds to p21 is brought about by an in-line water molecule , rather than the Mg^{2+} ion. This strongly suggests that water-175 is weakly interacting with the phosphorus atom of the $\gamma\text{-}PO_3^{2-}$ group.

6.4 Bond Length/Bond Strength/Vibrational Frequency Relationships.

For the P••O and P-O bonds of phosphates (and some other metal and nonmetal oxides), there exist very accurate empirically derived relationships between bond length/bond order and bond order/vibrational frequency. In this case, bond order is based on valence bond so that the sum of all the bond orders over all the bonds to the central phosphorus atom is its valence, i.e. 5. The equations are (Brown & Wu 1976; Hardcastle & Wachs 1991; chapter 4) :

$$s_{PO} = (r_{PO}/1.620)^{-4.29} \qquad (6.1)$$

where s is the bond order of the PO bond given in vu (valence units) and the length of the PO bond, r_{PO}, is given in Å, and

$$s_{PO} = [0.175*\ln(224500/\upsilon)]^{-4.29} \qquad (6.2)$$

where υ is the frequency of the phosphate stretch. The symmetric stretch frequency can sometimes be used in s/υ correlations in phosphates (Ray et al., 1993). However, in general, and particularly in situations where the changes in the angle of the O••P••O bonds in the $-PO_3^{2-}$ group are important in affecting the observed shifts of $\upsilon_s(-PO_3^{2-})$ and $\upsilon_a(-PO_3^{2-})$ as here, it is necessary to substitute the so-call 'fundamental' stretch frequency into equation 6.2, which is the geometric average of the symmetric and antisymmetric stretch frequencies, i.e. $\upsilon = [(\upsilon_s^2+2\upsilon_a^2)/(3)]^{1/2}$ (for dianionic phosphate esters). Hence, bond lengths and bond orders can be determined if the stretch frequencies are known. The error in these relationships is estimated to be about ±0.04 vu and ±0.004 Å for bond orders and bond lengths, respectively, and better estimates of changes in the parameters for a given molecule as it goes from one environment to another (chapter 4).

Application of these equations for the β-phosphate of Mg•GDP 1:1 complex in aqueous solution, yields $\upsilon = 1066$ cm^{-1} (υ_s=942 cm^{-1} and υ_a=1123 cm^{-1}, Table 6.1), and an average bond order of 1.327 vu and an average bond length of 1.517 Å for each of the three non-bonded P••O bonds. For p21 bound Mg•GDP, the fundamental stretch frequency of the P••O bonds of the β-phosphate shifts down to $\upsilon = 1042$ cm^{-1} (Table 6.1). The shift to lower frequency for the P••O bonds translates to somewhat lower bond order and longer bond length for the three non-bridge terminal P••O bonds: an average bond order of 1.303 vu and an average bond length of 1.523 Å for each of the three non-bonded P••O bonds. This derived bond length for p21 bound Mg•GDP is in excellent agreement with the result from x-ray diffraction studies, 1.528 Å (Tong, et al., 1991). Our results show that the bond order of the nonbonded P••O bonds of the β-PO_3^{2-} group decrease by 0.024 vu when GDP binds to p21. Since the total bond order about the phosphorus atom can be

taken to a good approximation to sum to 5, this means that the bridging O-PO_3^{2-} bond increases by 0.072 vu. The β-PO_3^{2-} group of GDP is strongly stabilized when it binds to p21.

For Mg•GTP in aqueous solution, the fundamental frequency of the γ-phosphate is 1065 cm-1 from υ_s=927 cm^{-1} and υ_a=1128 cm^{-1} (see Table 6.1), which yields a bond order of 1.326 vu and an average bond length of 1.517 Å for each of the three non-bonded P••O bonds of the γ-phosphate group using Equations 6.1 and 6.2. For p21 bound Mg•GTP, the P••O bonds symmetric stretch frequency of γ-phosphate shifts down to 917 cm^{-1} (Table 6.1). The position of υ_a(γ-PO_3^{2-}) for bound GTP has not been definitively assigned. Two bands at 1128 and 1140-cm^{-1} band, repectively, are observed in IR studies of p21-caged Mg•GTP-->p21:Mg•GTP (Cepus et al., 1997), and both are good candidates for the antisymmetric stretch. However in either case, the change in bond order (or bond length) upon binding to the nonbonded P••O bonds is very small, -0.003 vu or +0.006 vu respectively, consistent with the *ab initio* calulations. The downward shift of 9 cm^{-1} for υ_s(γ-PO_3^{2-}) upon binding and the *ab initio* analysis above suggests that the in-line water molecule is interacting with the γ-phosphorus atom of bound GTP. Using Eq. 6.1 and a distance of 3.7 Å between the in-line water-175 and the γ-phosphorus atom determined from the X-ray studies of p21 bound GppNp (Pai et al., 1990; Wittinghofer et al., 1991) , the bond order[3] of this incipient bond is 0.029 vu.

While the so-called fundamental frequency of a symmetric/antisymmetric set depends chiefly on force constant, we have shown that the symmetric and antisymmetric modes depends on the angle between the O••P••O bonds as well as the P••O stretch force constant (chapter 4). Hence, the angle between the O••P••O bonds can be calculated from measured values of the symmetric and antisymmetric stretch frequencies (θ in structure V). For the Mg•GTP 1:1

aqueous solution, υ_S=927 cm^{-1} and υ_a=1128 cm^{-1}, which yields an angle of 111° for the O••P••O bond of the γ-PO_3^{2-} group. The antisymmetric mode freqency is not known with precision for GTP bound to p21. However, assuming that the P••O stretch force constant is not affected by binding (a reasonably good assumption give the the results of the modeling above), the O••P••O bond is calculated to increases by 1.0° to 112°. Hence, it can be concluded that the O••P••O bond angle of GTP 'flattens' slightly when it binds to p21. This is in good agreement with the quantum mechanical *ab initio* calculations on the Mg•GTP protein complex model, which yields a change of angle of 0.9° (3.0 Å row in Table 6.3).

6.5 Discussion

Vibrational frequencies are determined by the force constants within chemical bonds and the geometry of the atoms that make up a molecule. Hence, vibrational frequencies report on bond orders, bond lengths, and geometry. A clear result from our investigation is that the ionization state of GDP or GTP does not change from its solution value when these nucleotides bind to the ras protein. This is so because the frequencies associated with the stretch motions of the various P••O bonds of bound GDP and GTP are not altered to the extent that would indicate protonation of one or more of these bonds. Hence, we see no evidence for substrate assisted catalysis wherein bound GTP activates an attacking water molecule by abstracting a proton to form hydroxyl (Schweins & Warshel, 1996; Langen et al., 1992; Schweins et al., 1995). However, our results would not show a protonated GTP species if it is present in small amounts in equilibrium with a much larger concentration of non-protonated bound GTP. Moreover, if the abstraction occured late in the reaction pathway (and at some point in the phosphotransfer reaction the proton from the water molecule must

be transferred to the phosphate moiety), there would be no evidence of it in the bound ground state.

Divalent cations are generally located in the binding sites of nucleotide phosphotransferases and complex directly to oxygens of bound phosphates, thereby strongly affecting binding of GDP and GTP as well as GTPase activity (Gilman, 1987; John et al., 1993; Sprang 1997). For ras, Mg^{2+} forms a very tight complex with GDP, reducing, for example, the GDP dissociation rate by four orders of magnitude compared to Mg^{2+} free ras (John et al., 1993). On the other hand, the dissociation rate of GTP is enhanced by only about a factor of 10 in Mg^{2+} free ras (John et al., 1988).

On the basis of our difference Raman spectroscopy studies of the ras•Mg•GDP and ras•Mg•GTP complexes, the following structural conclusions can be made. First, the frequency shifts of the specific P••O bonds of bound GDP indicate that Mg^{2+} interacts with ras bound GDP only with the β-phosphate group, in agreement with a previous EPR study (Feuerstein et al., 1987). This is in contrast to Mg•GDP complexes in solution, where vibrational studies indicate that there is a bidentate interaction to GDP to the α- and β-phosphates (chapter 5). Hence, the frequencies of β-PO_3^{2-} are decreased upon binding relative to Mg•GDP in solution while those of the α-PO_2^- group increase. This coordination pattern is in agreement with the x-ray studies of ras•Mg•GDP (Tong et al., 1991; Pai et al., 1990). It seems likely that the binding site Mg^{2+} ion is substantially responsible for the observed frequency shifts, and hence, a dominating factor in how the β-phosphate moiety of GDP interacts with the ras binding site. In the first place, although the x-ray structure of ras•Mg•GDP shows that there are a number of hydrogen bonds formed between binding site residues of ras and the β-PO_3^{2-} group of GDP, the partial charges on these are relatively very much smaller that that of Mg^{2+}, making

their electrostatic interactions correpondingly smaller. In addition, the *ab initio* calculations show that the interaction that Mg^{2+} has with GDP upon binding can easily account for the observed frequency changes. Nevertheless, the relative importance of the active site polar groups in affecting the electronic properties of bound nucleotides requires a systematic study, perhaps through the use of mutant proteins in vibrational studies like the current study and through modeling.

The non-bonded P••O bonds of the β-PO_3^{2-} group of bound GDP are strongly polarized upon binding to ras, reducing their bond order by 0.024 vu from the Mg•GDP solution value (equal to 1.327 vu), and increasing the average P••O bond length by 0.006 Å. This indicates a strong favorable electrostatic interaction between the binding site Mg^{2+} and GDP. Given the Brown and Wu paradigm (Brown & Wu 1976), which states that the sum of all bonds about a phosphorous atom sum to 5, the weakening of the nonbridging P••O bonds of the β-PO_3^{2-} group results in a strengthening of the bridging GMPO-PO_3^{2-} bond of 0.072 vu. Hence an interesting prediction from the present study is that the hydrolysis rate of GDP in ras should be greatly slowed compared to the rate in aqueous solution since the bridging bond is strengthened. In any case, it is clear that the terminal β-phosphate group of bound GDP interacts strongly with the ras binding site and that GDP is energetically stabilized. In contrast to bound GDP, the P••O bonds of the terminal -PO_3^{2-} group of GTP are not nearly as much affected by binding to ras. Importantly, spectroscopic studies (from IR, see ref. Cepus et al., 1997 & 1998) shows that the binding site Mg^{2+} maintains its interaction with the β-phosphorus group as judged by the shifts in the υ_a(β-PO_2^-) band from its solution value (Table 6.1). Hence, the bonds of the β-phosphorus groups of both bound GDP and GTP are strongly polarized, indicating a

substantial interaction with the ras binding site, while there is only a very small bond polarization of the P••O bonds of the γ-phosphorus group of bound GTP.

The frequencies of the symmetric and antisymmetric stretch modes of a $-PO_3^{2-}$ group are determined by a number of parameters, but two are by far most important: the force constant of the P••O bond (hence its bond order) and the O••P••O angle (ϑ in structure **V**, scheme 6.1) of the nonbonded P••O bonds (chapter 4). As shown by the modeling results and the analytical relationships relating these stretch frequencies to force constant and angle, the small 10 cm^{-1} downward shift of the symmetric stretch mode of bound GTP, $\upsilon_S(\gamma\text{-}PO_3^{2-})$, is well explained by a 1° increase in ϑ with little change in bond order. Hence, the structure of the $\gamma\text{-}PO_3^{2-}$ group of ras bound GTP is such that the three nonbonded P••O bonds approach a more planar arrangement compared to GTP in solution. The *ab initio* calculations suggest that the binding site Mg^{2+} is unable to produce even this small frequency shift for $\upsilon_S(\gamma\text{-}PO_3^{2-})$. Its geometry relative to the terminal phosphate group is such that the electrostatic interactions are calculated to produce negligible changes in the symmetric and antisymmetric stretch modes of the $\gamma\text{-}PO_3^{2-}$ group. On the other hand, a water molecule in line to the γ-phosphate, structure **V** of scheme 6.1, can reproduce just the experimentally observed shift because of their relative geometry. The *ab initio* calculations place the water molecule at a P—OH_2 distance of 3.0 Å to yield the correct shift in $\upsilon_S(\gamma\text{-}PO_3^{2-})$ (Table 6.3). This can be considered to be in good agreement with the 3.7 Å distance observed for water-175 in the ras•GppNp crystal structure, considering that our results are on the ras•GTP complex while the x-ray determined distance is of the ras•GppNp complex and also considering the inaccuracies in the calculations.

Generally, theories of phosphoryl transfer reactions for dianionic phosphate monoesters have a pentacoordinated phosphorous transition state in

which the nonbonded P••O bonds become planar and the leaving group and attacking nucleophile form apical bonds. Such a transition state is consistent for ras on the basis of crystal structures of guanine binding proteins with bound GDP•ALF_4^- (Sprang, 1997), which is believed to resemble the transition state of the pathway, and by studies of the hydrolysis stereochemistry in ras, which suggest a direct in-line transfer of the γ-phosphate from GTP to water with inversion of the configuration (Feuerstein et al., 1989). With this in mind, the 1° angle increase of the nonbonded O••P••O bonds of the γ-phosphate is quite significant. It is clear that the ground state of bound GTP is destabilized by its binding to ras in such a way that a small but a clear geometry change takes place that brings bound GTP closer to its transition state geometry. There has been much discussion of the role of Gln-61 in GTP hydrolysis. Mutations of this residue reduce the hydrolysis rate 10-fold or so, and it is within hydrogen bonding distance to water-175. Several possible catalytic roles have been advanced for this residue. One theory has this residue activating water-175 by abstraction of a proton to form the stronger hydroxyl nucleophile for attack. Our results suggest, rather, that it may have an important structural role in that it, and other residues interacting with water-175, hold this water close enough and tight enough to the phosphorus atom of the γ-phophate to cause a significant interaction between them. The calculations from the empirical relationships relating bond distance and bond order indicate a small incipient fifth bond between water-175 and the γ-phosphorus atom of GTP of approximately 0.03 vu. In addition to bringing the geometry of the bound GTP closer to its transition state, this interaction weakens the bridging GDPO-PO_3^{2-} bond in the ground state by a corresponding amount since most of the bond order formed by the phosphorus atom with water-175 is 'taken' from the bridging bond (see previous sections).

This study does not directly speak to the electronic nature of the transition state structure, that is whether it is dissociative or associative or in between (S_N2 like), because our results are on ground state complexes. However, the results are highly suggestive of a S_N2 like transition state where the bond making step is more or less synchronous with the bond breaking of the GDP leaving group, based on the following reasoning. Following the paradigm that the active sites of enzymes are designed to bind the transition state, it can then be expected that the bond distortions found in the ground state of the bound substrates are towards the transition state. Hence, the small formation of the incipient fifth bond between water-175 and corresponding weakening of the O–P bond between the GDP leaving group and the γ-phosphorus of bound GTP strongly suggests the synchronous motion of a S_N2 reaction. In addition as discussed above, the active site Mg^{2+} ion (with perhaps other active site residues) interacts strongly with the P••O bonds of the GDP leaving group β-phosphate rather than the γ-phosphate P••O bonds of bound GTP. The active site appears to be designed to hold and stabilize the GDP leaving group while allowing the phosphoryl moiety to move from the leaving group to the attacking (water) nucleophile. Finally, results on a Mg^{2+}•ADP•vanadate complex bound to the S1 subfragment of myosin, which is believed to resemble the transition state of the phosphoryl transfer reaction catalyzed by myosin (ATP -> ADP + phosphate), shows that the sum of the bond orders of the two apical bonds involving the attacking water molecule and the ADP leaving group is close to one, or again S_N2 like (see next chapter). Hence, assuming the reaction pathway of the ras and S1 enzymes are similar, and the active site structures are similar and both enzymes perform the same chemistry, this result reinforces the notion that the process in both proteins is S_N2 like.

Table 6.1. The frequencies (in cm^{-1}) of the phosphate modes of Mg•GTP in 1:1 complex in aqueous solution and their shifts for Mg•GDP/GTP bound to p21.

	mode	aqueous solution[a]	p21(Δυ)
GDP	$\upsilon_{st}(P\alpha\text{-}O\text{-}P\beta)$[b]	921	-28[e]
	$\upsilon_s(\beta\text{-}PO_3^{2-})$	942 (946)	-27[e]
	$\upsilon_{st}(P\alpha\text{-}O\text{-}P\beta)$[b]	1001	0[e]
	$\upsilon_s(\alpha\text{-}PO_2^-)$	1094 (1101)	0[e]
	$\upsilon_a(\beta\text{-}PO_3^{2-})$	1123	-23[c]
	$\upsilon_a(\alpha\text{-}PO_2^-)$	1215	+21[c]
GTP	$\upsilon_{st}(P\beta\text{-}O\text{-}P\gamma)$[b]	921	-38[e]
	$\upsilon_s(\gamma\text{-}PO_3^{2-})$	927	-10[e]
	$\upsilon_{st}(P\beta\text{-}O\text{-}P_g)$[b]	1019	+6
	$\upsilon_a(\gamma\text{-}PO_3^{2-})$	1128	?[d]
	$\upsilon_s(\text{in-}PO_2^-)$	1122	0[e]
	$\upsilon_s(\text{out-}PO_2^-)$	1088	+3[e]
	$\upsilon_a(\beta\text{-}PO_2^-)$	1247	-32[c]

[a]The number in parenthesis is the peak position observed in the solution difference spectra presented herein. This value is sometimes different that the position in the solution spectra due to some intenisty cancellation in the difference spectrum when the labeled and unlabeled bands are shifted by an amount smaller than their bandwidths (Chapter 5).

[b]The modes indicated by $\upsilon_{st}(P\alpha\text{-}O\text{-}P\beta)$ contain significant stretch motions of the Pα-O-Pβ linkage as indicated by their shifts in frequency upon ^{18}O labelling of the Pα-O-Pβ oxygen. Similarly for modes indicated by $\upsilon_{st}(P\beta\text{-}O\text{-}P\gamma)$.

[c]From ref. (Cepus et al., 1997; Cepus et al., 1998).

[d]There are two possible bands that could be assigned to $\upsilon_a(\gamma\text{-}PO_3^{2-})$, at 1128 or 1140 cm^{-1} (Cepus et al., 1997;Cepus et al., 1998, see text).

[e]From ref. (D. G. Xiao, 1995).

Table 6.2. Frequency shifts[a] of phosphate groups of Na•Methyldiphosphate (M^+•CH_3DP) and Na•methyltriphosphate (M^+•CH_3TP) calculated by *ab initio* methods to the HF/3-21g* level.

	mode	solution model	p21:GDP•M+	
		Structure **I**	Structure **II**	
M^+•CH_3DP	$\upsilon_s(\beta\text{-}PO_3^{2-})$	1050	-34	
	$\upsilon_a(\beta\text{-}PO_3^{2-})$	1335	-30	
	$\upsilon_s(\alpha\text{-}PO_2^{-})$	1234	-1	
	$\upsilon_a(\alpha\text{-}PO_2^{-})$	1368	+20	
		solution model	p21•GTP•M^+	p21•GTP•M^+•H_2O
		Structure **III**	Structure **IV**	Structure **V**
M^+•CH_3TP	$\upsilon_s(\gamma\text{-}PO_3^{2-})$	1000	+1	-9
	$\upsilon_a(\gamma\text{--}PO_3^{2-})$	1287	+2	-1

[a]All values are in cm^{-1}.

Table 6.3 The O••P••O angle, P_{γ}-O bond length, P••O bond length of γ-phosphate group as a function of water-methyltriphosphate distance in the model of the active site of p21•MgGTP complex from *ab initio* calculations in HF/3-21g* level.

Na•MeTP···OH_2 distance (Å)	$\Delta\upsilon_S(\gamma\text{-}PO_3^{2-})$	$\Delta\upsilon_a(\gamma\text{-}PO_3^{2-})$	O••P••O angle[a]	P••O bond length (Å)	P-O bond length (Å)
infinite	0	0	114.9	1.513	1.7187
4.0	-3	+2	115.3	1.512	1.7311
3.7	-4	+2	115.3	1.512	1.7331
3.5	-5	+2	115.4	1.512	1.7359
3.25	-6	+1	115.6	1.513	1.7394
3.00	-9	-1	115.8	1.513	1.7447
2.75	-12	-3	116.1	1.513	1.7528
2.50	-18	-8	116.6	1.515	1.7647

[a]bond angles are in degrees..

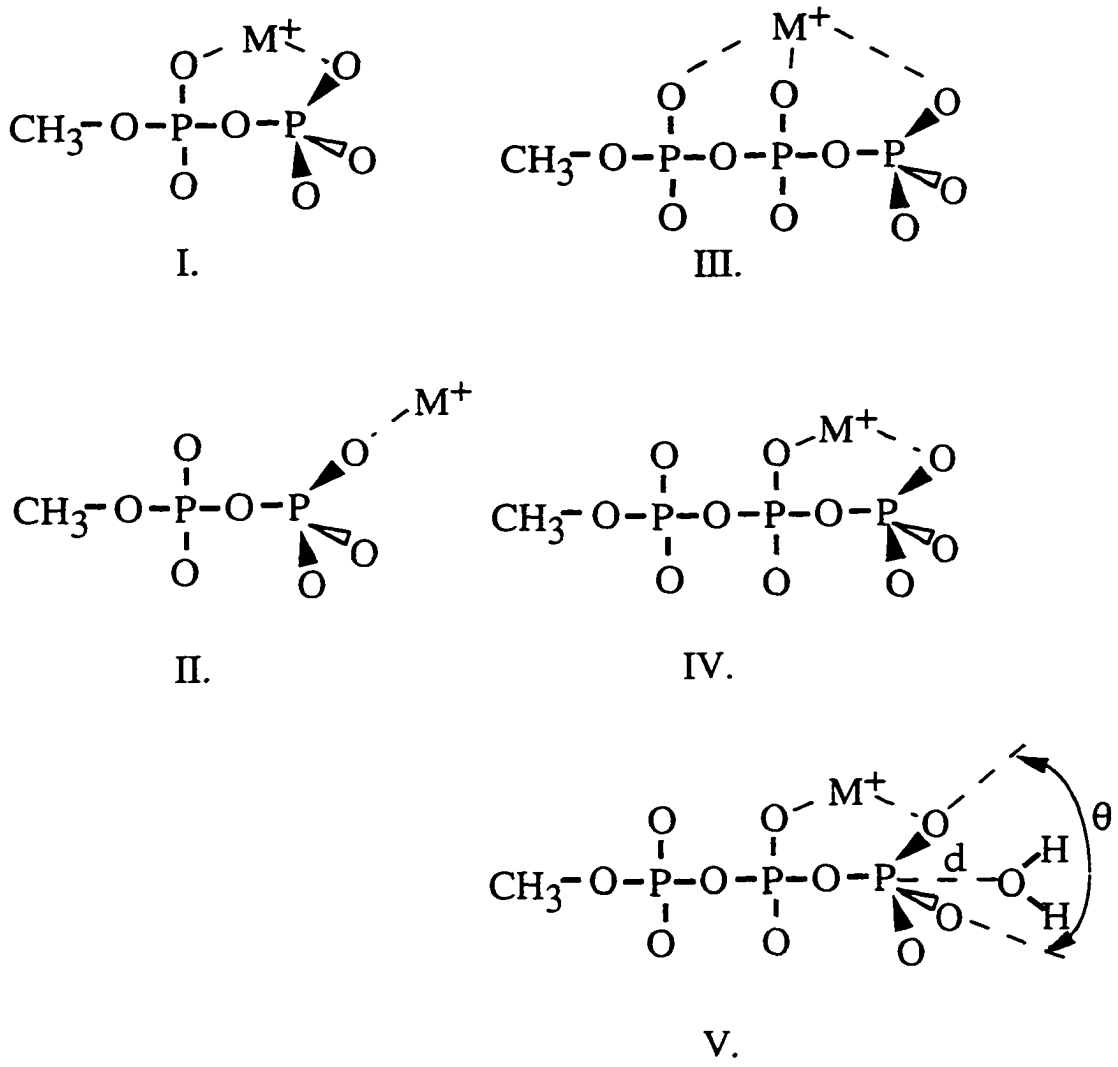

Scheme 6.1. The various structures used to model the environment of GDP in solution (I) and in p21 (II) and the environment of GTP in solution (III) and in p21 (IV and V).

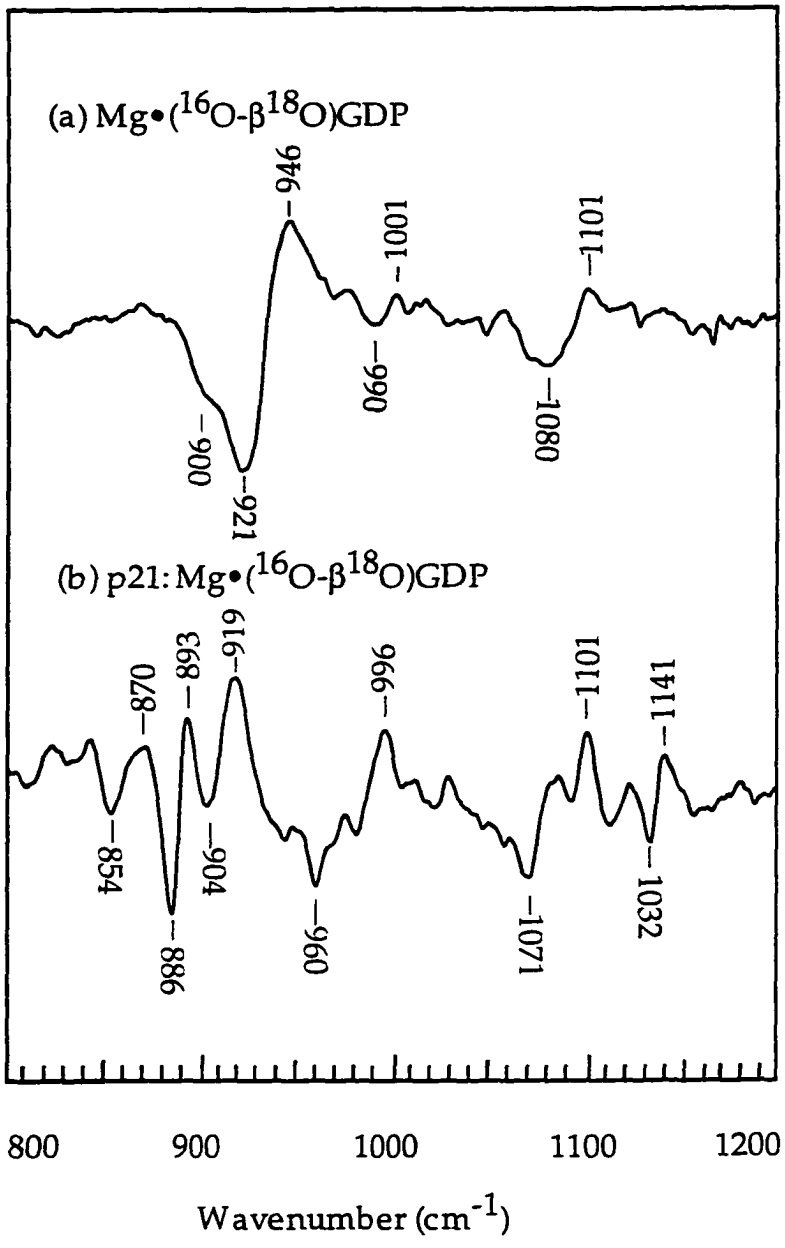

Figure 6.1. Raman difference spectra of the Mg•GDP 1:1 complex minus Mg•(β-$^{18}O_3$)GDP 1:1 complex in (a) aqueous solution and (b) p21, both at pH 7.5. Raman scattering was excited with the 150 mW 5682nm line from a Kr+ ion laser. The temperature of the sample was maintained at 4 °C during the Raman measurements [adapted from Xiao's thesis (1995)].

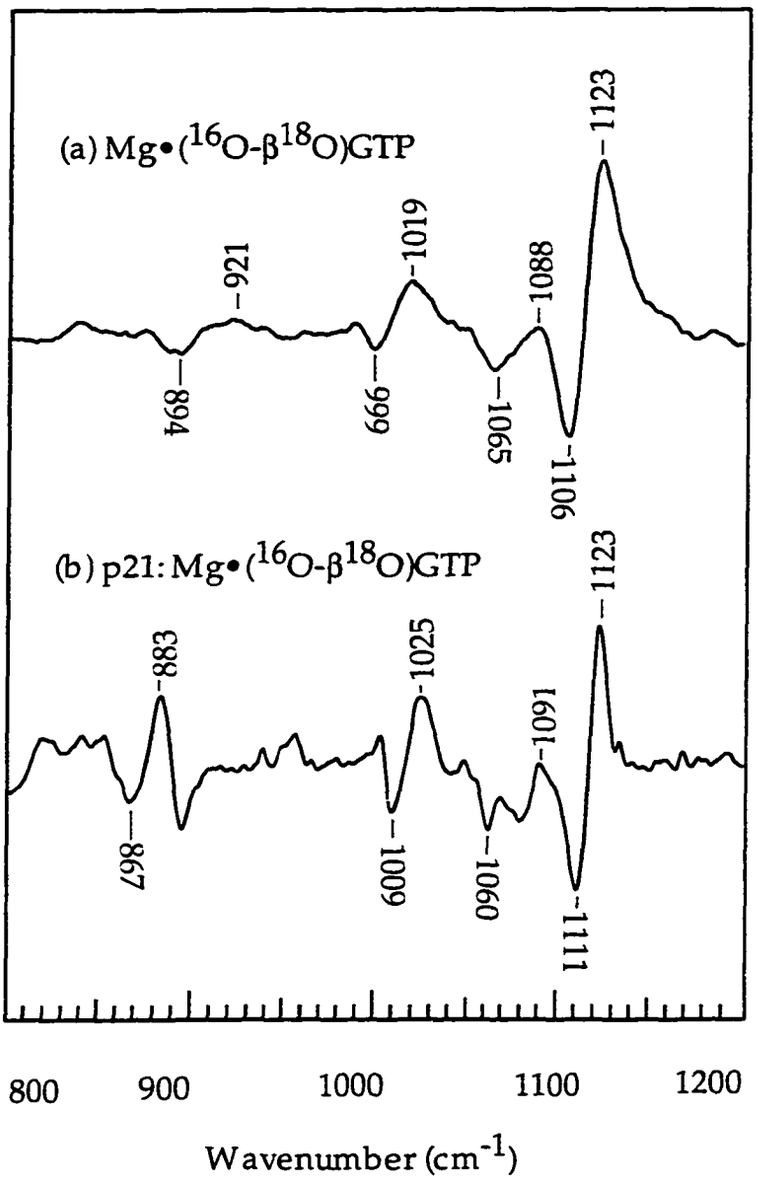

Figure 6.2. Raman difference spectra of Mg•GTP 1:1 complex minus Mg•(β-$^{18}O_2$,βγ-^{18}O)GTP 1:1 complex in (a) aqueous solution and (b) p21, both at pH 7.5. The concentration of p21 was ca. 4 mM. Raman scattering was excited with 150 mW at 568.2nm from a Kr^+ ion laser. The temperature of the sample was maintained at 4 °C during the Raman measurements [adapted from Xiao's thesis (1995)].

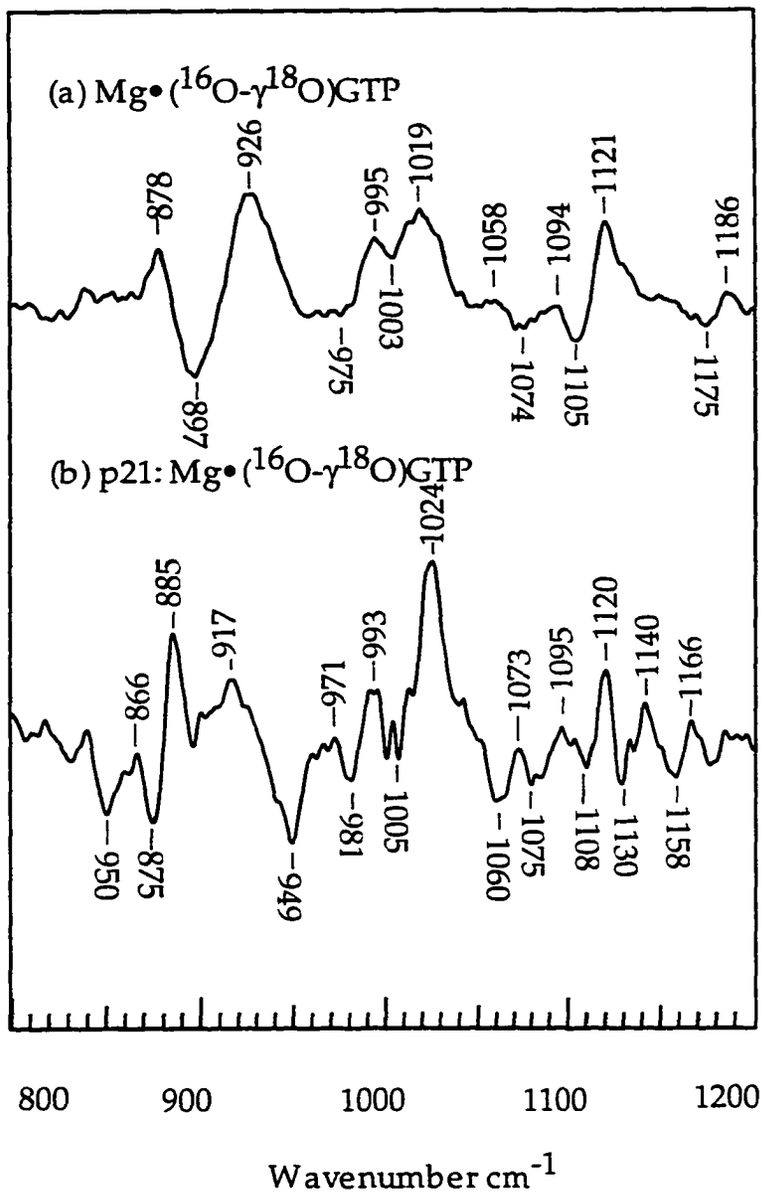

Figure 6.3. Raman difference spectra of Mg•GTP 1:1 complex minus Mg•(γ-$^{18}O_3$)GTP 1:1 complex in (a) aqueous solution and (b) p21, at pH 7.5 and at 4 °C. The concentration of p21 was ca. 4 mM. Raman scattering is excited by 150 mW at 568.2 nm from a Kr^+ ion laser. [adapted from Xiao's thesis (1995)].

CHAPTER 7

Vibrational Studies of Myosin S1•MgADP-Vanadate

It is well established that muscle contraction occurs when the thick and thin filaments, which are built primarily of myosin and actin respectively, slide past each other. The movement occurs through the interaction of the head of myosin with actin and is driven by the hydrolysis of ATP. The binding of ATP reduces the affinity of myosin for actin, and the subsequent hydrolysis of ATP results in a metastable ternary complex myosin•ADP•Pi. The release of ADP and Pi is catalyzed by rebinding of actin. The myosin head fragment can be isolated, the so called subfragment-1 (S1), and it contains both the ATPase and actin binding sites.

Vanadate has been used extensively in the studies of enzyme catalyzed phosphoryl transfer reactions since it does not only demonstrate physical and chemical similarities with phosphate but also exhibits considerable plasticity in the formation of VO bonds with large variations of bond strengths and the readiness to form an additional fifth ligand. Because of these properties, vanadate has been shown to be a potent inhibitor of many enzymes that catalyze phosphoryl transfer (Gresser & Tracey, 1990). Vanadate inhibits myosin ATPase activity by forming a complex with MgADP. This complex is believed to mimic either the transition state of the hydrolysis reaction or the ADP•Pi intermediate (Goodno & Taylor, 1982). Recently, a three-dimensional crystallographic structure of myosin S1 and its complexes with MgADP-vanadate has been determined (Smith & Rayment, 1996). The vanadate moiety in the myosin S1•MgADP-Vi complex is trigonal bipyramidal, with three short equatorial V••O bonds and two long apical V-O bonds. One of the three equatorial V••O bonds interacts with a structural Mg^{2+} while each of

the other two equatorial bonds are hydrogen bonded to protein residues. One of the vanadium apical V••O bonds is formed with oxygen of the β-phosphate of the ADP leaving group while the other is formed with a water molecule. The two apical V••O bonds are quite long, 2.09 and 2.27Å respectively, which suggest that the bond orders are weak.

It has been shown that Raman difference spectroscopy (Callender et al., 1994) is well suited for the determination of high resolution VO bond lengths and bond orders of vanadate complexes in enzymes (Deng et al., 1993; Ray et al., 1993a). In such studies, the Raman spectrum of the protein-vanadate complex is measured, as is that of the protein. The difference spectrum contains bands arising from the vanadate group. The vanadate bands dominate the difference spectrum due to their intrinsic large intensity and because most of the protein background spectrum subtracts out (Deng et al., 1993). Definitive assignment of the bands is accomplished by studies of isotopic (^{18}O) labeled vanadates. The bond lengths and bond orders of the nonbridging V••O bonds are determined from empirical correlations relating the vibrational stretch frequencies to these quantities (Hardcastle & Wachs, 1991; Ray et al., 1993a).

We analyze here the previously obtained Raman difference measurements of the nonbridging V••O stretch mode frequencies of the myosin S1•MgADP-Vi complex and model compounds in solution (measured by H. Deng). Large changes of the vanadate Raman spectra were observed when vanadate binds to the complex. Employing both the previous empirical relationships between bond orders/lengths and frequecies as well as vibrational analysis from *ab initio* calculations, the spectral changes can be explained by a small decrease of the nonbridging V••O bond orders of the ADP-Vi moiety in the myosin S1•MgADP-Vi complex and an increase of the angle between adjacent nonbridging V••O bonds. Our results show that formation of a fifth long

V••O bond with a structural water molecule (or OH group of an amino acid side chain), opposite to the bridging V-OR bond, can induce the V••O bond order change and geometry change of the three nonbridging V••O bonds determined from the stretching modes frequency shifts. Implications of these structural results on the reaction mechanism of ATP hydrolysis catalyzed by the ATPase will be discussed.

7.1 Raman Difference Spectra

Figure 7.1a shows the Raman spectrum of vanadate in aqueous solution at pH 10 (H. Deng, personal communication). The parallel polarized spectrum is plotted on top of the perpendicularly polarized spectrum. Figure 7.1b shows the spectrum of the vanadate sample prepared in ^{18}O water for the parallel and perpendicularly polarized Raman excitation laser beam as in Figure 7.1a. At pH 10, vanadate is dianionic and therefore contains one V-OH bond and three nonbridging V••O bonds with similar bond lengths. The stretch motions of these three bonds are strongly coupled to form a symmetric V••O stretch mode and a doubly degenerate asymmetric V••O stretch. The most prominent Raman band is the symmetric mode, which lies at 870 cm^{-1}, and the much weaker antisymmetric mode lies at virtually the same place, 869 cm^{-1}. This is shown in Figure 7.1a since the symmetric mode dominates the parallel polarized Raman spectrum (underneath the 870 cm^{-1} band in Figure 7.1a) but becomes the minor band in the Raman spectrum when the perpendicularly polarized laser beam was used for Raman excitation. This is because the depolarization ratio of the symmetric mode is close to zero while that of an asymmetric stretch mode is 6/7 in ideal situations under our experimental conditions. The assignment of these bands to V••O stretch modes is confirmed by ^{18}O labeling of the dianionic vanadate; the frequencies of these two modes

shift down by about 45 cm^{-1} (Figure 7.1b). The relative positions of the symmetric and antisymetric modes are important for structural determinations, as will be shown below. The Raman spectra of another vanadate model compound, methylvanadate monoester dianion, shows the same symmetric and asymmetric V••O stretch frequencies at 870 cm^{-1} in solution (Ray et al., 1993a). Therefore the V••O stretch modes due to the three nonbridging V••O bonds in dianionic vanadate derivatives are little affected by the other bond formed with vanadium, as long as this bond is formed with an oxygen atom.

Raman difference spectra between the S1•MgADP-Vi complex and myosin S1 has been obtained (data not shown). However, this difference spectrum contains many protein Raman bands in addition to the Raman bands from the MgADP-Vi moiety, presumably because the binding of MgADP-Vi induces significant protein changes that show up in the difference spectrum, and this substantially obscures the assignment of the Raman bands of the vanadate moiety. Previous X-ray crystallographic studies have shown that the protein conformations are similar in the myosin S1•MgADP-Vi and myosin S1•MgADP-AlF_4 complexes (Fisher et al., 1995; Smith & Rayment, 1996). Thus, the Raman difference spectrum between these two complexes, which shows substantially less contributions from protein, is presented (Figure 7.2a). Two clearly resolved Raman bands in the spectral region between 600 to 1000 cm^{-1} can be assigned to the V••O stretch modes of the bound vanadate moiety on the basis of their shift upon ^{18}O labeling of the nonbridging V••O bonds in S1•MgADP-Vi complex (Figure 7.2b). In addition, a nearly resolved band at 840 cm^{-1} (best seen in the perpendicularly polarized spectrum of Figure 7.2a) can also be assigned to a V••O stretch. Based on the relative intensities of the band at 870 cm^{-1} and 829 cm^{-1} (Figure 7.2a) and on their respective depolarization ratios as determined by depolarization studies (Figure 7.2b), they

are assigned to 'nearly' asymmetric and symmetric V••O stretch modes, respectively. The presence of a third band at 840 cm^{-1}, which has a depolarization ratio intermediate between a symmetric (perpendicular to parallel polarized intensity ratio near zero) and an antisymmetric mode (ratio of 6/7) suggests that the C_{3v} symmetry of the vanadate dianion in solution has been broken when vanadate binds to the S1•ADP subfragment. That the symmetry of the three V••O bonds in the complex is somewhat altered from a nearly perfect C_{3v} symmetry in solution is also consistent from the observation that the depolarization ratio of the 'symmetric' V••O stretch mode in the complex at 829 cm^{-1} is significantly larger than zero, as shown by the finite intensity of the band at 829 cm^{-1} in the perpendicularly polarized spectrum (Figure 7.2a). These observations are additionally consistent with our analaysis below and with the crystalographic results on this complex (Smith & Rayment, 1996) which show that the three V••O bonds interact with different groups at the protein binding site and that the three V••O bonds are slightly different.

Since the binding site of the S1 subfragment has been designed to bind dianionic ATP, it is expected that the ionic state of vanadate in the binding pocket is also dianionic. Our results are in agreement with this. In the first place the trianion, which has a solution pKa of 13.0, would be very difficult to form under the pH 7 conditions of the measurement. Moreover, this ion has only one V••O stretch mode while three are observed. The monoanion, which is stable at the pH 7 of the experiment in solution (pKa of 8.5), shows a symmetric Raman V••O band in solution at ca. 930 cm^{-1}, much higher than the observed bands of the bound vanadate. A ca. 100 cm^{-1} shift in the non-bonded V••O bonds implies a large reduction of V••O bond order with a large concomitant increase in the bond order of the bridging oxygens (see below). The predicted bond order of the bridging oxygens is much too large to be consistent with the

crystallographic results. In addition monoanionic vanadate can yield only two Raman bands of V$\underline{\bullet\bullet}$O character while three are observed. We conclude that the ionic state of the bound vanadate is dianionic.

7.2 Empirical Relationships

Accurate structural information about bonding in both metal and nonmetal oxides often can be obtained from vibrational spectroscopy by using two types of empirical relationships. One is the bond-length/bond-strength correlation pioneered by Brown and coworkers (Brown et al., 1992; Brown et al., 1976); the other is the bond strength-vibrational frequency correlation formulated by Hardcastle and Wachs (1991). In the Brown and Wu relationship, a network paradigm is used to define bond order, s, in terms of the average number of electron pairs per bond, so that Σs for any atom in a crystalline compound is equal to the formal valence of that atom. When defined in this way, bond strength can be referred to as valence bond strength and is expressed in terms of valence units, vu.

In the case of vanadate, where the valence of vanadium is 5, Σs calculated from Eq 7.1 is expected to be close to 5.0 vu, where r_{VO} is measured bond length (in Å) given by:

$$s_{VO} = (r_{VO}/1.791)^{-5.1} \qquad (7.1)$$

An empirical strength/frequency relationship can be cast in the same form as the Brown and Wu length/strength equation. Parameters for such an expression have been evaluated that allow bond strengths to be calculated from vibrational frequencies in crystalline oxymolybdenum and oxyvanadium compounds (Hardcastle et al., 1991). Calculated values of Σs_{VO} are close to the formal valence of vanadate (and the other metal that was studied), thus

allowing VO bond lengths to be related to vibrational frequencies via the Brown and Wu strength/length relationship. The validity of the Hardcastle/Wachs relationship, Eq (7.2), can be evaluated from the rather minimal scatter in their frequency/strength plot for the VO bonds in a number of different crystalline oxyvanadium compounds where strengths/ frequencies vary widely (Hardcastle et al., 1991).

$$s_{VO} = [0.2912*\ln(21349/\nu]^{-5.1} \qquad (7.2)$$

Within their data set, which contains a variety of different oxyvanadium compounds, Hardcastle and Wachs show that the correlation of Eq. 7.2 is accurate to within ± 20 cm^{-1}. In the case of vanadates, this translates, via Eq 7.1, into the an absolute error in length of ±0.01 Å. Changes in length can be obtained much more accurately, to within ±0.001 Å.

The question arises as to which frequency, ν, should be substituted into Eq. 7.2. We have shown recently that the symmetric and antisymmetric modes of the vanadate V••O bonds in solution are functions of force constant of the V••O bond and the O••V••O angle (similarly for the corresponding phosphate bonds) . It can be shown that the average or 'fundamental' frequency, ν, as defined by $[(\nu_s^2+d\nu_a^2)/(d+1)]^{1/2}$ (ν_s is the symmetric stretch, ν_a the antisymmetric stretch, and d is the degeneracy of the asymmetric modes), depends directly on the stretch force constant of the V••O bond and is affected to a smaller extent by geometrical and bond-bond coupling terms than is either ν_s or ν_a alone (e. g. Bansil, 1980; unpublished results). This parameter is thus the appropriate frequency for use in Eq. 7.2 (for vanadates in solution, $\nu_s \approx \nu_a$ so that this distinction makes no practical difference; however, this is not true for phosphates). In contrast to what is observed in solution, crystal forces can differ for one VO bond compared to another and lift the coupling of these VO

vibrational modes that otherwise would produce a symmetric and asymmetric pair. This 'crystal like' behavior is what is seen for the S1•MgADP-Vi complex in that three V••O bands are observed. Treating each V••O bond as an 'independent oscillator', as did Hardcastle and Wachs in their analysis of vanadate crystals, then yields three somewhat different V••O bond orders and, via Eq. 7.1, three different bond lengths.

The 'fundamental' frequency of the vanadate solution model is calculated to be 869 cm^{-1} from ν_s = 870 cm^{-1} and ν_a = 869 cm^{-1}, which yields a bond order of 1.430 vu and a bond length of 1.669 Å for each of the three non-bonded V••O bonds using Equations 7.1 and 7.2. The shift to lower frequency for the V••O bonds in the S1 subfragment bound vanadate translates to a somewhat higher bond order and lower bond length for the three bonds. From Eqs. 7.1 and 7.2, the three frequencies at 829, 844, and 870 cm^{-1} yield bond orders of 1.327, 1.365, and 1.433 vu and bond lengths of 1.694, 1.685, and 1.669 Å respectively. The total bond order of the three non-bonded V••O bonds sums to 4.29 vu for the vanadate model in solution and 4.125 for the bonded vanadate. This means that, since the bond orders sum to five in both cases, the total remaining bond order for all other bonds has increased by 0.16 vu when vanadate binds to the subfragment.

While the average frequency of a symmetric/antisymmetric set depends chiefly on force conatant, it can be shown that the difference between the symmetric and antisymmetrc modes depends an the angle between the O••V••O bonds as well as the V••O stretch force constant (Chapter 4). Therefore, it is clear from the data that the the O••V••O angle changes when vanadate binds to the S1•ADP complex since the difference between the symmetric and antisymmetric modes for the vanadate in solution is close to zero but is around 40 cm^{-1} in S1•ADP Vi. Using the simple analytical

expressions for the symmetric and antisymmetric frequencies of dianionic vanadate (Chapter 4) and assuming (1) normal values for the V••O stretch force constant and the stretch-stretch coupling constant and (2) that these force constant values are unaffected by binding (approximately true given the small change in the bond orders as calculated above), then a 7° angle increase is predicted for the O••V••O angle upon binding. Because the modes of the bound vanadate no longer appear to form a symmetric/antisymmetric pair and because the force constants must change some, quantum mechanical *ab initio* calculations were performed to model the vanadate binding. These calculations are also of value because the interactions assumed to take place at the binding site can be well modeled by these methods, as is shown just below.

7.3*Ab initio* vibrational analysis of dianionic vanadate

It is well known that chemical bond lengths, especially those bonds which contain oxygen, are underestimated by *ab initio* methods at the Hatree-Fock level compared with those observed values. This is due to the neglect of correlation forces in the calculations, the limited basis set, and also that the calculations are done in 'gas phase', which does not treat the interactions with solvent. Consequently, the calculated stretch frequencies of these bonds are significantly (about 20%) overestimated. However, the overestimation of the calculated spectral differences compared to experimentally determined values between different configurations/conformations of a given molecule tends to remain constant (Deng et al., 1992; Deng et al., 1996; Deng et al., 1994). Thus a scaling procedure was adopted to reduce the errors in the absolute frequencies calculated by *ab initio* methods but retain its predicting value on the spectral change of the molecule when the configuration of the molecule is changed by external perturbation.

In this procedure, Cartesian force constants and the Raman polarization tensor of an isolated dianionic vanadate or methylvanadate are calculated by Gaussian 94 program (Frish et al., 1994) at the HF/3-21g* level. The Cartesian force field is then converted to internal force field by the program REDONG (Allouche, QCPE) and subsequently "scaled" (by a set of scaling factors) so that the calculated vibrational frequencies and isotopic shifts of the vanadate derivatives are in good agreement with those observed ones. The Raman intensities and depolarization ratios of the new vibrational modes are also calculated, by using the Raman polarization tensor obtained in the initial *ab initio* calculations and the new normal mode eigenvectors obtained by the scaled force field. These quantities are then compared with the experimental spectra to evaluate the scaling factors. Once a set of satisfactory scaling factors is obtained, calculations on a series of models of the vanadate moiety simulating S1•MgADP-Vi complex are then performed by Gaussian 94. The calculated force fields from these model vanadate complexes are scaled, using the scaling factors determined from the calculations on the isolated model complex, to produce the vibrational modes, Raman intensities, and depolarization ratios. Raman spectra of these vanadate model complexes are then compared with that found of the bound vanadate in S1•MgADP-Vi complex.

The model systems used in our *ab initio* calculations are vanadate and methylvanadate dianions. The results of geometry optimizations on these model vanadates indicate that the bridging V-O bond is not collinear with the bridging O-C(H) bond at equilibrium. One of the nonbridging V••O bonds is longer compared to the other two, so that the C3v symmetry expected for the three nonbridging V••O bonds is slightly broken. Thus, three nonbridging V••O stretch modes, at 869, 865 and 851 cm^{-1}, respectively, are predicted after application of the scaling procedure described above (Figure 7.3). Thus the

calculations do not take into account that fast rotation of the methyl group about the bridging bond would result in an average equal environment for each of the three non-bridging V••O bonds. However, this effect of the calculations is not important for our purposes. For a VO3 group with perfect C_{3v} symmetry, the displacements of the three oxygens in the symmetric stretch mode are in phase and with the same magnitude. One asymmetric mode has an eigenfunction where one oxygen has zero displacement while the other two non-bridging oxygens are out of phase with the same magnitude. The second asymmetric mode shows a displacement of one out of phase oxygen with the other two whose displacement magnitude is twice as large. Although the VO3 group in our solution model compound does not have a perfect C_{3v} symmetry, the resultant stretch modes can still be identified based on the above classification. The 869 cm^{-1} mode corresponds to the symmetric stretch mode, with the depolarization ratio very close to zero (Figure 7.3). The character of the 865 cm^{-1} mode is the quite close to the asymmetric modes for VO3 with C_{3v} symmetry since the two (shorter) V••O bonds have out of phase displacements and there is no displacement of the third oxygen, and also they have the expected depolarization ratio for an asymmetric mode. Likewise the 851 cm^{-1} mode resembles the second asymmetric mode discussed closely above, and has an intermediate depolarization ratio (0.12, Table 7.3).

The simulated Raman spectra of vanadate dianion in the V••O stretch mode region based on the *ab initio* calculations and empirical scaling of the force field are presented in Figure 7.3. Also presented is the effect of replacing the non-bridging oxygens by ^{18}O. For presentation, all bands were assigned a bandwidth that matches the experimentally determined bandwidth; the bandwidth do not come out of the calculations. It can be seen that the agreement between the measured (Figure 7.1) and calculated Raman spectra

(Figure 7.3) is reasonable. Thus the scaling factors obtained here will be used in subsequent Raman spectrum calculations of vanadate complexes simulating that found in S1•MgADP-Vi.

To simulate the vanadate moiety in S1•MgADP-Vi complex, a water molecule opposite the bridging V-O bond of methylvanadate dianion was placed at various distances. The geometry of the complex, with the vanadium-water oxygen distance fixed at various lengths, was optimized with 3-21g* basis set. The force field and Raman depolarization ratios of normal modes were obtained in subsequent frequency calculations. Using the scaling factors obtained in the solution model calculations, the scaled force field and resulting frequencies were then calculated. Table 7.1, 7.2 and 7.3 show the results of calculations on several model complexes with V-- $O(H_2)$ distance ranging from 2.25 Å to 4.0Å. It was found that for a water oxygen-vanadium distance of about 2.5 Å the calculated Raman spectrum of the nonbridging V••O bonds shows a pattern quite similar to that observed in the Raman spectrum of S1•MgADP-Vi complex. The Raman spectra calculated from this 2.5Å model complex are presented in Figure 7.4. As can be seen, the calculated pattern of bands and their depolarization ratios, and shifts upon ^{18}O substitution, is in quite good agreement with the observed spectra (compare Figures 7.2 and 7.4).

The results in Table 7.1 show that to push a water molecule toward vanadium of a vanadate dianion along the bridging V-O bond from the vanadium end causes two general changes in the VO_3 geometry: the first is to increase the average V••O bond length; the second is an increase of the average bond angle between two V••O bonds, resulting in a more planar VO3 moiety. For example, the average V••O bond length is about 0.009Å longer in the 2.5 Å model complex than that in isolated vanadate while the average angle between two adjacent nonbridging V••O bond is increased by about 4.4°, from 111.2° in

isolated vanadate dianion to 115.6° in the 2.5Å model complex. One of the antisymmetric frequencies of V••O virtually doesn't change while its symmetric stretching frequency is shifted from 1051(848) cm^{-1} to 1009 (821) cm^{-1} (see Table 7.2 and 7.3. the values in paretheses is the frequency after scaling). It is consistent with the experimental result. We also used HO^- instead of H_2O toward vanadium along V-O bridge. For 2.27-Å V--$^-$OH model complex, the stretch frequencies of V••O are listed in the Table 7.3 and those frequencies are far smaller than the experimental data. Table 7.4 shows the bond order calculated by empirical equation 7.1, where bond length comes from ab initio calculation and r_1=1.7578. Although the calculated bond length is underestimated, the sum of all bond orders is close to 5 (Column 4th, Table 7.4). It's consistent with the empirical assumption.

Test calculations on model compounds including a Mg^{2+} or Na^+ ion next to one of the nonbridging oxygens were not successful because the interaction between Mg^{2+} and the vanadate moiety was greatly overestimated by *ab initio* methods. The results predict that the nonbridging V••O bond interacting with Mg^{2+} would be too greatly polarized (data not shown). Such effects are not observed in our Raman data. Therefore, much more complex model systems, involving hydrogen bonding or ionic interactions on all three nonbridging V••O bonds and with the metal ions, are required to reproduce the observed Raman spectrum of vanadate moiety in S1•MgADP-Vi complex if ions are to be included in the model complex.

7.4 The Structure of vanadate moiety bound in S1·MgADP-Vi complex

On the basis of our difference Raman spectroscopy studies of the S1•MgADP•Vi complex, empirical and *ab initio* vibrational analyses of the Raman data, the following conclusions can be made. First, the average bond

order of the nonbridging V••O bonds in the complex is decreased by 0.05 vu, from 1.43 vu in solution to 1.38 vu in the complex. This means that, the although the ionic and hydrogen bonding interactions between the nonbridging V••O bonds and Mg^{2+}/protein residues are well coordinated in the S1•MgADP-Vi complex, the average strength of such interactions are not much stronger than that observed between the nonbridging V••O bonds and counterion/water in aqueous solution since larger interactions would polarize the V••O bonds and bring about a proportional decrease in their bond orders. The average V••O bond length calculated from Eq. 7.1 and 7.2 is correspondingly slightly increased to 1.683 Å in the S1•MgADP-Vi complex, which is 0.014Å larger when compared to the solution value. The Brown and Wu paradigm (Brown & Wu, 1976) predicts that the sum of the bond orders of all VO bonds in the S1•MgADP-Vi complex is equal to 5. Thus, the total bond order of the two apical bonds should be about 0.88 vu, which corresponds to two V-O bonds with average bond length of 2.10 Å, about 0.08 Å shorter than that observed in the X-Ray structure. The three equatorial V••O bond lengths found from the present vibrational results at 1.694, 1.685, and 1.669 Å are on average about 0.02Å longer than that the corresponding V••O bonds reported in X-ray crystallographic studies, 1.67, 1.67, and 1.64 Å (Smith & Rayment, 1996).

Our results from the *ab initio* analysis also suggest that the average angle between two nonbridging V••O bonds increases by 4-5° from the solution value. Larger changes of the bond angle, which can be induced either by forcing the apical water molecule closer to vanadate or by lengthening the second apical V-O bond in the model complexes can be readily obtained, but this results in too large a frequency difference between symmetric and asymmetric nonbridging V••O stretch modes compared to that observed in Raman experiments. The 4-5° increase of the angle between two nonbridging

V••O bonds corresponds to a decrease of 5-6° of the angle between one nonbridging V••O bond and the apical V-O bond when the vanadate moiety has an approximate C3v symmetry. According to the *ab initio* calculations, the angle between any one of the three equatorial V••O bonds and the apical V-O bond in isolated dianion vanadate is about 108°, and this angle decreases to about 102-103° in the 2.5 Å model complex. Since it is unlikely that this angle is less than 100° in solution, our predicted geometry of the vanadate moiety in the S1•MgADP•Vi complex is somewhat different from that obtained in X-ray crystallographic studies, in which the equatorial V••O bonds are essentially planar (have an almost 90° angle with the apical V-O bond).

7.5 Implications for the reaction mechanism of the myosin ATPase catalyzed ATP hydrolysis

As discussed in the Introduction, the mechanism of phosphoryl transfer can be classified according to the summed bond order between the oxygens of the attacking and leaving groups with the central vanadium metal: a summed bond order near zero is dissociative, near one is S_N2, and larger than one is associative. A dissociative mechanism is observed in phosphoryl transfer reactions of dianionic phosphates in solution while the process in enzymic catalyzed reactions is much less clear and appears to vary from enzyme to enzyme (see Chapter 1, Introduction). Our results show that the summed bond order of apical bonds of vanadate in the S1•MgADP-Vi complex is 0.88 vu. Thus, to the extent that the S1•MgADP-Vi complex is a good transition state mimic for the phophoryl transfer reaction in myosin, our results are consistent with a S_N2 process, possibly with a small associative character.

Table 7.1. The O••V••O angle, $CH_3O\text{-}VO_3^{2-}$ bondlength, and V••O bond length as a function of water-methylvanadate distance in the model of the active site of myosin S1•MgADP Vi complex from *ab initio* calculations.

$CH_3O\text{-}VO_3$•••$0H_2$ bond length (Å)	O••V••O angle (degrees)	$CH_3O\text{-}VO_3$ bond length (Å)	V••O bond length (average, Å)
$CH_3OVO_3^{2-}$	111.2	1.907	1.636
4.0	112.1	1.914	1.636
3.5	112.4	1.915	1.637
3.0	113.3	1.917	1.639
2.75	114.3	1.918	1.641
2.5	115.6	1.925	1.645
2.25	117.2	1.931	1.651

Table 7.2. The V••O symmetric and antisymmetric stretching frequencies, Raman intensity (R. I.) and depolization ratio (Dep. R.) as a function of water-methylvanadate distance in the model of the active site of myosin S1•MgADP Vi complex from *ab initio* calculations (before scale).

CH_3O-VO_3•••$0H_2$ bond length (Å)	υ_s(R. I. /Dep. R.)	υ_a(R. I. /Dep. R.)	υ_a(R. I. /Dep. R.)
$CH_3OVO_3^{2-}$	1057 (22.7/0.01)	1080 (8.41/0.15)	1091 (3.82/0.75)
4.0	1051 (23.1/0.01)	1081 (7.26/0.17)	1095 (3.98/0.70)
3.5	1047 (23.2/0.01)	1079 (7.19/0.18)	1094 (4.20/0.67)
3.0	1038 (24.5/0.01)	1073 (5.47/0.22)	1093 (5.07/0.59)
2.75	1027 (25.3/0.01)	1068 (4.81/0.25)	1092 (5.66/0.57)
2.5	1009 (25.7/0.01)	1058 (4.45/0.30)	1090 (6.56/0.58)
2.25	986 (25.4/0.02)	1042 (4.80/0.37)	1082 (7.67/0.63)
2.27*	965(19.13/0.03)	1029(6.08/0.63)	1058(6.11/0.75)

*Indicating the distance between vanadium and the oxygen atom of HO^-, not of H_2O

Table 7.3. The V••O symmetric and antisymmetric stretching frequencies, Raman intensity (R. I.) and depolization ratio (Dep. R.) as a function of water-methylvanadate distance in the model of the active site of myosin S1•MgADP Vi complex from *ab initio* calculations (after scale)

CH_3O-VO_3•••$0H_2$ bond length (Å)	υ_s(R. I. /Dep. R.)	υ_a(R. I. /Dep. R.)	υ_a(R. I. /Dep. R.)
$CH_3OVO_3^{2-}$	869 (23.8/0.03)	865 (3.46/0.75)	851 (5.72/0.12)
4.0	848 (15.7/0.06)	866 (8.14/0.06)	869 (8.33/0.19)
3.5	864 (16.2/0.06)	846 (9.26/0.04)	870 (6.80/0.50)
3.0	841 (13.1/0.02)	858 (12.1/0.07)	870 (7.47/0.30)
2.75	834 (16.8/0.01)	853 (9.10/0.10)	870 (7.40/0.35)
2.5	821 (19.7/0.01)	845 (6.70/0.14)	869 (7.70/0.42)
2.25	804 (20.8/0.02)	835 (5.99/0.22)	864 (8.21/0.50)
2.27*	792(16.0/0.04)	828(6.77/0.45)	847(6.12/0.75)

*Indicating the distance between vanadium and the oxygen atom of HO^-, not of H_2O

Table 7.4. CH_3O-VO_3^{2-} bond order, and V••O bond order as a function of water-methylvanadate distance in the model of the active site of myosin S1•MgADP Vi complex from *ab initio* calculations.

CH_3O-VO_3•••$0H_2$ bond length (Å)	CH_3O-VO_3 bond[a] order (vu)	V••O bond order[a] (vu)	Sum(bond order)[b] (vu)
$CH_3OVO_3^{2-}$	0.6598	1.4432	4.9894
4.0	0.6483	1.4409	4.9862
3.5	0.6462	1.4382	4.9908
3.0	0.6435	1.4293	4.9969
2.75	0.6409	1.4200	5.0029
2.5	0.6298	1.4029	5.0045
2.25	0.6196	1.3780	5.0374

[a]bond order is calucluated by (bond length/1.7578)$^{-5.1}$, in which bond length comes from the Table 7.1 column 3rd and 4th.

[b]Sum(bond order) is the sum of the bond oder of V••O, bridge V-O and the incoming V-O.

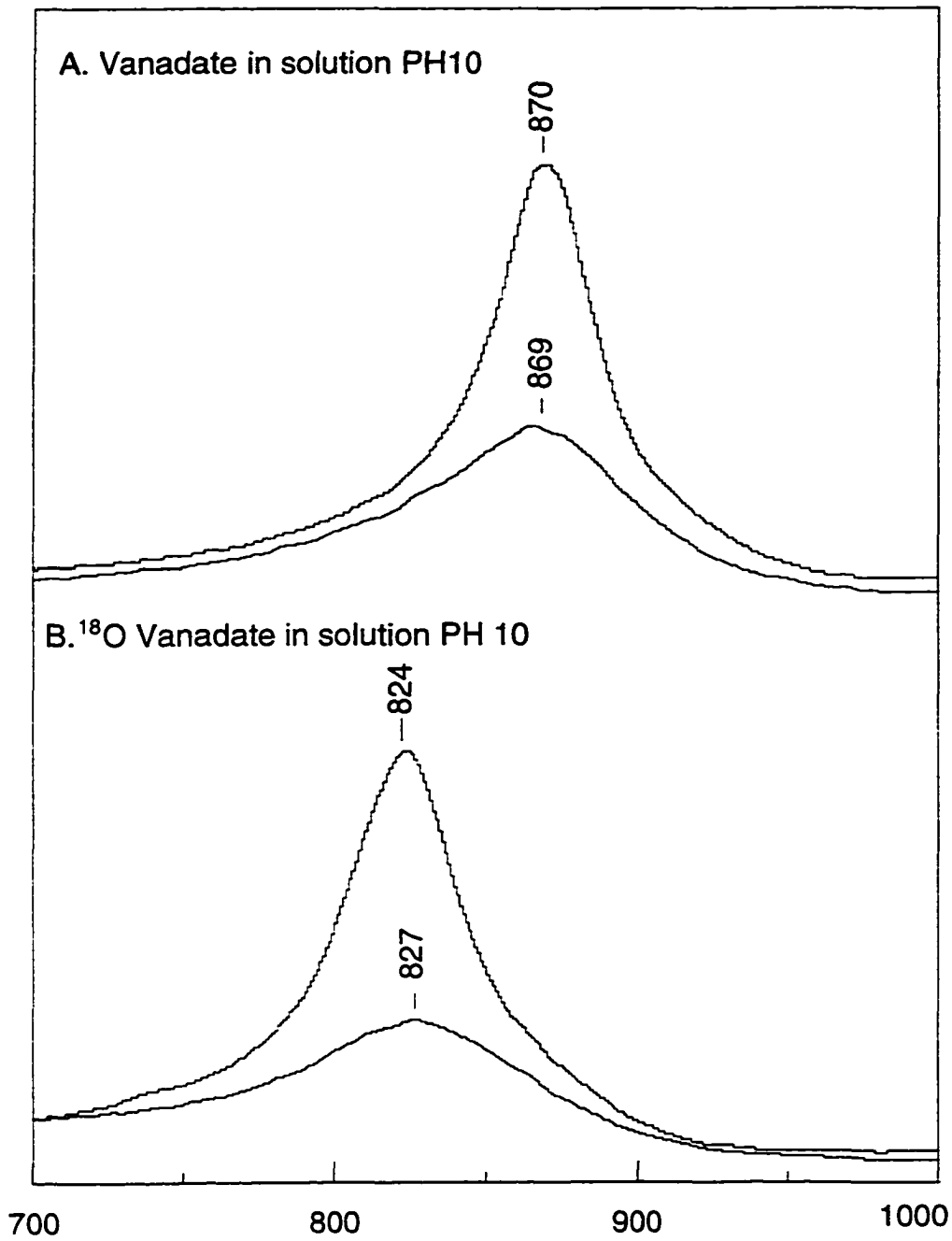

Figure 7.1. (a) Raman spectrum of 100mM HVO_4^{2-} at pH10.5. The top curve is the parallel polarized spectrum with the Raman excitation laser beam parallel to the spectrometer's entrance slit plane while the bottom graph is the perpendicular specrum (excitation laser beam perpendicular to the spectrometer's entrance slit plane). (b) same as (a) except prepared in ^{18}O water. A 100 mW of the 514.5nm laser line from an argon ion laser was used, and the spectral resolution was 8 cm^{-1}(measured by H. Deng).

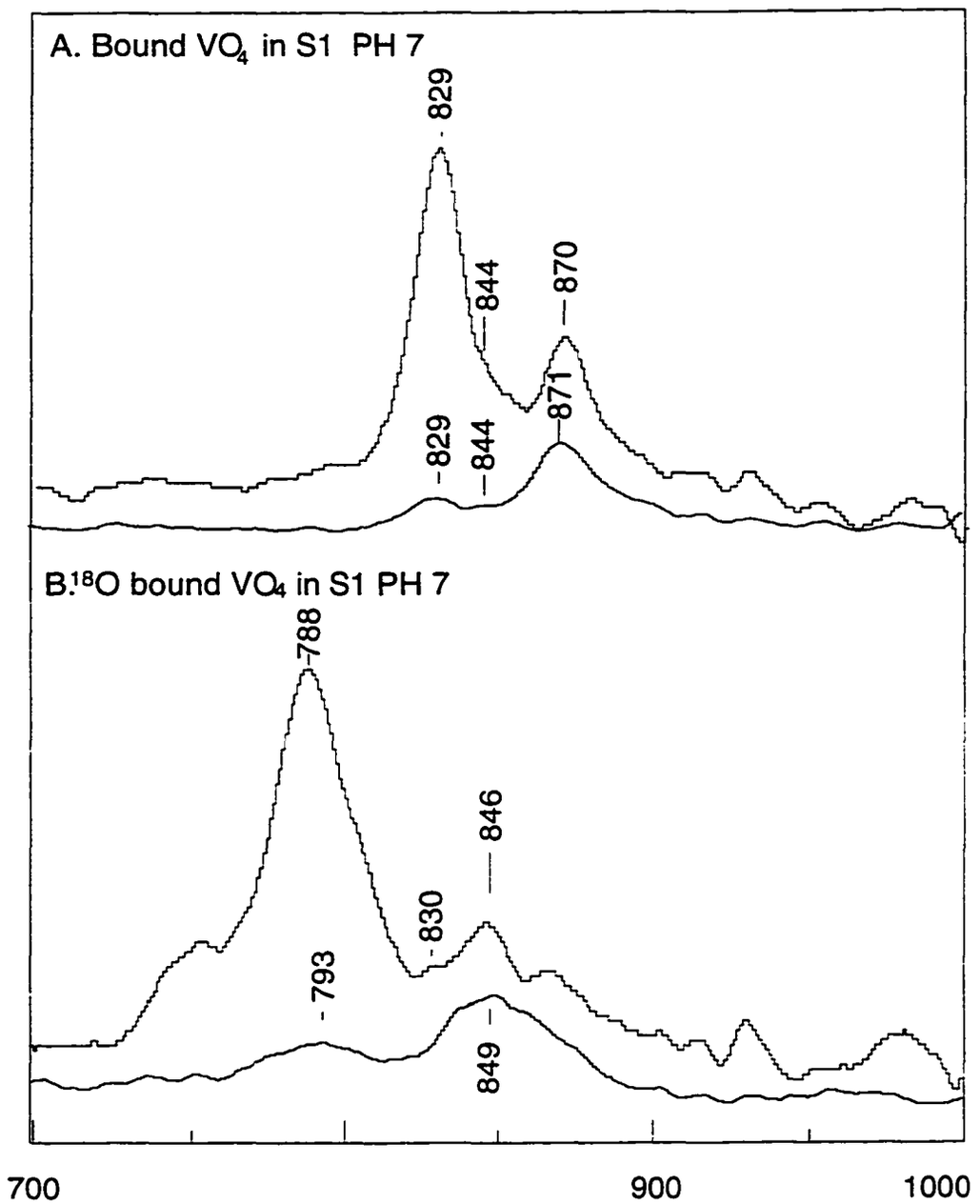

Figure 7.2. (a) Raman difference spectrum between myosin S1•MgADP-Vi complex and myosin S1•MgADP•AlF_4^- complex. The top curve is the parallel polarized spectrum with the Raman excitation laser beam parallel to the spectrometer's entrance slit plane while the bottom graph is the perpendicular specrum (excitation laser beam perpendicular to the spectrometer's entrance slit plane). (b) same as (a) except prepared in ^{18}O water. 100 mW 514.5 nm laser line from an argon ion laser was used, and the spectral resolution was 8 cm^{-1} The temperature of the sample was maintained at 4 °C during the measurements (measurements were done by H. Deng).

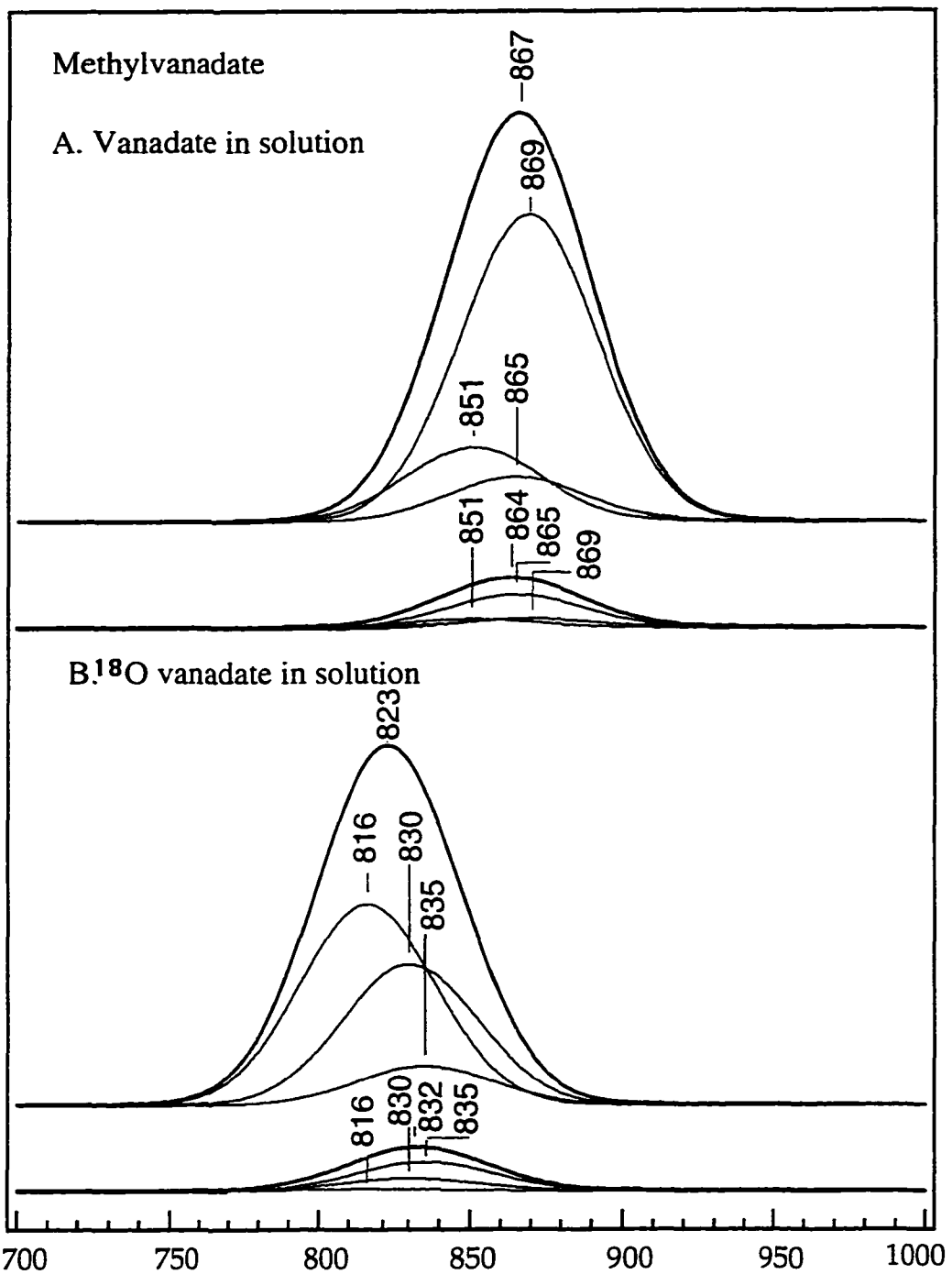

Figure 7.3. (a) Calculated Raman spectrum of dianionic methylvanadate from ab initio calculations as described in the text. The top curve is the simulated parallel polarized spectrum and the bottom curve is the perpendicular polarized spectrum. (b) same as (a) except ^{16}O are replaced by ^{18}O. The Raman bands are simulated by a guassian function and the band width is set to 22 $cm.^{-1}$

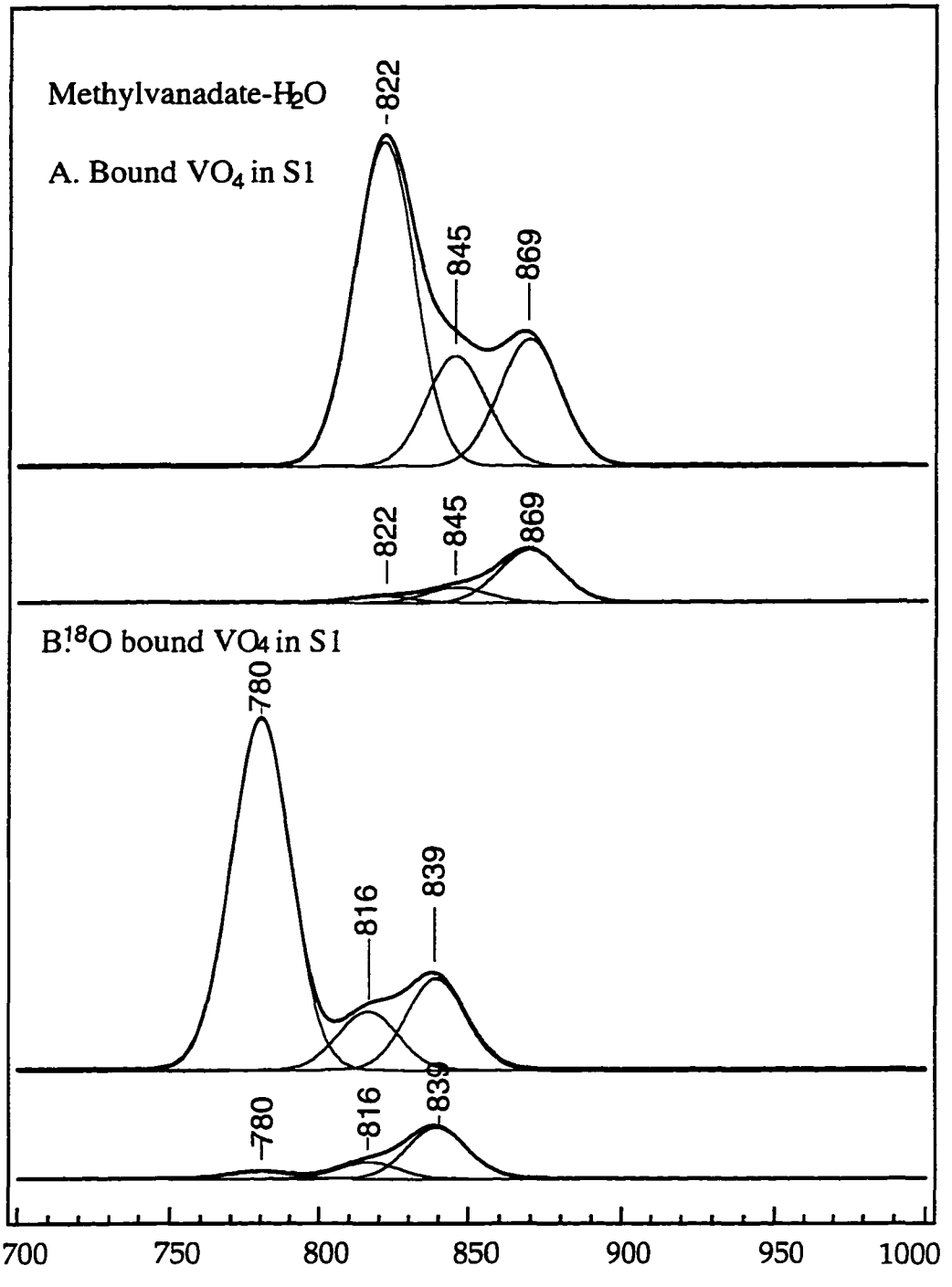

Figure 7.4. (a) Calculated Raman spectrum of dianionic methylvanadate complexed with a water molecule. The water oxygen-vanadium distance is fixed at 2.5Å. The top curve is the simulated parallel polarized spectrum and the bottom curve is the perpendicular polarized spectrum. (b) same as (a) except ^{16}O are replaced by ^{18}O. The Raman bands are simulated by a guassian function and the band width is set to10 $cm.^{-1}$

REFERENCES

Adari, H., Lowy, D. R., Willumsen, B. M., Der, C. J. , & McCormick, F. (1988) *Science.* **240,** 518-521.

Admiraal, S. , & Herschlag, D. (1995) *Chemistry & Biology.* **2,** 729-739.

Badger, R. M. , & Bauer, S. H. (1937) *J. Chem. Physics.* **5,** 839-855.

Bagshaw, C. R. , & Trentham, D. R. (1973) *Biochemistry J.* **133,** 323-328.

Bagshaw, C. R. , & Trentham, D. R. (1974) *Biochemistry J.* **141,** 331-349.

Bansil, R., Day, J., Meadows, M., Rice, D., & Oldfield, E. (1980) *Biochem.* **19,** 1938-1943.

Barbacid, M. (1987) *Ann. Rev. Biochem.* **56,** 779-827.

Barth, A., Corrie, J. E. T., Gradwell, M. J., Maeda, Y., Mantele, W., Meier, T. , & Trentham, D. R. (1997) *J. Am. Chem. Soc.* **119,** 4149-4159.

Barth, A., Hauser, K., Mantele, W., Corrie, J. E. T. , & Trentham, D. R. (1995) *J. Am. Chem. Soc.* **117,** 10311-10316.

Bishop, E. O., Kimber, S. J., Orchard, D. , & Smith, B. E. (1981) *Biochim. Biophys. Acta.* **635,** 63-72.

Boguski, M. S. , & McCormick, F. (1993) *Nature.* **366,** 643-653.

Bourne, H. R., Sanders, D. A. , & McCormick, F. (1990) *Nature.* **348,** 125-131.

Bourne, H. R., Sanders, D. A. , & McCormick, F. (1991) *Nature.* **349,** 117-127.

Bourne, N. , & Williams. (1984) *J. Org. Chem.* **49,** 1200-1204.

Brown, I. D. (1992) *Act. Crystallogr.* **B48,** 553-572.

Brown, I. D. , & Wu, K. K. (1976) *Acta Cryst.* **B32,** 1957-1959.

Callender, R., Chen, D., Lugtenburg, J., Martin, C., Ree, K. W., Sloan, D., VanderSteen, R. , & Yue, K. T. (1988) *Biochemistry.* **27,** 3672-3681.

Callender, R. , & Deng, H. (1994) *Ann. Rev. Biophys. Biomol. Struct.* **23,** 215-245.

Callender, R., Gilmanshin, R., Dyer, R. B. , & Woodruff, W. (1994). *Physics World. 7,* 41-45.

Carey, P. R. (1982) *Biochemical Applications of Raman and Resonance Raman Spectroscopy.* Academic Press, New York.

Cepus, V., Ulbrich, C., Allin, C., Troullier, A. , & Gerwert, K. (1997) "FTIR Photolysis Studies of Caged Compounds." *Preprint.*

Cepus, V., Goody, R. S., & Gerwert, K. (1998) "Time resolved FTIR studies of the GTPase reaction of H-ras p21: The phosphate vibrations." *Preprint.*

Chen, D., Yue, K. T., Martin, C., Rhee, K. W., Sloan, D. , & Callender, R. (1987) *Biochemistry.* **26,** 4776-4784.

Cohen, M. , & Hughes, T. R. J. (1962) *J. Biol. Chem.* **237,** 176-186.

Cook, P. Enzyme Mechanism from Isotope Effects, CRC Press, Inc(1991). 1-500.

Cooperman, B. S. (1976) *M. Decker, Inc., New York.* **5,** 79-125.

Darwish, A. A. , & Prichard, R. K. (1981) *J. Liq. Chromat.* **4,** 1511-1524.

de Vos, A. M., Tong, L., Milburn, M. V., Matias, P. M., Jancarik, J., Noguchi, S., Nishimura, S., Miura, K., Ohtsuka, E. , & Kim, S.-H. (1988) *Science.* **239,** 888-893.

Dean, Johna, Hand Book of Organic, Published by McGraw-Hill, (1987).

Deng, H. , & Callender, R. (1993) *Comments Mol. Cell. Biophys.* **8,** 137-154.

Deng, H. , & Callender, R. H. (1987) *Biochem.* **26,** 7418-7426.

Deng, H., Chan, A. Y., Bagdassarian, C. K., Estupinan, B., Ganem, B., Callender, R. H. , & Schramm, V. L. (1996) *Biochemistry.* **35,** 6037-6047.

Deng, H., Huang, L., Groesbeek, M., Lugtenburg, J. , & Callender, R. H. (1994) *J. Am. Chem. Soc.* **98,** 4776-4779.

Deng, H., Manor, D., Weng, G., Chen, C.-X., Balogh-Nair, V. , & Callender, R. (1993a). *Proccedings of International Society for Optical Engineering. 1890,* 114-122.

Deng, H., Ray, W. J., Burgner, J. W. , & Callender, R. (1993b) *Biochemestry.* **32,** 12984-12992.

Deng, H., Zheng, J., Burgner, J. , & Callender, R. (1989) *Proc. Nat'l. Acad. Sci. (USA).* **86,** 4484-4488.

Deng, H., Zheng, J., Sloan, D., Burgner, J. , & Callender, R. (1992) *Biochem.* **31,** 5085-5092.

Diem, M. (1993) *Introduction to Modern Vibrational Spectroscopy, published by John Wiley & Sons.* 65-77.

Eckstein, F. (1985) *Annu. Rev. Biochem.* **54,** 367-402.

Fasano, O., Aldrich, T., Tamanoi, F., Taparowsky, E., Furth, M. , & Wigler, M. (1984) *Proc. Natl. Acad. Sci. U.S.A.* **81,** 4008-4012.

Feuerstein, J., Goody, R. S. , & Webb, M. R. (1989) *J. Biol. Chem.* **264,** 6188-6190.

Feuerstein, J., Kalbitzer, H. R., John, J., Goody, R. S. , & Wittinghofer, A. (1987) *Eur. J. Biochem.* **162,** 49-55.

Fisher, A. J., Smith, C. A., Thoden, J. B., Smith, R., Sutoh, K., Holden, H. M. , & Rayment, I. (1995) *Biochemistry.* **34,** 8960-8972.

Frisch, M. J., Trucks, G. W., Head-Gordon, M., Gill, P. M. W., Wong, M. W., J. B. Foresman, Johnson, B. G., Schlegel, H. B., Robb, M. A., E. S. Replogle, Gomperts, R., Andres, J. L., Raghavachari, K., J. S. Binkley, Gonzalez, C., Martin, R. L., Fox, D. J., Defrees, D. J., Baker, J., Stewart, J. J. P. , & Pople, J. A. (1992) *Gaussian 92, Revision C.* Gaussian, Inc., Pittsburgh PA.

Frisch, M. J., Trucks, G. W., Head-Gordon, M., Gill, P. M. W., Wong, M. W., J. B. Foresman, Johnson, B. G., Schlegel, H. B., Robb, M. A., E. S. Replogle, Gomperts, R., Andres, J. L., Raghavachari, K., J. S. Binkley, Gonzalez, C., Martin, R. L., Fox, D. J., Defrees, D. J., Baker, J., Stewart, J. J. P. , & Pople, J. A. (1994) *Gaussian 94.* Gaussian, Inc., Pittsburgh PA.

Gibbs, J. B., Sigal, I. S., Poe, M. , & Scolnick, E. M. (1984) *Proc. Natl. Acad. Sci.* **81,** 5704-5708.

Gilman, A. G. (1987) *Ann. Rev. Biochem.* **56,** 615-649.

Goldman, Y. E. (1987) *Annu. Rev. Physiol.* **49,** 637-654.

Goodno, C. C. (1979) *Proc. Natl. Acad. Sci. U.S.A.* **76,** 2620-2624.

Goodno, C. C. , & Taylor, E. W. (1982) *Proc. Natl. Acad. Sci. U. S. A.* **79,** 21-25.

Gordy, W. (1946) *J. Chem. Phys.* **14,** 305-320.

Greene, L. E. , & Eisenberg, E. (1980) *J. Biol. Chem.* **255,** 543-548.

Gresser, M. J. , & Tracey, A. S. (1990) in *Vanadium in Biological Systems,* (Chasteen, N. D. E., Ed.) Kluwer Academic Publishers, The Netherlands.

Hardcastle, F. D. , & Wachs, I. E. (1991) *J. Phys. Chem.* **95,** 5031-5041.

Herschlag, D. , & Jencks, W. (1987) **109,** 4665-4674.

Herschlag, D. , & Jencks, W. P. (1990) *Biochemistry.* **29,** 5172-5179.

Heyde, M. E. , & Rimai, L. (1971) *Biochemistry.* **10,** 1121-1128.

Hinchliffe, A. (1989) *Computational Quantum Chemistry, published by John Wiley & Sons, Inc.* 3-26.

Hollfelder, F. , & Herschlag, D. (1995) *Biochem.* **34,** 12255-12264.

Huang, L., Deng, H., Koutalos, Y., Ebrey, T., Groesbeek, M., Lugtenburg, J., Tsuda, M. , & Callender, R. H. (1996) *Biochemistry.* **35,** 8504-8510.

Huang, S. L. , & Tsai, M. D. (1982) *Biochemistry.* **21,** 951-959.

John, J., Frech, M. , & Wittinghofer, A. (1988) *J. Biological Chem.* **263,** 11792-11799.

John, J., Rensland, H., Schlichting, I., Vetter, I., Borasio, G. D., Goody, R. S. , & Wittinghofer, A. (1993) *J. Biol. Chem.* **268,** 923-929.

John, J., Sohmen, R., Feurstein, J., Linke, R., Wittinghofer, A. , & Goody, R. S. (1990) *Biochem.* **29,** 6058-6065.

Jones, P. G. , & Kirby, A. J. (1984) *J. Am chem. Soc.* **106,** 6207-6212.

Kirby, A. J. , & Varvoglis, A. G. (1967) *J. Am. Chem. Soc.* **87,** 415-423.

Kjeldgaard, M. , & Nyborg, J. (1992) *J. Mol. Biol.* **223,** 721-742.

Knight, W. B., Weiss, P. M. , & Cleland, W. W. (1986) *J. Am. Chem. Soc.* **108,** 2759-2761.

Knowles, J. R. (1980) *Annu. Re. Biochem.* **49,** 877-919.

Krengel, U., Schlichtig, I., Schere, A., Schumann, R., Frech, M., John, J., Kabsch, M., Pai, E. F. , & Wittinghofer, A. (1990) *Cell.* **62,** 539-548.

Langen, R., Schweins, T. , & Warshel, A. (1992) *Biochem.* **31,** 8691-8696.

Lewis, A., Nelson, N. , & Racker, E. (1975) *Biochemistry.* **14,** 1532-1535.

Lymn, R. W. , & Taylor, E. W. (1971) *Biochemistry.* **10,** 4617-4624.

Maegley, K. A., Admiraal, S. J., & Herschlag, D. (1996) *Proc. Natl. Acad. Sci. (USA).* **93,** 8160-8166.

Manor, D., Weng, G., Deng, H., Cosloy, S., Chen, C. X., Balogh-Nair, V., Delaria, K., Jurnak, F. , & Callender, R. H. (1991) *Biochemistry.* **30,** 10914-10920.

Mathews, C. K. and Holde, K. E., *Biochemistry,* published by The Benjamin/Cummings Published Company, Inc. 1990.

Milburn, M. V., Tong, L., DeVos, A. M., Brunger, A., Yamaizumi, Z., Nishimura, S. , & Kim, S. (1989) *Science.* **247,** 939-945.

Miller, D. L. , & Weissbach, H. (1974) *Adv. Enzymol.* **30,** 219-232.

Pai, E. F., Kabsch, W., Krengel, U., Holmes, K. C., John, J. , & Wittinghofer, A. (1989) *Nature.* **341,** 209-214.

Pai, E. F., Krengel, U., Petsko, G. A., Goody, R. S., Kabsch, W. , & Wittinghofer, A. (1990) *EMBO J.* **9,** 2351-2359.

Pulay, P. , & Fogarasi, G. (1981) *J. Chem. Phys.* **74(7),** 3999-4014.

Ramirez, F. , & Marecek, J. F. (1980) *Biochim. Biophys. Acta.* **589,** 21-29.

Ray, J. W. J., Burgner, I. J. W., Deng, H. , & Callender, R. (1993a) *Biochemistry.* **32,** 12977-12983.

Ray, W. J., Post, C. B., Liu, Y. , & Rhyu, G. I. (1993b) *Biochem.* **32,** 48-57.

Rayment, I., Rypniewski, W. R., Schmidt-Base, K., Smith, R., Tomchick, D. R., Benning, M. M., Winkelmann, D. A., Wesenberg, G. , & Holden, H. M. (1993) *Science.* **261,** 50-58.

Schlichting, I., Almo, S. C., Rapp, G., Wilson, K., Petratos, K., Lentfer, A., Wittinghofer, A., Kabsch, W., Pai, E. F., Petsko, G. A. , & Goody, R. S. (1990) *Nature.* **345,** 309-315.

Schweins, T., Geyer, M., Scheffzek, K., Warshel, A., Kalbitzer, H. R. , & Wittinghofer, A. (1995) *Nature St. Biology.* **2,** 36-44.

Schweins, T. , & Warshel, A. (1996) *Biochem.* **35,** 14232-14243.

Shimanouchi, T., Tsuboi, M. , & Kyogoku, Y. (1964) *Adv. Chem. Phys.* **7,** 435-498.

Sigal, I. S. (1988) *nature.* **332,** 485-486.

Smith, C. , & Rayment, I. (1996) *Biochemistry.* **35,** 5404-5417.

Smith, C. A. , & Rayment, I. (1995) *Biochemistry.* **34,** 8973-8981.

Smith, S. J. , & Eisenberg, E. (1990) *Eur. J. Biochem.* **193,** 69-73.

Sprang, S. R. (1997) *Annu. Rev. Biochem.* **66,** 639-678.

Struve. (1989) *Fundamentals of Molecular Spectroscopy.* published by John Wiley & Sons, Inc., 321-329.

Takeuchi, H., Murata, H. , & Harada, I. (1988) *J. Am. Chem. Soc.* **110,** 392-397.

Takeuchi, H., Nemoto, Y. , & Harada, I. (1990) *Biochemistry.* **29,** 1572-1579.

Taylor, E. W. (1977) *Biochemistry.* **16,** 732-740.

Tong, L., de Vos, A. M., Milburn, M. V. , & Kim, S. H. (1991) *J. Mol. Biol.* **217,** 503-516.

Tran-Dinh, S., Roux, M. , & Ellenberger, M. (1975) *Nucleic Acids Res.* **2,** 1101-1110.

Trybus, K. M. , & Taylor, E. W. (1982) *Biochemistry.* **21,** 1284-1294.

Tsuboi, M., Nishimura, Y., Hirakawa, A. Y. , & Peticolas, W. L. (1987) in *Biological Application of Raman Spectroscopy,* (Spiro, T. G., Ed.) John Wiley & Sons.

Tu, A. T. (1982) *Raman Spectroscopy in Biology, Principles and Applications. John Wiley & Sons., Inc.*

Tucker, J., Sczakiel, G., Feurstein, J., John, J., Goody, R. S. , & Wittinghofer, A. (1986) *EMBO J.* **5,** 1351-1358.

Wells, C. , & Bagshaw, C. R. (1984) *J. Muscle Res. Cell Motil.* **5,** 97-112.

Weng, G., Manor, D., Chen, Z., Balogh-Nair, V. , & Callender, R. (1994) *Protein Science.* **3,** 22-29.

Werber, M. M., Peyser, M. , & Muhlrad, A. (1992) *Biochemistry.* **31,** 7190-7197.

Williams, A. (1989) *Accs. Chem. Res.* **22,** 387-392.

Willis, H. A., Van der Mass, J. C. , & Miller, R. G. J. (1987) *Laboratory Methods in Vibrational Spectroscopy, published by John Wiley &Sons, Inc.* 565-567.

Wilson, E. B. J., Decius, J. C. , & Cross, P. C. (1955) *Molecular Vibrations.* Mcgraw-Hill, New York.

Wittinghofer, A., Krengel, U., John, J., Kabsch, W. , & Pai, E. F. (1991) *Envirom. Hlth. Perspec.* 11-15.

Wittinghofer, A. , & Pai, E. (1991) *TIBS.* **16,** 382-387.

Wooley, P. , & Clark, B. F. C. (1989) *Bio/technology.* **7,** 913-920.

Xiao, D. G. (1995) *CUNY Ph.D. Thesis.*

Yue, K. T., Deng, H. , & Callender, R. (1989) *J. Raman Spec.* **20,** 541-546.

Yue, K. T., Yang, J. P., Martin, C. L., Lee, S. K., Sloan, D. , & Callender, R. (1984) *Biochem. Biophys. Res. Comm.* **122,** 225-229.

Zhao, Y. , & Zhang, Z.-Y. (1996) *Biochem.* **35,** 11797-11804.

IMAGE EVALUATION TEST TARGET (QA-3)

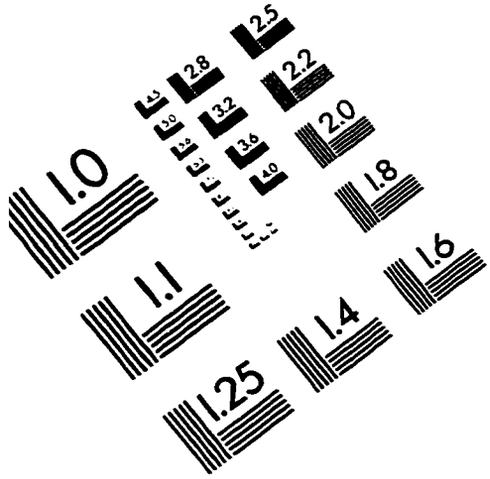

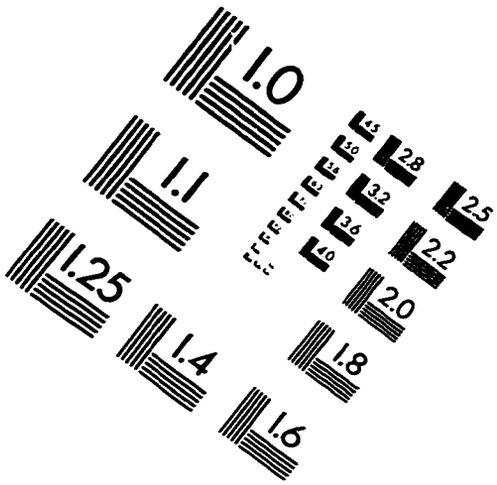

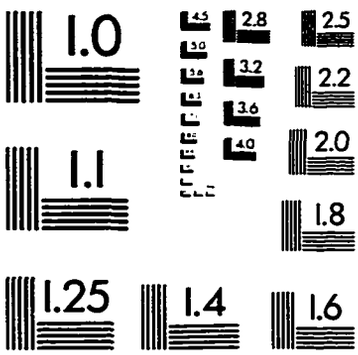

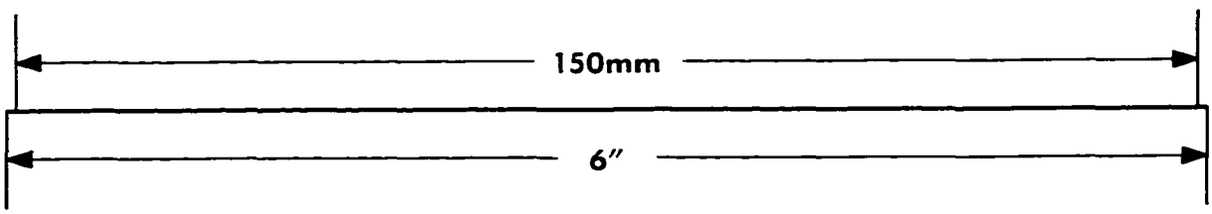

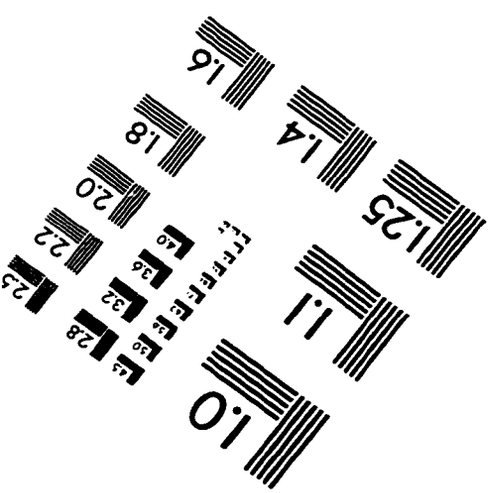

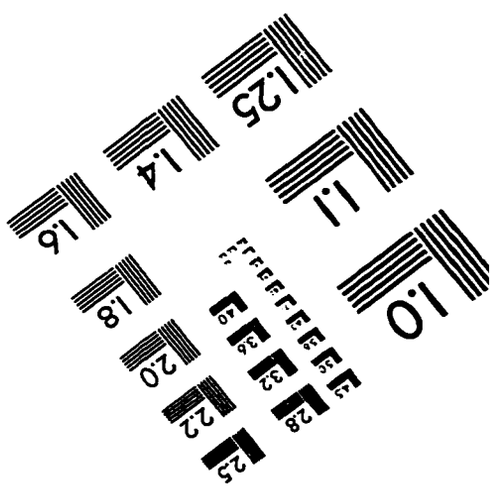

APPLIED IMAGE, Inc
1653 East Main Street
Rochester, NY 14609 USA
Phone: 716/482-0300
Fax: 716/288-5989